



NTNU – Trondheim
Norwegian University of
Science and Technology

Simulation model for an LNG ferry

Andreas Rolland Moss

Marine Technology (2-year)
Submission date: June 2014
Supervisor: Tor Einar Berg, IMT

Norwegian University of Science and Technology
Department of Marine Technology



NTNU Trondheim
Norwegian University of Science and Technology
Department of Marine Technology

MASTER THESIS IN MARINE TECHNOLOGY

SPRING 2014

FOR

Andreas Moss

Simulation model for a LNG ferry

Simulators are widely used by the shipping community in feasibility studies, engineering, operational planning and training. The need for quality of the simulation model depends on the actual application and varies from a representative representation of a class of vessels to specific models for single ships. This MSc thesis will be linked to a Research Council of Norway project studying methods to validate simulation models through use of model tests and sea trials. The student will obtain sea trial data for a LNG ferry and PMM data from tests done at MARINTEK.

The main objective for this thesis is to develop, test and validate a deep and calm water simulation model for the actual LNG ferry "MF Landegode". The final simulation model should be based on simulation tools developed and applied by MARINTEK such as the manoeuvring plug-in SIMAN in the ShipX tool box or the simulation tool VeSim. In addition to IMO's standard manoeuvres ship specific low speed manoeuvres shall be used for validation of the simulation model.

Secondary objectives of this MSc thesis are to:

- Understand the process of verification and validation of simulation models
- Calculate and/or estimate manoeuvring forces/moments in applied simulation tools
- Compare calculation results with manoeuvring characteristic specified in IMO MSC Res. 137(76) and vessel specific low speed manoeuvres
- Compare simulated manoeuvres with sea trial results
- Compare simulation results with similar results from the training simulator at Bodin
- Discuss needs for improvement of input parameters and physical models used in MARINTEK's simulation tools for studies of ship manoeuvring performance

In the thesis the candidate shall present his personal contribution to the resolution of problem within the scope of the thesis work.

Theories and conclusions should be based on mathematical derivations and/or logic reasoning identifying the various steps in the deduction.

The candidate should utilize the existing possibilities for obtaining relevant literature.

The thesis should be organized in a rational manner to give a clear exposition of results, assessments, and conclusions. The text should be brief and to the point, with a clear language. Telegraphic language should be avoided.



NTNU Trondheim
Norwegian University of Science and Technology
Department of Marine Technology

The thesis shall contain the following elements: A text defining the scope, preface, list of contents, summary, main body of thesis, conclusions with recommendations for further work, list of symbols and acronyms, reference and (optional) appendices. All figures, tables and equations shall be numerated.

The supervisor may require that the candidate, in an early stage of the work, present a written plan for the completion of the work. The plan should include a budget for the use of computer and laboratory resources that will be charged to the department. Overruns shall be reported to the supervisor.

The original contribution of the candidate and material taken from other sources shall be clearly defined. Work from other sources shall be properly referenced using an acknowledged referencing system.

The thesis shall be submitted in two copies:

- Signed by the candidate
- The text defining the scope included
- In bound volume(s)
- Drawings and/or computer prints that cannot be bound should be organized in a separate folder.
- The bound volume shall be accompanied by a CD or DVD containing the written thesis in Word or PDF format. In case computer programs have been made as part of the thesis work, the source code shall be included. In case of experimental work, the experimental results shall be included in a suitable electronic format.

Supervisor : Professor II Tor Einar Berg
Start : 14.01.2014
Deadline : 10.06.2014

Trondheim, 10.01.2014

Tor Einar Berg
Supervisor

Abstract

Developing regulations for improving safety at sea has been a concern since international trading became a reality. The International Maritime Organization (IMO) has become the international adopted treaty, which regulates the manoeuvring performance of ships to maintain the safety, security and to prevent marine pollution at sea. Manoeuvring tests for evaluating the performance of vessels have been established to ensure this.

Early estimations of the manoeuvring performance is an essential part and simulation models are therefore a critical tool, as alterations to the vessel can be of large costs after the vessel is built. Alterations and modifications can be made in an early design stage with a good simulation model, avoiding such great costs.

A set of full-scale trial data has been provided and processed for comparison with the simulated manoeuvres. The results show that the IMO standard manoeuvres are within the required abilities set for each specific full-scale manoeuvre.

The simulation of the manoeuvres were carried out using the simulation model VeSim. VeSim uses two pre-processors to calculate the motions and hydrodynamic characteristics of the vessel. All the IMO standard manoeuvres were well within the requirements. The comparison between the full-scale trials and simulated manoeuvres give a clear indication of over- and underestimation of the simulated manoeuvres in the range of 20 – 50% as an average value. This is mainly caused by questionable results of the hydrodynamic characteristics.

VeSim is believed to be a satisfying simulation model regarding the results presented in this thesis. But with regard to the aberrations in the hydrodynamic calculations, the model should be studied in more detail before making a conclusive decision on whether or not to use VeSim as a validated simulation model.

Sammendrag (Norwegian Abstract)

Utvikling av vedtekter for forbedring av sikkerheten til havs har vært et viktig tema siden internasjonal handelsvirksomhet ble en virkelighet. Den internasjonale sjøfartsorganisasjonen (IMO) har blitt den internasjonale traktaten som skal regulere manøvreringsferdighetene til skip for å opprettholde trygghet, sikkerhet og motvirke maritim forurensning til havs. Forskjellige manøvreringstester for evaluering av skipets ferdigheter har blitt etablert for å sikre at slike tilstander blir opprettholdt.

Tidlig estimering av slike manøvreringsferdigheter er en essensiell del og simuleringsmodeller er derfor et viktig verktøy ettersom endringer av fartøy kan ha store kostnader etter at det er ferdigstilt. Endringer av fartøyer kan gjøres i en tidlig fase i design stadiet med en god simuleringsmodell, og dermed unngå slike store kostnader.

Et sett av fullskala test data har blitt besørget og prosessert for å sammenlignes med simulerte tester. Resultatene av fullskala dataene viser at alle IMO kravene er opprettholdt.

Simuleringen av manøvrene ble utført med simuleringsmodellen VeSim. VeSim bruker to pro-kalkulerings programmer for å kalkulere skipets bevegelser og hydrodynamiske karakteristikk. Alle standard testene beskrevet av IMO er godkjent med hensyn på resultatene fra simuleringene. Sammenligningen mellom fullskala testene og simuleringene gir en klar indikasjon på over- og underestimering av de simulerte forsøkene. De simulerte manøvrene ligger i gjennomsnitt på rundt 20 – 50% over eller under resultatene fra fullskala testene. Dette er forårsaket av tvilsomme resultater av de karakteristiske hydrodynamiske egenskapene.

VeSim er likevel antatt å være en godkjent simuleringsmodell med tanke på resultatene som er blitt presentert i denne avhandlingen. Men i forhold til de store avvikene grunnet de hydrodynamiske kalkuleringene, burde denne simuleringsmodellen bli studert i mere detalj før en håndfast avgjørelse blir gitt, med hensyn på om VeSim kan bli brukt som en validert simuleringsmodell.

Acknowledgement

This thesis is submitted as a part of a 2-year Master of Science program at the Norwegian University of Science and Technology, department of Marine Technology.

The thesis is developed in cooperation with MARINTEK, which supplied technical support regarding hull lines and properties of the ship. In that note, I would like to express my gratitude to Ørjan Selvik who has supplied the information and offered technical guidance. I would also like to express my gratitude to Dariusz Fathi who has offered guidance and support regarding the simulation tool used in the thesis.

Finally, I want to express my gratitude to my supervisor Tor Einar Berg for guidance throughout the study. And a special thanks to my office-mates, for a good study environment and a memorable time.

Andreas Rolland Moss
Trondheim, June 2014

Contents

1	Introduction	1
1.1	Background	1
1.2	Objectives	1
1.3	Limitations	2
1.4	Approach	2
1.5	Structure of the thesis	3
2	Verification and validation of simulation models	4
2.1	The process	4
2.2	Validation	5
2.3	The SIMMAN initiative	5
2.4	Further work	5
3	Ship manoeuvring	7
3.1	Manoeuvring characteristics	8
3.2	IMO Standard manoeuvring tests and criteria	9
3.2.1	Turning circle manoeuvre	9
3.2.2	Zig-zag manoeuvre	10
3.2.3	Stopping test	11
3.2.4	Test conditions	12
3.2.5	Test criteria	13
3.2.6	Comments to the IMO Standards	13
3.3	Additional manoeuvres	14
3.3.1	Low speed manoeuvres	14
3.4	Manoeuvring prediction methods	17
3.4.1	Database method	17
3.4.2	Model tests	18
3.4.3	Mathematical and empirical methods	19
4	Mathematical model	21
4.1	Motions and axis system	21
4.2	Linear 3-DOF model	23
4.2.1	Dynamically stable vessel	24
4.3	Structure of VeSim	26

4.3.1	HullVisc	27
4.3.2	Vessel Response	32
4.3.3	Vessel Model (VeSim)	36
5	Full-scale trials	44
5.1	Gauges and data acquisition	45
5.2	Analysis of trials	45
5.3	Turning circle manoeuvre	49
5.3.1	Post-processing	49
5.3.2	Results	52
5.4	Zig-zag manoeuvre	53
5.4.1	Results	54
5.5	Stopping test	54
5.5.1	Results	55
5.6	Thruster turning manoeuvre	56
5.6.1	Results	56
5.7	Accelerating turn manoeuvre	57
5.7.1	Results	58
6	Simulations in VeSim	59
6.1	Results from VeSim	61
6.1.1	Turning circle manoeuvre	61
6.1.2	Zig-zag manoeuvre	62
6.1.3	Stopping test	62
6.1.4	Thruster turning manoeuvre	63
6.1.5	Accelerating turn manoeuvre	65
6.2	Comparison of simulated and full-scale results	66
6.2.1	Turning circle manoeuvre	66
6.2.2	Zig-zag manoeuvre	67
6.2.3	Thruster turning manoeuvre	69
6.2.4	Accelerating turn manoeuvre	71
7	Summary and Conclusion	73
7.1	Discussion	73
7.1.1	Manoeuvring results compared with IMO MSC Res. 137(76)	73
7.1.2	Simulation results compared with full-scale results	75
7.1.3	Influencing parameters in VeSim and error sources	78
7.1.4	Verification and validation of the model	79
7.2	Summary and conclusion	79
7.3	Recommendations for further work	81
Appendix A Ship specifications: MF Landegode		II
Appendix B Non-dimensional coefficients		IV

Appendix C Full-scale manoeuvres	VI
C.1 Turning circle manoeuvre	VII
C.1.1 Port turning circle	VII
C.1.2 Starboard turning circle	VIII
C.2 Zig-zag manoeuvre	IX
C.2.1 Port 10/10 zig-zag manoeuvre	IX
C.2.2 Starboard 10/10 zig-zag manoeuvre	X
C.2.3 Port 20/20 zig-zag manoeuvre	XI
C.2.4 Starboard 20/20 zig-zag manoeuvre	XII
C.3 Stopping test manoeuvre	XIII
C.4 Thruster turning manoeuvre	XIV
C.5 Accelerating turn manoeuvre	XV

Appendix D VeSim simulated manoeuvres	XVI
D.1 Turning circle manoeuvre	XVII
D.1.1 Port turning circle	XVII
D.1.2 Starboard turning circle	XIX
D.2 Zig-zag manoeuvre	XXI
D.2.1 Port 10/10 zig-zag manoeuvre	XXI
D.2.2 Starboard 10/10 zig-zag manoeuvre	XXIII
D.2.3 Port 20/20 zig-zag manoeuvre	XXV
D.2.4 Starboard 20/20 zig-zag manoeuvre	XXVII
D.3 Full astern stopping manoeuvre	XXIX
D.4 Thruster turning manoeuvre	XXXII
D.5 Accelerating turn manoeuvre	XXXVII

List of Figures

2.1	MF Landegode	6
3.1	Turning circle manoeuvre	10
3.2	10°/10° zig-zag manoeuvre	11
3.3	Stopping test manoeuvre	12
3.4	Test results of thruster turning test	15
3.5	Test results of accelerated turn test	16
3.6	MARINTEK's hexapod mounted at the multipurpose carriage	19
3.7	Sink/source principle	20
4.1	Body-fixed axis system used in manoeuvring	21
4.2	Flowchart of VeSim structure	26
4.3	NED-frame	27
4.4	The notation used by Newman and standard notation	30
4.5	Added mass, damping, and restoring forces and moments	35
4.6	Excitation loads	36
5.1	MF Landegode's position during sea trials	46
5.2	Port turning circle trajectory before and after rotation	50
5.3	Starboard turning circle trajectory before and after rotation	50
5.4	Starboard turning circle with original and corrected trajectory	51
5.5	Starboard turning circle with corrected trajectory before rotation	52
5.6	Full-scale stopping test trajectory	55
5.7	Full-scale stopping test speed and propeller pitch	56
5.8	Vessel heading from the full-scale thruster turning manoeuvre	57
5.9	Full-scale accelerating turn trajectory and heading in degrees	58
6.1	List of available manoeuvres in the calm water simulation model	60
6.2	Scenario manager in the time domain simulator	64
6.3	Vessel heading from the simulated thruster turning manoeuvre	64
6.4	Comparison of full-scale and simulated turning circle results	66
6.5	Comparison of full-scale and simulated zig-zag overshoot angles	68
6.6	Comparison of full-scale and simulated zig-zag results	69
6.7	Comparison of full-scale and simulated thruster turning results	70
6.8	Heading with colour equivalent to time parameters	70

6.9	Comparison of full-scale and simulated accelerating turn results . . .	71
7.1	Full-scale turning circle and simulation in percentage difference . . .	75
7.2	Full-scale stopping test and simulation in percentage difference . . .	76
7.3	Full-scale zig-zag and simulation in percentage difference	77
7.4	Full-scale thruster turning and simulation in percentage difference .	77
7.5	Full-scale accelerating turn and simulation in percentage difference .	78
A.1	Rolls Royce's integrated propeller and rudder system "PROMAS" .	III
C.1	Full-scale port turning circle	VII
C.2	Full-scale starboard turning circle	VIII
C.3	Full-scale port 10/10 zig-zag manoeuvre	IX
C.4	Full-scale starboard 10/10 zig-zag manoeuvre	X
C.5	Full-scale port 20/20 zig-zag manoeuvre	XI
C.6	Full-scale starboard 20/20 zig-zag manoeuvre	XII
C.7	Full-scale stopping test manoeuvre	XIII
C.8	Full-scale thruster turning manoeuvre	XIV
C.9	Full-scale accelerating turn manoeuvre	XV
D.1	Port turning circle summary report	XVII
D.2	Port turning circle trajectory	XVIII
D.3	Starboard turning circle summary report	XIX
D.4	Starboard turning circle Trajectory	XX
D.5	Port 10/10 zig-zag summary report	XXI
D.6	Port 10/10 zig-zag heading and yaw angle	XXII
D.7	Starboard 10/10 zig-zag summary report	XXIII
D.8	Starboard 10/10 zig-zag heading and yaw angle	XXIV
D.9	Port 20/20 zig-zag summary report	XXV
D.10	Port 20/20 zig-zag heading and yaw angle	XXVI
D.11	Starboard 20/20 zig-zag summary report	XXVII
D.12	Starboard 20/20 zig-zag heading and yaw angle	XXVIII
D.13	Stopping test summary report	XXIX
D.14	Stopping test engine power	XXX
D.15	Stopping test propeller rpm	XXXI
D.16	Thruster turning heading	XXXII
D.17	Thruster turning heading yaw rate	XXXIII
D.18	Thruster turning thruster 1 power	XXXIV
D.19	Thruster turning thruster 2 power	XXXV
D.20	Thruster turning thruster 3 power	XXXVI
D.21	Accelerating turn summary report	XXXVII
D.22	Accelerating turn heading	XXXVIII
D.23	Accelerating turn rudder angle	XXXIX
D.24	Accelerating turn main engine power	XL
D.25	Accelerating turn thruster 1 power	XLI
D.26	Accelerating turn thruster 2 power	XLII

D.27 Accelerating turn thruster 3 power XLIII

List of Tables

4.1	Forces and motion parameters in manoeuvring	22
4.2	Hydrodynamic forces based on slender body theory	30
4.3	Input data to SIMAN	31
4.4	Hydrodynamic coefficients from HullVisc	31
5.1	Test conditions for the respective days	46
5.2	Full-scale port turning circle results	53
5.3	Full-scale starboard turning circle results	53
5.4	Full-scale zig-zag results	54
5.5	Full-scale stopping test results	55
5.6	Full-scale thruster turning results	57
5.7	Full-scale accelerating turn results	58
6.1	Simulated turning circle results	61
6.2	Simulated 10/10 and 20/20 zig-zag results	62
6.3	Simulated stopping test results	63
6.4	Simulated thruster turning results	65
6.5	Simulated accelerating turn results	65
6.6	Markers for comparison of simulated and full-scale turning circle results	67
6.7	Markers for comparison of simulated and full-scale zig-zag results	69
6.8	Markers for comparison of simulated and full-scale thruster turning results	71
6.9	Markers for comparison of simulated and full-scale accelerating turn results	72

Nomenclature

a	Acceleration [m/s^2]
a_{jk}	2D added mass coefficient in the j th mode due to k th motion
A_{jk}	Elements of the added mass matrix
A_ω	Frequency dependent added mass matrix
A_∞	Added mass at infinite frequency
B	Ship's breadth
B_{jk}	Elements of the linear damping matrix
C	Coriolis matrix
C_b	Block coefficient
C_D	Cross flow drag coefficient
C_{jk}	Elements of the stiffness matrix
C_ω	Frequency dependent potential damping matrix
C_∞	Damping matrix at infinite frequency
D	Drag force component; Differential operator
$D(x)$	Sectional draught in longitudinal direction
$D_{1,2}$	Linear (1) and quadratic (2) damping matrix
D_{50}	Median grain size
d_{em}	Mean draught including depth of keel at mid-ship
f	Vector function
F	Force [kgm/s^2]
$F_D^{(1)}$	Longitudinal polynomial resistance
$F_D^{(2)}$	Cross flow drag in sway
$F_D^{(6)}$	Cross flow drag in yaw
g	Acceleration of gravity
G (COG)	Centre of gravity
$h(\tau)$	Retardation function
H_{m0}	Significant wave height calculated using wave spectra
I	Moment of inertia
I_{zz}	Ship mass moment of inertia
k	Relative seabed roughness
K	Roll moment; Restoring matrix
kg	Kilogram
L	= L_{pp} = Ship's length between perpendiculars
ln	Natural logarithm

$m(M)$	Meters; Mass [kg]; Pitch moment; Body mass matrix
M_{jk}	Elements of the generalized mass matrix
N	Yaw moment
N'_r	Coefficient for yaw damping
N'_v	Coefficient for yaw damping due to sway velocity
$N'_\dot{r}$	Coefficient for hydrodynamic mass moment of inertia in yaw
$N'_\dot{v}$	Coefficient for hydrodynamic mass moment of inertia in yaw due to sway
p	Roll rate of turning
P, V_1, V_2	Potential, linear and quadratic viscous damping terms
q	Pitch rate of turning; Excitation forces
q_{wind}	Wind drag force
$q_{wave}^{(1)}$	First order wave excitation force
$q_{wave}^{(2)}$	Second order wave drift force
q_{prop}	Propulsion force
q_{man}	Manoeuvring force
q_{ext}	Remaining force
r	Yaw rate of turning
Re	Reynolds number
s	Seconds
t	Time in seconds
T	Ship's draught
u	Longitudinal velocity component
$u_c^{(i)}$	Current velocity
u_D	Relative velocity between vessel and surrounding fluid
$u_v^{(i)}$	Vessel velocity
$u_w^{(i)}$	Wave particle velocity at COB
$U(V)$	Speed of vessel
v	Lateral velocity component
V	Depth averaged velocity
V_L	Threshold speed
\vec{v}_{cx}	Current velocity in longitudinal direction
\vec{v}_{cy}	Current velocity in transverse direction
w	Vertical velocity component
\vec{w}	Rotational motion
W	Sustained wind speed at 10m above water surface
(x, y, z)	Cartesian coordinate system. Body-fixed in manoeuvring analysis.
(x_n, y_n, z_n)	NED coordinate system. Earth-fixed.
(x_b, y_b, z_b)	Body-fixed coordinate system
x_T	x-coordinate at transom stern
X	Longitudinal force component
$X_{\dot{u}}$	Added mass coefficient in surge
X_{res}	Ship resistance
X_{rr}	Longitudinal resistance due to yaw velocity
X_{vr}	Longitudinal resistance due to combined sway and yaw velocity

X_{vv}	Longitudinal resistance due to sway velocity
X_{vvvv}	Longitudinal resistance due to sway velocity
Y	Lateral force component
y_0	Water depth
Y'_r	Coefficient for sway damping due to yaw velocity
Y_{Ur}	Froude number dependent linear damping coefficient
Y_{Uv}	Froude number dependent linear damping coefficient
Y'_v	Coefficient for sway damping
$Y'_\dot{r}$	Coefficient for hydrodynamic mass in sway due to yaw acceleration
$Y'_\dot{v}$	Coefficient for hydrodynamic mass in sway
Z	Vertical force component

Greek symbols

β	Drift angle
δ	Rudder angle
η_k	Motion amplitude, where k=1,2,3,..6 refers to the 6-DOF
θ	Phase angle
$\rho(water)$	Density of water
ρ_{air}	Density of air
τ	Trim; Wind stress exerted on water surface
τ_{bed}	Shear stress exerted on seabed
$\tau_{surface}$	Shear stress exerted on the water surface
ϕ	Roll angle
ψ	Heading angle
ω_0	Wave frequency
ω	Angular frequency of encounter
Γ	Dihedral angle
Δ	Vessel's weight displacement; "Change of"
∇	Vessel's volume displacement
Σ	Summation
Ω_2	Non-dimensional yaw velocity

List of Abbreviations

AP	Aft Perpendicular
BL	Base Line
CFD	Computational Fluid Dynamics
CL	Center Line
CO	Coordinate Origin
COB	Centre Of Buoyancy
COG	Centre Of Gravity
CP	Controllable Pitch
DOF	Degrees Of Freedom
FP	Fore Perpendicular
GMT	Greenwich Mean Time
IMO	International Maritime Organization
ISO	International Organization for Standardization
ITTC	International Towing Tank Conference
MAROFF	Maritime activities and Offshore operations
MCR	Maximum Continuous Revolution
MF	Motor Ferry
NED	North East Down
NTNU	Norges Teknisk-Naturvitenskapelige Universitet Norwegian University of Science and Technology
ODE1	Ordinary Differential Equations 1
OMAE	Conference on Ocean, Offshore and Arctic Engineering
PMM	Planar Motion Mechanism
PT	Port
RANS	Reynolds-Averaged Navier-Stokes
SB	Starboard
SNAME	Society of Naval Architects and Marine Engineers
SOLAS	Safety Of Life At Sea
VeRes	Vessel Response
VeSim	Vessel Simulator
WAMIT	Wave Analysis MIT

Chapter 1

Introduction

1.1 Background

The course TMR 4220 - Naval hydrodynamics lectured at NTNU gives an introduction to the standard simulation tests and requirements. The lecture notes to this course provided by Tor E. Berg is used throughout the study, along with the International Maritime Organization's (IMO) resolutions and explanatory notes. The thesis include explanatory chapters and sections explaining the different methods of retrieving the input parameters to the simulation model and how they are applied. References are given throughout the thesis showing where the information has been found and gives the reader the opportunity to further investigate what has been presented in the thesis.

This thesis has its origin in the project thesis written autumn 2013 [1]. A validation of the simulation tool SIMAN was presented as a comparison of simulated manoeuvres, IMO requirements and preliminary full-scale trials. The initial results were not as satisfactory as hoped and resulted in a conclusion that SIMAN was not a suited simulation tool for MF Landegode at the present time.

1.2 Objectives

The main objectives of this thesis are to

- Give a brief introduction on how to validate a simulation model
- Give a brief introduction on the International Maritime Organization and its purpose
- Give an introduction to the IMO standard manoeuvring tests and criteria
- Give an introduction to additional low speed manoeuvring tests

- Give an introduction to the simulation model Vessel Simulator (VeSim) and the structure of the model
- Give an explanatory note on the mathematical model used in the simulation model
- Gather and process full-scale trial measurements, and present the trial conditions and results in a lucid manner
- Simulate the IMO standard manoeuvres, in addition to low speed manoeuvres and compare the results with full-scale results
- Discuss the validity of the simulation model based upon the presented results and comparisons
- Give a conclusion on whether or not this is a suitable simulation model for the case vessel
- Suggest further work

1.3 Limitations

The full-scale results presented are affected by weather conditions. These are not easy to account for in post-processing of the data and will have an effect on the similarity of the simulations. Some of the manoeuvres have been treated to account for weather conditions, which will be described. The simulation tool used was preliminary unknown to the student, and getting to know the program is therefore a part of the study. Due to time restraints, a brief study of all the manoeuvres will be addressed instead of a higher detailed study of a specific manoeuvre or aspect of the simulation model. Regarding the ship's hull lines and properties supplied by MARINTEK, they are confidential and will not be reproduced in the thesis. One of the bullet points in the scope of the thesis suggests comparing the simulation results with results from the training simulator at Bodin. The hydrodynamic coefficients that were intended for analysis from the PMM tests conducted at MARINTEK and used in the training simulator, were not obtainable within the time of completing the study. The secondary objective is hence not evaluated in the thesis.

1.4 Approach

To understand the purpose and process of validating and verifying a simulation model, a literature study has been conducted. This includes reading different papers published by amongst others, the ITTC, OMAE and SIMMAN initiative, and studying the different parameters that are of interest in the specific manoeuvres. To evaluate these manoeuvres, different organizations as the IMO and ISO are studied. Here, the manoeuvres are explained in detail, along with limitations to

the standard tests. The mathematical formulations behind manoeuvring theory is studied with the simulation model used as a basis. The simulation model Vessel Simulator is used, which is developed by MARINTEK. The manual of the plug-in has been studied to get an overview of the model. Input parameters, restrictions and assumptions have been addressed to understand how the program calculate and estimate the motions of the vessel.

The result of the simulations are compared with the IMO requirements and post-processed full-scale trials, conducted in August 2013, to evaluate the similarity and give an assessment on the validity of the simulation model. A discussion of any influencing sources and errors in the calculation is given on the basis of the results, also to address the validity of the model.

As a concluding remark, further work is suggested on the basis of information extracted from the findings, and which areas of the process that needs to be studied in more detail to give a more tangible decision on the validity of this model.

1.5 Structure of the thesis

A brief explanation of the different chapters are presented below. Chapter 2, 3 and 4.1-2 are mainly an abridged version of what was presented in the project thesis, with modifications and alterations to the text [1].

Chapter 2 gives an introduction to validation of simulation models. A step by step explanation of the process is given. Work regarding validation models are also presented along with future plans for validation assessment workshops.

Chapter 3 gives an introduction to the IMO initiative and its purpose, along with an explanation of the standard manoeuvres and requirements. The chapter also includes additional manoeuvres, along with low speed manoeuvres and different manoeuvring prediction methods.

Chapter 4 gives an introduction to the basic 3-DOF mathematical model. It gives an overview of the structure of VeSim and presents the mathematical model it uses.

Chapter 5 presents the full-scale trials and the post-processed results compared with the IMO standard requirements and other parameters to be obtained.

Chapter 6 presents the simulated manoeuvres according to the IMO requirements. A comparison of the simulated and full-scale manoeuvres are given by various graphs and a discussion of these.

Chapter 7 gives a summary of the thesis, a discussion of influencing parameters and a conclusion on whether or not VeSim is a suitable simulation model for MF Landegode. Suggestions for further work are given as a concluding note to the thesis.

Chapter 2

Verification and validation of simulation models

Development of ship manoeuvring simulators have been of great concern in recent time when international manoeuvring standards have been developed. Ship manoeuvring simulation models can be separated by models for prediction of manoeuvrability and models for use in simulators [2]. High-quality simulation models are often used for the study of advanced marine operations and investigations of maritime accidents, as for instance collisions and groundings [3]. To ensure the validity of the models, careful consideration and verification of the simulation models must be conducted and gathered. Maritime simulation models will require a larger degree of validation than of the prediction in ship manoeuvrability, because of the large amount of different parameters involved, such as wind, current, waves and operating conditions of the vessel. This thesis will focus on the manoeuvrability of a ship and the validation of the model will therefore be less detailed than for maritime simulation models. The main details of the validation procedure of a manoeuvrability model will be discussed in the following.

2.1 The process

The main content of a manoeuvring model and intention of a well validated model will contain the following aspects and procedures [2]:

- Ship particulars
- Prediction of hydrodynamic forces
- Modelling of forces in a structured mathematical model
- Integration method
- Simulation software
- Simulated manoeuvres

The process of the simulation and the documentation should be given such that it clearly shows the validity of the model and the simulated manoeuvres. That be the standard manoeuvres defined by the IMO, along with the low speed manoeuvres and the accuracy of the model.

2.2 Validation

When a manoeuvre has been simulated and the results have been presented, the normal procedure for validation is by comparing the results with known benchmarking data. The documentation of the validation should be available in the form of a report or published paper [2]. Benchmarking data are used for comparing of the various methods for predicting ship manoeuvrability. There are little full-scale benchmark data available on the open market. The *Esso Osaka* is a much used ship for comparison of manoeuvring data [4]. However, due to its outdated hull design and lack of a bulb, the *Esso Osaka* is a poor comparison ship with regard to new ships with more modern design. Captive model tests, as well as free running model tests are frequently used as substitutes for full-scale trials and are thought to be as precise as the full-scale trials. Although scale effects are not well documented, the control of environment and test parameters can be fairly controlled.

2.3 The SIMMAN initiative

The SIMMAN 2008 initiative is a workshop where new benchmarking models, data as well as proceedings have been documented [5]. The main purpose of the workshop was to obtain, as mentioned, new benchmarking data for newer vessels and document the different simulation models' different capabilities including systems and CFD based methods, through comparison of the different ship hulls. The ships used in the SIMMAN 2008 workshop included a tanker (KVLCC1 and KVLCC2), a container ship (KCS) and a surface combatant hull (5415). The different simulation models were compared with PMM and rotating arm tests. None of these ships exist in full-scale, but only as scaled models. They are provided with geometrical data for hull, propeller, rudder and appendages for the public to view.

2.4 Further work

Further work on establishing more benchmarking data is planned. A new session of a SIMMAN workshop is being planned, and institutes like NTNU are constantly developing their simulation tools with comparison of new vessels, like the MF Landegode. The vessel is depicted in Figure 2.1.



Figure 2.1: MF Landegode [6]

Chapter 3

Ship manoeuvring

Manoeuvring and ship handling has always been a challenge for ship designers and naval architects. To have an adequate understanding and an anticipated knowledge about the vessel's manoeuvring characteristics and behaviour in confined waters, is an important aspect of the marine safety and protection of the marine environment. In addition, the safety of the crew and staff operating the vessel needs to be maintained.

As long as travelling at sea has been possible and trading across continents have been a sustainable development of countries, there have always been a need for a standardization of ship design and operational safety aspects. Developing international regulations for improving safety at sea that is followed by all shipping nations have been adapted several times from the mid-19th century. After the accident of the Titanic in 1912, the first convention addressing the safety of life at sea (SOLAS) was held. Which is the most important treaty addressing marine safety [7].

It was first in the year 1948 that such a convention was adopted. In Geneva, the formal establishment of the International Maritime Organization (IMO) was conducted. Ten years later, in 1958 the convention entered into force. The IMO is a United Nations agency regulating manoeuvring performances of ships to ensure safety, which is the key driving force of the organization. Its main purpose is related to security and safety of shipping and the prevention of marine pollution.

IMO's **mission statement** [7]:

"The mission of the International Maritime Organization (IMO) as a United Nations specialized agency is to promote safe, secure, environmentally sound, efficient and sustainable shipping through cooperation. This will be accomplished by adopting the highest practicable standards of maritime safety and security, efficiency of navigation and prevention and control of pollution from ships, as well as through consideration of the related legal matters and effective implementation of IMO's instruments with a view to their universal and uniform application."

To confirm the vessel's compliance with the Standards, full-scale trials must be conducted [8]. The full-scale trials must also be performed according to the Standards. The Standards refers to IMO's three required manoeuvring tests, presented later in Section 3.2. Some of the parameters influencing the manoeuvrability are the main dimensions of the vessel, its hull shape, speed and propulsion system. These are all decided and calculated in the design stage.

3.1 Manoeuvring characteristics

IMO addresses the Standard manoeuvrability characteristics for a ship by typical measurements of the vessel's performance quality and handling ability [8].

Inherent dynamic stability/straight line stability

If a vessel on a straight course is exposed to a small disturbance, which sets it off course, and soon after settles a new straight course, without needing to correct with a rudder, the vessel is said to be dynamically stable.

The degree of inherent stability and the magnitude and duration of the disturbance will affect the resulting deviation.

Course-keeping ability

The course-keeping ability is a measure of the steered vessel's ability to maintain a straight predetermined path direction without having to use corrective rudder. If the vessel suffers from small inherent dynamic stability, reasonable course control is allowed.

Initial turning/course-changing ability

The change-of-heading response to a moderate helm is defined as the the vessel's initial turning ability. This can be measured in terms of either heading deviation per unit distance sailed, or in terms of the distance sailed before a certain heading deviation (e.g. time to second execute in a zig-zag manoeuvre) is reached.

Yaw checking ability

The measure of the counter-rudder applied in a certain state of turning is called the yaw checking ability of the vessel. E.g. for a zig-zag manoeuvre, this can be the heading overshoot reached before the yawing tendency has been cancelled by the counter-rudder.

Turning ability

The measure of the vessel's ability to turn using the hard-over rudder is called the turning ability. The results may be given by either minimum advance or tactical diameter, where both can be determined by a turning circle manoeuvre.

Stopping ability

The measured "track reach" and "time to dead in water" is the vessel's stopping ability. This can be measured in a stop engine-full astern manoeuvre, executed in the end of a steady approach at full test speed.

3.2 IMO Standard manoeuvring tests and criteria

Three required manoeuvring tests has been defined by IMO to help assist in design, construction and operation of ships [8]. These tests are used in evaluating the ship's manoeuvring performance according to the Standard [8]. The tests are hence referred to as the Standard manoeuvring tests. These tests will measure the manoeuvrability of the vessel and evaluate its characteristics based on the conventional trial manoeuvres. The three manoeuvring tests are the turning circle manoeuvre, the zig-zag manoeuvre and the stopping test manoeuvre. By executing a turning circle, the turning ability of the vessel can be determined. The course-keeping and initial turning/course-changing ability can be determined by a zig-zag manoeuvre. Finally, the vessel's stopping ability can be found from the stopping test manoeuvre. The following sections describe the three manoeuvres in more detail.

3.2.1 Turning circle manoeuvre

The turning circle manoeuvre is performed to both starboard and port. The vessel is set to a fixed heading with no measured yaw rate. When heading and test speed is achieved, the rudder is set to a 35° angle or maximum design rudder angle permissible at the test speed. When the vessel has performed a 360° change of heading, the test is complete. The essential information extracted from this manoeuvre are tactical diameter, advance and transfer, see Figure 3.1. Transfer is the transfer (deviation perpendicular to the original heading) at a 90° change of heading. Tactical diameter is the transfer at a 180° change of heading. Advance is the distance travelled by the vessel along the original course until a 90° change of heading is achieved. The distance is measured from the point where the rudder is put over.

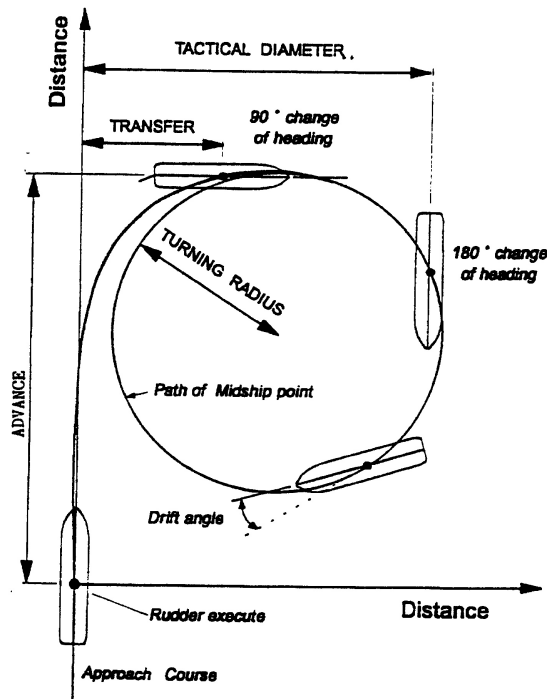


Figure 3.1: Turning circle manoeuvre [9]

3.2.2 Zig-zag manoeuvre

The zig-zag manoeuvre is also executed to both starboard and port. When the vessel is on a straight course, a specific amount of rudder angle is applied ("first execute"). When the specific course alteration from the original heading is achieved, the rudder is alternately shifted to either side ("second execute" and so on). There are two types of zig-zag manoeuvres described in the Standards. The $10^\circ/10^\circ$ and the $20^\circ/20^\circ$ zig-zag test. The $10^\circ/10^\circ$ zig-zag test uses a 10° rudder angle until a course change of 10° from the original heading is achieved. The $20^\circ/20^\circ$ zig-zag test is executed correspondingly with 20° . The desired information to extract from this test are the overshoot angles, initial turning time to second execute and the time to check yaw (the time between the rudder execute and the time of the maximum heading change in the original direction). The overshoot angle is the difference in angle between the rudder execute and the continuous turning of the vessel until it changes its direction (corresponding to the yaw checking ability). The first and second overshoot angle corresponds to the second and third rudder execute, respectively [10]. See Figure 3.2.

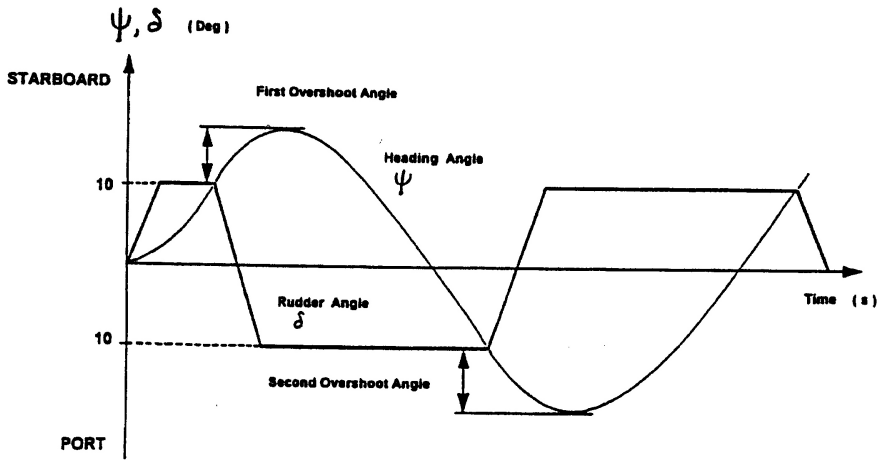


Figure 3.2: 10°/10° zig-zag manoeuvre [9]

3.2.3 Stopping test

The stopping test is performed when the vessel is at full ahead speed. At this moment, the full astern power command is given and the ship's speed reduces until a zero value of the speed is achieved. During the trial, the rudder should be placed in midship position. The parameters of interest are the head reach, track reach and the lateral deviation. The head reach is the distance travelled along the ship's original course from the astern order command is given, until the ship is "dead in water". The track reach is the total distance sailed in the ship's path. Lateral deviation is the distance to either starboard or port, perpendicular to the ship's initial course. See Figure 3.3.

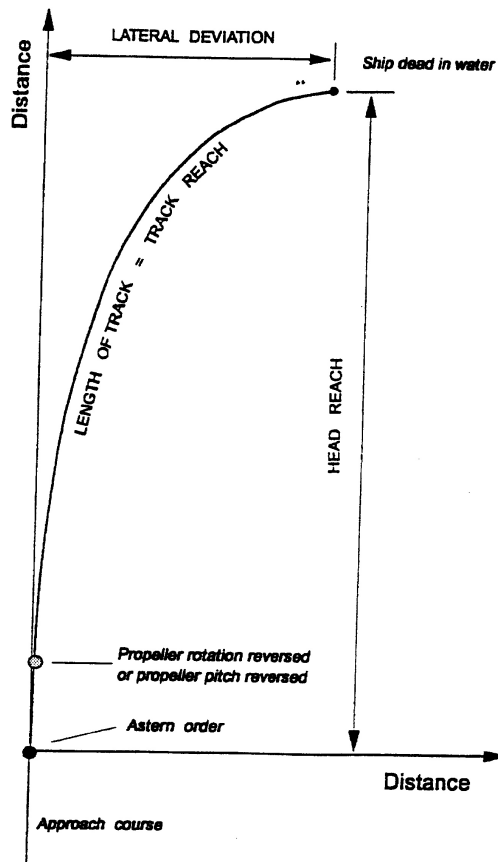


Figure 3.3: Stopping test manoeuvre [9]

3.2.4 Test conditions

In order to evaluate the manoeuvring tests and characteristics properly, the manoeuvring tests should be conducted to both starboard and port under the following conditions [9]:

- deep, unrestricted water: more than 4 times the draught,
- calm environment,
- full load, even keel condition,
- steady approach at the test speed, and
- the test speed is at least 90% of the ship's speed, corresponding to 85% of the maximum engine output

3.2.5 Test criteria

The test criteria defined by the IMO are explained as follows [8];

- Turning ability;
 - tactical diameter should not exceed 5 ship lengths in the turning circle manoeuvre
- Initial turning ability;
 - with the application of a 10° rudder angle to port/starboard, the ship should not travel more than 2,5 ship lengths by the time the heading has changed by 10° from the original heading
- Yaw checking abilities and Course keeping ability
 - the value of the first overshoot angle in the $10^\circ/10^\circ$ zig-zag test should not exceed:
 - * 10° , if L/V is less than 10 seconds (L = ship length, V = test speed)
 - * 20° , if L/V is 30 seconds or more
 - * $(5 + \frac{1}{2}(L/V))$ degrees, if L/V is 10 seconds or more but less than 30 seconds
 - The value of the second overshoot angle in the $10^\circ/10^\circ$ zig-zag test should not exceed the above criterion values for the first overshoot by more than 15°
 - The value of the first overshoot angle in the $20^\circ/20^\circ$ zig-zag test should not exceed 25°
- Stopping ability
 - the track reach in the full astern stopping test should not exceed 15 ship lengths

3.2.6 Comments to the IMO Standards

Since the IMO resolution A751(18) was accepted in 1993, compliance of these standards have been the foundation in design of ships [11]. The standards are focused on conventional vessels such as displacement ships, like bulk carriers and tankers, propelled by standard propulsion (propellers and rudders). Sailing in restricted waters and impact of environment (i.e. wind, waves and other vessels) are not a part of the standards, with an exception of current in the turning circle manoeuvre. As a consequence of this, ships are constructed to "only" fulfil the design criteria given by the IMO resolution A751(18). Some vessels should, in addition to the IMO requirements, fulfil specific "mission-related" requirements. Which could be

specific low speed manoeuvres for determining the manoeuvring abilities in quay areas. Such performance qualities would not be needed for other vessels such as bulk carriers and tankers, as they are guided by tugs near port. In the wide selection of different ship designs and special purpose vessels available to this date, the IMO requirements relate to only a small portion of what is considered as safe manoeuvring [11]. The standards should be viewed as a minimum requirement to fulfil and several more tests, especially mission-related tests, should be conducted and reviewed before letting a vessel sail.

3.3 Additional manoeuvres

In addition to the mandatory manoeuvring tests listed in IMO's standards there are several other tests recommended by various organizations. These tests are however not examined in this thesis and will not be explained in detail. For further information about the different tests, it is referred to the ITTC - Recommended Procedures [10]. An overview of some different manoeuvring tests are listed below:

- Modified zig-zag manoeuvre test
- Zig-zag manoeuvre at low speed test
- Direct spiral test
- Reverse spiral test
- Pullout test
- Stopping inertia test
- Parallel course manoeuvre test
- Thruster turning test
- Accelerating turn test

3.3.1 Low speed manoeuvres

The thruster turning test and the accelerating turn test are considered low speed manoeuvres. As MF Landegode needs to perform turning manoeuvres in the quay area, these tests have been conducted during sea trials and will be explained in the following.

Thruster turning manoeuvre

The thruster turning test is not specified in the "IMO MSC Circ.1053" and is not viewed as a standard manoeuvring test. The manoeuvre is explained in the "International Standard ISO 13643-2 Ships and marine technology - Manoeuvring of ships" [12].

The vessel is turned by means of its thrusters to starboard by 60° from its initial heading (into the wind). The time measured at heading changes of 15° , 30° and 60° are to be obtained. When a heading change of 60° is reached, the thrusters are reversed and the overshoot angle and time are recorded. The test is then performed to port. The test should be performed with all possible combinations of bow and stern thrusters. The results of the thruster turning test at zero speed can be presented as shown in Figure 3.4.

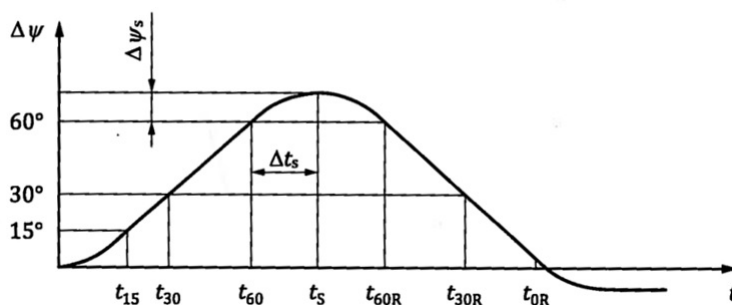


Figure 3.4: Test results of thruster turning test [12]

The data to be obtained from the thruster turning test are:

- time to turn 15° t_{15}
- time to turn 30° t_{30}
- time to turn 60° t_{60}
- time to return to 60° t_{60R}
- time to return to 30° t_{30R}
- time to return to 0° t_{0R}
- overshoot time Δt_s
- overshoot angle ψ_s
- threshold speed V_L

Accelerating turn test

The accelerating turn test is, as the thruster turning test, not described by the "IMO MSC Circ.1053" standards. A description of the manoeuvre can be found in the "International Standard ISO 13643-2", with guidelines of what to obtain from the measured data [12].

The manoeuvre starts with zero speed and the main propulsion unit set at half MCR. At the same time, the rudder is applied hard over, or the desired degree of interest, in the specific direction as quickly as possible. The settings are kept in these conditions until the vessel achieves a steady turn and the manoeuvre is complete, i.e. the vessel has performed a turn of at least 180° . Figure 3.5 depicts the trajectory of the manoeuvre and the data to be obtained.

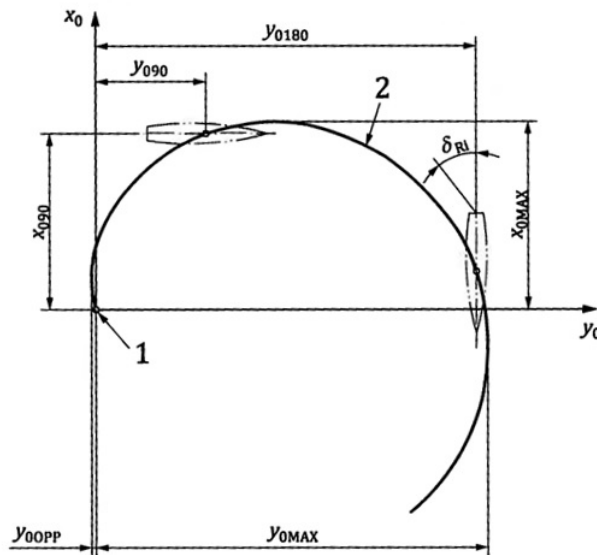


Figure 3.5: Test results of accelerated turn test [12]

The key **1** denotes the point where the manoeuvre commence and **2** denotes the trajectory.

The data to be obtained from the accelerating turn test are:

- advance x_{090}
- maximum advance x_{MAX}
- maximum opposite transfer y_{0OPP}
- transfer y_{090}

- tactical diameter y_{0180}
- maximum transfer y_{0MAX}
- time to turn 90° t_{90}
- time to turn 180° t_{180}
- speed at 90° of heading V_{90}
- speed at 180° of heading V_{180}

3.4 Manoeuvring prediction methods

To be able to predict a vessel's manoeuvring behaviour at the design stage is very useful in means of detecting errors and characteristics that need alteration or modification. It is then easy to do changes on the model to get the preferred results. The predictions must be made on the basis of the vessel's main dimensions, line drawings and other relevant information available at the design stage. There are a variety of manoeuvring predictions available, varying in accuracy and cost. There are mainly three basic methods.

- Database method,
- Model test, and
- Mathematical and empirical methods

3.4.1 Database method

The database method uses predictions and experience from existing data [9]. When using the database method, the existing ships must preferably have similar manoeuvring characteristics as that which are intended for the new ship. The manoeuvring performance of the new ship is then predicted without having to do simulations or model tests. The predictions are based on the vessel's main dimensions, line drawings and relevant information available at design stage. Typical ranges for the main parameters of the ships are set so that there is a form of similarity requirement between the investigated ship and the ships in the database. Typical parameters and ranges can be viewed below [13].

$$2,6 < L/B < 7,1, \quad 0,25 < d_{em}/B < 0,46$$

$$0,51 < C_b < 0,65, \quad 0 < \tau' = trim/d_{em} < 1,17$$

3.4.2 Model tests

Predictions made on the basis of model tests are considered to be the most reliable method [9]. However, the lack of full-scale trials and manoeuvring standards has made this prediction method less accurate than other model test areas. All though, more and more full-scale trials are being conducted, and manoeuvring standards for the vessels have been introduced. This will result in a need of more accurate validation of model tests. There are mainly two model test methods used in manoeuvring prediction. The free-running model test, which duplicates the full-scale manoeuvring tests and provide a direct result to the manoeuvring characteristics. The other, a captive model test that measures the forces which are needed to excite the model in a specific manner. The manoeuvring coefficients are provided and used for the prediction of the response.

- **Free-running model**

The same model that is used for resistance and self-propulsion tests can be used when doing a free-running model test. This will reduce the cost, since a separate model for manoeuvring tests won't be needed. The large model is also beneficial regarding scale effects. The free-running test can be conducted in a towing tank, if the tank is wide enough to perform a $10^\circ/10^\circ$ zig-zag manoeuvre. Large ocean basins are also well suited for free-running tests. Manoeuvring tests with a free-running model will always suffer from scale effects [9]. The most common free-running model tests are turning circle, zig-zag manoeuvre and spiral test. The results can be directly compared with the Standards for manoeuvrability. Deriving the manoeuvring coefficients from free-running model tests has recently become more frequent. The coefficients are used in mathematical models predicting the manoeuvring characteristics. Oblique towing and propulsion tests have been combined with parameter identification to provide the coefficients.

- **Captive model**

Captive model tests are performed using oblique towing, rotating-arm facilities and Planar Motion Mechanism (PMM) systems [9].

PMM systems are the most commonly used methods for captive model tests [9]. By combining static or oscillatory modes of drift and yaw, the PMM system can simulate any kind of motion. Captive model tests will also suffer from scale effects. The intention of the motion simulation is to retrieve information on specific parts of the larger complete manoeuvres. The forces measured on the model are used to derive its hydrodynamic coefficients. The hydrodynamic coefficients are then used in mathematical models to predict the manoeuvring characteristics. The PMM system is mainly used in long and narrow towing tanks. The PMM tests conducted at MARINTEK are executed using a multi-purpose carriage with a 6 DOF hexapod motion platform in the towing tank. With a maximum carriage speed of 5 *m/s*, the

hexapod is free to move in all DOF.

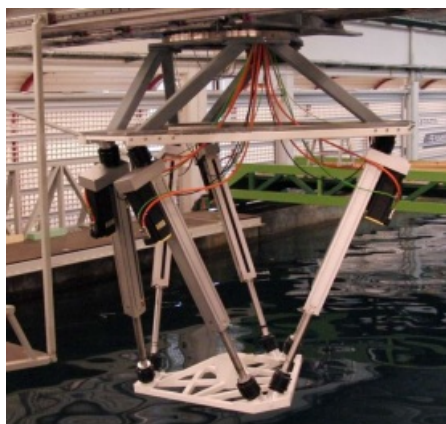


Figure 3.6: MARINTEK's hexapod mounted at the multipurpose carriage [14]

The rotating-arm facility is in principal a basin with an arm in the centre. The model is mounted on the arm, which rotates in circles while varying the diameter for each test. The coefficients related to turning and the combination of turning and drift, are determined as the hydrodynamic coefficients. The results are, as in the PMM test, used in a mathematical model predicting the manoeuvring characteristics.

3.4.3 Mathematical and empirical methods

The dynamics of a manoeuvring ship can be described by numerical simulations. A set of equations are used in prediction at the design stage. This can be helpful in order to obtain a quick prediction of the manoeuvring characteristics at an early stage of design. The hydrodynamic forces used in the equations are found by empirical methods or theoretical methods. Empirical methods are low cost methods that provide quick results.

The empirical methods have a restriction regarding the similarity needed between the vessels that they are based upon.

Often used theoretical methods are slender body theory and viscous flow methods using computational fluid dynamics (CFD). The CFD methods are mainly used with Reynolds averaged Navier Stokes (RANS) calculations [15]. The limitations of using CFD-methods are high computational time and large computer resources, like supercomputers, to achieve better results and calculate larger operations [16]. Sink/source models can be used to represent the flow caused by a ship as a source (sink) distribution along the ship's hull. Velocity vectors are generated and the forces acting from the ship can be calculated. MARINTEK uses such models in

their calculation programs VeRes and WAMIT [17] [18]. The sink/source principle is depicted in Figure 3.7.

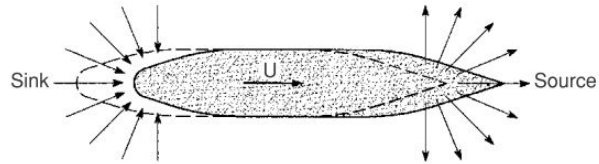


Figure 3.7: Sink/source principle [19]

Chapter 4

Mathematical model

To be able to validate a simulation model, the mathematical model used for describing the forces and motion of the vessel have to be properly documented [10]. An introduction to the elementary ship motions, the reference frame used for ship manoeuvring and a description of the basic 3-DOF model will be addressed. This will be followed by a descriptive overview of the mathematical model used for the simulation tool Vessel Simulator (VeSim).

4.1 Motions and axis system

A ship experiences motion in 6 degrees of freedom (DOF) [20]. The DOF describe the independent displacements and rotations of the ship. The motions in the horizontal plane are referred to as *surge* (longitudinal motion), *sway* (sideways motion) and *yaw* (rotation about the vertical axis) and describes the heading of the ship. The last three DOF are *roll* (rotation about the longitudinal axis), *pitch* (rotation about the transverse axis) and *heave* (vertical motion). See Figure 4.1.

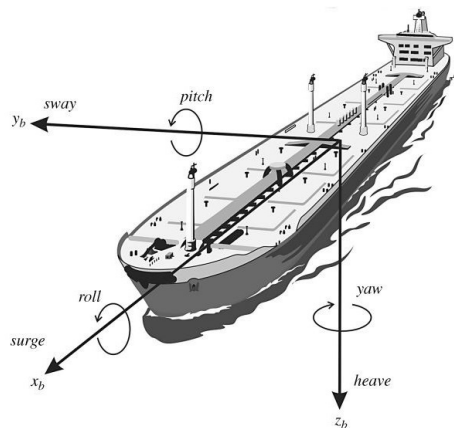


Figure 4.1: Body-fixed axis system used in manoeuvring [20]

For development of mathematical models for ships there exist various approach methods. Manoeuvring theory states that a ship moving in restricted, sheltered water can be described with a linear 3-DOF (*surge*, *sway* and *yaw*) equation based on Newton's second law [20]. Newton's second law is given as $\vec{F} = m\vec{a}$, and states that the alteration of motion is proportional to the motive force impressed; and is made in the direction of the right line in which that the force is impressed [21]. The manoeuvring model is derived for a ship moving with the velocity U in a positive direction, with a zero-frequency wave excitation. This enables the added mass and damping to be represented by the use of hydrodynamic derivatives (constant parameters). The motions are given relative to a body fixed reference frame, see Figure 4.1 for visualization.

Note!: The zero-frequency assumption is only valid for *surge*, *sway* and *yaw*.

This linear approximation is the simplest representation of a manoeuvring model. A non-linear approximation can be derived using an Euler-Lagrangian approach, cross-flow drag, quadratic damping or a Taylor-series expansion. The non-linear approximation uses a 6 DOF model (*surge*, *sway*, *heave*, *roll*, *pitch* and *yaw*) which is a fully coupled equation of motion.

It is desirable to derive the equations of motion for a ship from an arbitrary point, CO. This is to take advantage of the vessel's geometric properties. The hydrodynamic forces and moments are often computed in CO. The point CO is specified by the control engineer and is commonly located on the centerline midships as seen in Figure 4.1.

The forces and moments are listed in Table 4.1 and the nomenclature follows the SNAME and ITTC standard used for manoeuvring problems [15].

Table 4.1: Forces and motion parameters in manoeuvring

DOF	Motion type		Forces and moments	Linear and angular velocities
1	Linear x-axis	Surge	X	u
2	Linear y-axis	Sway	Y	v
3	Linear z-axis	Heave	Z	w
4	Rotation about x-axis	Roll	K	p
5	Rotation about y-axis	Pitch	M	q
6	Rotation about z-axis	Yaw	N	r

For study of the non-linear 6-DOF model, it is referred to [21].

4.2 Linear 3-DOF model

When using the linear 3-DOF model, only the motions in the horizontal plane (*surge*, *sway* and *yaw*) are evaluated in the mathematical equation. The relationship between the forces from the fluid and the motion of the vessel can be derived from Newton's second law and given as:

$$\frac{d}{dt}(M\vec{U}_A) = \vec{F}_1 \quad (4.1)$$

where the hydrodynamic forces and control forces from rudders are included in the force \vec{F}_1 . The absolute velocity in the centre of gravity is given as \vec{U}_A and M is the mass of the body.

The rotational equation of motion can be expressed as:

$$\frac{d}{dt}(I\vec{\omega})_G = \vec{F}_2 \quad (4.2)$$

where the hydrodynamic moments and control moments from rudders are included in the moment \vec{F}_2 . The moment of inertia-matrix is given as I and $\vec{\omega}$ is the rotation. The equation applies to an axis system with origin in the hull's centre of gravity, indicated by the index G .

This gives rise to equations of motions expressed as:

$$\begin{aligned} X &= M\dot{u} \\ Y &= M(\dot{v} + x_G\dot{r} + ur) \\ N &= I_{zz}\dot{r} + Mx_G(\dot{v} + ur) \end{aligned} \quad (4.3)$$

where x_G is the distance between the vessel's centre of gravity and the origin in the axis system. I_{zz} is the moment of inertia about the vertical axis, through the midship point (CO).

When the hydrodynamic hull forces and control forces from the rudder are included, the following linear equations of motions are given:

$$\begin{aligned} (X_{\dot{u}} - M)\dot{u} &= 0 \\ (Y_{\dot{v}} - M)\dot{v} + (Y_{\dot{r}} - Mx_G)\dot{r} + Y_v v + (Y_r - Mu)r + Y_{\delta}\delta &= 0 \\ (N_{\dot{v}} - Mx_G)\dot{v} + (N_{\dot{r}} - I_{zz})\dot{r} + N_v v + (N_r - Mx_G u)r + N_{\delta}\delta &= 0 \end{aligned} \quad (4.4)$$

With this linear equation, no speed loss is predicted. For this reason, the linear equation can only be valid when:

- the vessel has straight line stability
- there is straight line motion at constant speed

The sway and yaw equations (4.4), can be made dimensionless by dividing the expressions by $\frac{1}{2}\rho L_{pp}^2 U^2$ and $\frac{1}{2}\rho L_{pp}^3 U^2$, respectively. The non-dimensional sway and yaw equations are then expressed as:

$$\begin{aligned} (Y'_v - M')\dot{v}' + (Y'_r - M'x'_G)\dot{r}' + Y'_v v' + (Y'_r - M')r' + Y'_\delta \delta &= 0 \\ (N'_v - M'x'_G)\dot{v}' + (N'_r - I'_{zz})\dot{r}' + N'_v v' + (N'_r - M'x'_G)r' + N'_\delta \delta &= 0 \end{aligned} \quad (4.5)$$

where ' denotes that the parameter is dimensionless.

4.2.1 Dynamically stable vessel

By introducing a differential operator $D = \frac{d}{dt}$, the straight line stability of a vessel can be investigated. The accelerations are written as

$$\begin{aligned} \dot{v}' &= Dv' \\ \dot{r}' &= Dr' \end{aligned} \quad (4.6)$$

Equation (4.5) can thereby be re-written as:

$$\begin{aligned} \left((Y'_v - M')D + Y'_v \right) v' + \left((Y'_r - M'x'_G)D + (Y'_r - M') \right) r' + Y'_\delta \delta &= 0 \\ \left((N'_v - M'x'_G)D + N'_v \right) v' + \left((N'_r - I'_{zz})D + (N'_r - M'x'_G) \right) r' + N'_\delta \delta &= 0 \end{aligned} \quad (4.7)$$

the sway velocity term may be eliminated by:

- multiplying the sway equation with $\left((N'_v - M'x'_G)D + N'_v \right)$
- multiplying the yaw equation with $\left((Y'_v - M')D + Y'_v \right)$
- subtracting the resulting sway equation from the yaw equation.

The result is given by

$$(AD^2 + BD + C)r' = (ED + F)\delta, \quad (4.8)$$

where

$$\begin{aligned} A &= (N'_r - I'_{zz})(Y'_v - M') - (Y'_r - M'x'_G)(N'_v - M'x'_G) \\ B &= (N'_r - I'_{zz})Y'_v + (N'_r - M'x'_G)(Y'_v - M') - (Y'_r - M'x'_G)N'_v - \\ &\quad (Y'_r - M')(N'_v - M'x'_G) \\ C &= (N'_r - M'x'_G)Y'_v - (Y'_r - M')N'_v \\ E &= Y'_\delta(N'_v - M'x'_G) - N'_\delta(Y'_v - M') \\ F &= Y'_\delta N'_v - Y'_\delta Y'_v \end{aligned} \quad (4.9)$$

Equation (4.8) is a first order differential equation, where the yaw speed can be written as:

$$r'(t') = r'_H + r'_P = C_1 \exp(D_1 t') + C_2 \exp(D_2 t') + r'_P \quad (4.10)$$

where r'_H is the homogeneous solution and r'_P is the particular solution. Setting the rudder angle to zero, the homogeneous solution r'_H , can be calculated using:

$$\begin{aligned} AD^2 + BD + C &= 0 \\ D_{1,2} &= \frac{-B \pm \sqrt{B^2 - 4AC}}{2A} \end{aligned} \quad (4.11)$$

For a ship with straight line stability the homogeneous solution goes to zero as the time goes to infinity, which is obtained when the exponential coefficients $D_{1,2}$ have real parts. This implies that in order to have straight line stability,

$$C > 0. \quad (4.12)$$

This is satisfied if:

$$\frac{N'_r - M'x'_G}{Y'_r - M'} > \frac{N'_v}{Y'_v} \quad (4.13)$$

4.3 Structure of VeSim

The Vessel Simulator (VeSim) model developed by MARINTEK is a time domain simulation tool. The model combines manoeuvring and seakeeping into one common simulation model [22].

The VeSim simulation model consists of several pre-processors and input variables. HullVisc and VeRes computes the hydrodynamic properties, and the wave loads and motions in the frequency domain, respectively. These are then input to the Vessel Model along with propulsion and wind input. The Vessel Model computes the vessel motions and retardation functions in the time domain along with the manoeuvring forces. The user can then calculate the different calm water manoeuvres. The flow of the total model is graphically presented in the flowchart in Figure 4.2 below.

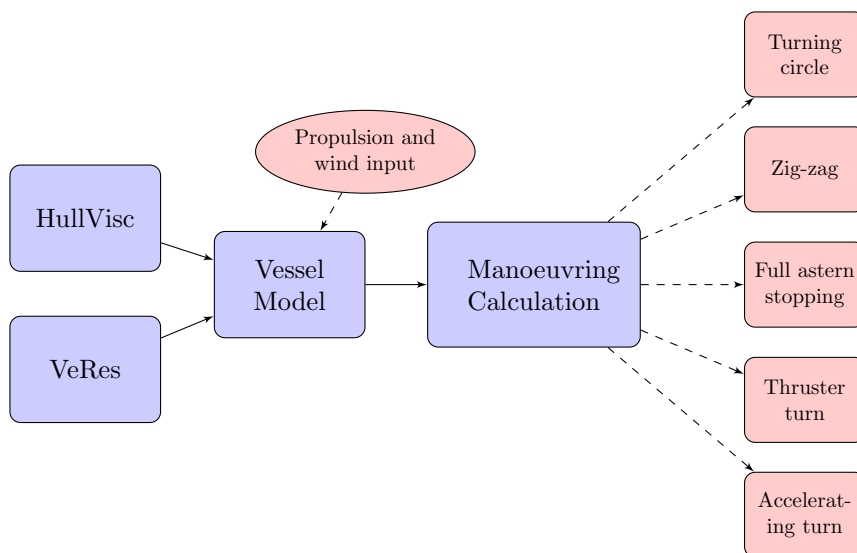


Figure 4.2: Flowchart of VeSim structure

Definition of coordinate systems in VeSim

The simulation model (VeSim) applies in total, three different reference frames [23]. The **NED-frame** and the **body-frame**, which are applied when calculating the ship motions. And the **naval-frame**, which is used for describing the positions on the vessel.

The **north-east-down (NED)** reference frame is defined relative to the Earth's ellipsoid, see Figure 4.3. The x_n -axis is positioned along the northern axis, the

y_n -axis is directed towards the east and to uphold the right-hand rule, the z_n -axis is directed downwards, towards the center of the Earth. The NED-frame is used when the computations of the motions are performed.

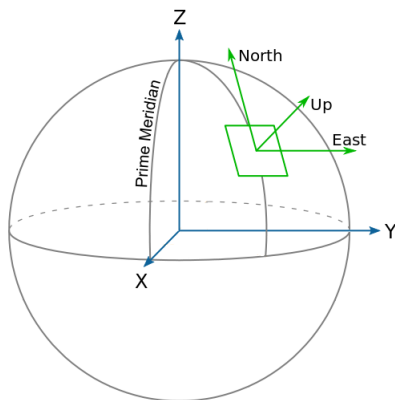


Figure 4.3: NED-frame [24]

The **body-frame** is fixed to the vessel. The origin of this frame is fixed in the center of gravity of the vessel. The x_b -axis is directed towards the bow, the y_b axis is directed towards starboard and to uphold the right-hand rule, the z_b -axis is directed downwards. This is the same reference frame which is depicted in Figure 4.1. The body-frame is used when describing the cross-sectional geometry of the vessel and when calculating the external forces on the vessel.

The **naval-frame** is used to describe positions on the vessel and is commonly used in design and naval architecture, hence the term naval-frame. Unlike the previous reference frames, this frame is a left-handed system. The origin of the frame is located at the intersection between the aft perpendicular (AP), the centerline (CL) and the base line (BL) of the vessel. The x-axis is directed forwards, towards the bow. The y-axis is directed towards starboard and the z-axis is then directed upwards. The naval-frame is used for the graphical interface in ShipX.

4.3.1 HullVisc

The hydrodynamic coefficients have been calculated using ShipX. ShipX is an interface program that allows the user to analyse the ship at an early design stage [25]. ShipX uses amongst others, an additional plug-in for manoeuvring prediction called SIMAN. SIMAN uses a pre-processor called HullVisc to calculate the hydrodynamic coefficients. HullVisc allows the user to predict the hydrodynamic coefficients on the basis of the ship's geometry, which is accessible in the early stages of design.

Strip theory

A combination of slender body and strip theory is used to describe the acceleration dependent forces and moments excited during the calm water manoeuvre. Lighthill's theorem is used to calculate the linear velocity dependent forces and moments with a sectional distribution of the added mass [26]. HullVisc compare results from model tests of approximately 25 different ships, the calculations are modified using expressions based on regression analysis of these models [15].

HullVisc uses an uneven distribution of the hull sections, concentrating the number of sections at the fore part of the ship and in the aft. This is to get a more correct measurement in these parts of the ship, as they include more complicated lines than the mid-section. The hull's cross sections are increased along the ship's length, from bow to the stern. This is to give the hull a more realistic boundary layer. It will also give a correction at the stern for the full body forms when using slender body theory.

The forces derived from Lighthill's theorem are adopted by John Nicholas Newman in "Marine Hydrodynamics" and Odd Magnus Faltinsen in "Hydrodynamics for high speed marine vehicles". These forces are briefly explained in the following [19] [26]. It should be mentioned that Lighthill uses a different notation from what is used in the ITTC/SNAME standard [27].

By evaluating a slender fish moving in the water, Lighthill stated that the force in heave (equivalent to sway, see Figure 4.4) can be described as:

$$f_3^{HD} = -\left(\frac{\partial}{\partial t} + U\frac{\partial}{\partial x}\right)\left[a_{33}\left(\frac{\partial w}{\partial t} + U\frac{\partial w}{\partial x}\right)\right] \quad (4.14)$$

Where a_{33} is the two-dimensional infinite-frequency added mass in heave. But because a ship-fixed coordinate system is used, the term $U\frac{\partial w}{\partial x}$ does not appear [19]. By evaluating equation (4.14) in a manoeuvring aspect, the equation can be expressed as:

$$f_2^{HD} = -\left(\frac{\partial}{\partial t} + U\frac{\partial}{\partial x}\right)[a_{22}(\dot{\eta}_2 + x\dot{\eta}_6)] \quad (4.15)$$

where f_2^{HD} is the two-dimensional horizontal force on the hull. η is the vessel motion in the direction of the subscripts 2 and 6, given as sway and yaw, respectively. $\dot{\eta}$ and $\ddot{\eta}$ represents the velocity and acceleration for the respective motions. a_{22} is the low-frequency two-dimensional added mass in sway.

The total force acting on the body can be obtained by strip-theory and integration over the length of the ship.

The following hydrodynamic sway force is obtained:

$$F_2^{HD} = - \left[\int_L a_{22} dx \ddot{\eta}_2 + \int_L a_{22} x dx \ddot{\eta}_6 + U a_{22}(x_T) \dot{\eta}_2 + U x_T a_{22}(x_T) \dot{\eta}_6 \right] \quad (4.16)$$

Where x_T is the x-coordinate of the transom stern.

Similarly, by multiplying equation (4.16) by the moment arm x , and integrating over the length of the ship, the yaw moment is found.

$$F_6^{HD} = - \left\{ \int_L x a_{22} dx \ddot{\eta}_2 + \int_L a_{22} x^2 dx \ddot{\eta}_6 + U \left\{ \left[x_T a_{22}(x_T) - \int_L a_{22} dx \right] \dot{\eta}_2 + \left[x_T^2 a_{22}(x_T) - \int_L x a_{22} dx \right] \dot{\eta}_6 \right\} \right\} \quad (4.17)$$

Equation (4.16) and (4.17) give the sway force and yaw moment acting on the hull according to the slender body theory. Table 4.2 shows the Hydrodynamic coefficients derived from Lighthill's theorem of a swimming slender fish compared with the standard notation of the manoeuvring forces and the slender-body theory.

Table 4.2: Hydrodynamic forces based on slender body theory

Notation from Newman	Standard Notation	Slender body theory
$\partial F_3/\partial U_3$	Y_v	$-U a_{22}(x_T)$
$\partial F_3/\partial \Omega_2$	$-Y_r$	$-U x_T a_{22}(x_T)$
$\partial F_3/\partial \dot{U}_3$	$Y_{\dot{v}}$	$-\int_L a_{22} dx$
$\partial F_3/\partial \dot{\Omega}_2$	$-Y_{\dot{r}}$	$-\int_L x a_{22} dx$
$\partial M_2/\partial U_3$	$-N_v$	$U \left[\int_L a_{22} dx - x_T a_{22}(x_T) \right]$
$\partial M_2/\partial \Omega_2$	N_r	$U \left[\int_L x a_{22} dx - x_T^2 a_{22}(x_T) \right]$
$\partial M_2/\partial \dot{U}_3$	$-N_{\dot{v}}$	$-\int_L x a_{22} dx$
$\partial M_2/\partial \dot{\Omega}_2$	$N_{\dot{r}}$	$-\int_L x^2 a_{22} dx$

- x_T denotes the added-mass coefficient at the stern
- a_{22} , $x a_{22}$ and $x^2 a_{22}$ is the sway added-mass coefficient, the cross-coupling added-mass between sway and yaw, and the added moment of inertia for yaw acceleration, respectively.
- U , U_3 and Ω_2 is the non-zero velocity components of the ship in forward, sway and yaw motion, respectively.

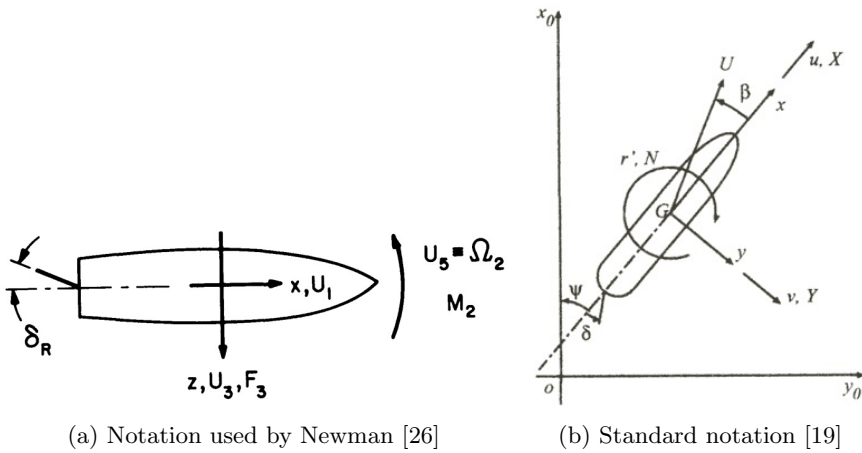


Figure 4.4: The notation used by Newman, a) and standard notation, b)

In Figure 4.4 the notation used by Newman describes x as positive forward, y upward and z to starboard. The velocity components are U_1 , U_3 and Ω_2 which denotes forward, sway and yaw velocity, respectively. F_3 , M_2 and δ_R is defined as the sway force, yaw moment and rudder angle, respectively [26]. As Figure 4.4 illustrates, this differs from the standard notation given by figure b). Here, z is positive downward, x forward and y towards starboard. X and Y is the hydrodynamic force components along the x - and y -axis, and N is the hydrodynamic yaw-moment about the z -axis. u , v , r and δ is the longitudinal, lateral, yaw angular velocity and rudder angle, respectively [19].

For a further understanding and more complete evaluation of the mathematical derivations, it is referred to [19] and [26].

HullVisc Results

The input data specified in SIMAN are shown in Table 4.3

Table 4.3: Input data to SIMAN

Definition	Nomenclature		Units
Draught	T	=3,6	m
Length	Lpp	=90	m
Breadth	B	=16,81	m
Displacement	∇	=2494,634	m^3
Block coefficient	C_B	=0,396	[-]
Weight	Δ	=2557	tons
Speed	V	=19	knots

The resulting hydrodynamic coefficients calculated by HullVisc are tabulated in Table 4.4.

Table 4.4: Hydrodynamic coefficients from HullVisc

Hydrodynamic coefficients for Landegode			
Y'_v	-0,00539 [-]	$Y'_\dot{v}$	-0,00353 [-]
Y'_r	0,00182 [-]	$Y'_\dot{r}$	0,00018 [-]
N'_v	-0,00140 [-]	$N'_\dot{v}$	0,00018 [-]
N'_r	-0,00072 [-]	$N'_\dot{r}$	-0,00026 [-]

Validity of HullVisc

There is reason to question the results given by HullVisc due to the benchmark data used in the regression analysis, as these ships are mainly offshore vessels and of older design. MF Landegode is hence, not in the same category as the benchmark vessels, with different characterisation of the bow and aft design and with a generally more modern hull shape. This may lead to inaccurate values of the coefficients, which consequently may lead to incorrect straight line vessel stability. This will affect some of the manoeuvres, the turning circle being a specific example. The block coefficient calculated by HullVisc is remarkably low and should be treated with care and investigated properly for further studies.

4.3.2 Vessel Response

The Vessel Response (VeRes) processor can be divided into two different main processes [28]. The first and the most important for the intended simulations, is the process which calculates the transfer functions for the vessel motions and loads, given in a frequency domain. It may also perform time simulations. The second process is a post-processor which enables the user to make reports and presentations of the data. Further calculations based on the transfer functions may also be carried out.

Some of the main VeRes calculations that the first process can carry out are listed below [28]:

- Motion transfer functions in 6-DOF
- Relative motion transfer functions
- Motion transfer functions at specified points
- Global wave induced loads given by forces and moments
- Time simulations of motions and loads including important non-linear effects

When calculating ship motions and loads, general assumptions and simplifications are made [19] [20] [29]. Computer programs used to calculate and estimate these forces and motions are configured with such simplifications. The user must be aware of the simplifications used by the program and be able to validate the results by knowing the limitations and restrictions of the computer software. The main assumptions in VeRes are the use of linear, potential and strip theory.

For a more detailed understanding of these assumptions it is referred to [19], [20] and [29].

The main simplifications and assumptions applied in VeRes are listed below [28]:

- The ship is oscillating with the same frequency as the wave encounter frequency.
- Linearity is assumed between the responses and the incident wave amplitude because of linear theory.
- The loads and motions on a vessel in a sea state is derived by use of the superposition principle.
- Potential theory is applied when evaluating sea loads and motions. Potential theory states that the fluid is incompressible, inviscid, homogeneous and irrotational. Empirical formulas are used when accounting for viscous roll damping.
- Slender-body theory is assumed, which states that the length of the ship is much larger than the breadth and draught. ($L \gg B, T$).
- Strip theory is applied in the frequency domain when evaluating hydrodynamic problems. The ship is divided into small two-dimensional cross sectional strips and integrated along the ship length to obtain three-dimensional values.
- The vessel is assumed to be symmetric about its centerline.

Equation of motion

VeRes is primarily based upon linear strip theory. The main assumptions for linear theory are [29]:

- The velocity potential is proportional to the wave amplitude and is valid if the amplitude is small relative to a characteristic wavelength and body dimension.
- The wave steepness is small, i.e. the waves are far from breaking.

In "Sea Loads on Ships and Offshore Structures" by O.M. Faltinsen it is stated that:

By adding together results from regular waves with different amplitudes, wavelengths and propagation directions, it is possible to obtain results of irregular waves.

If the ship is analysed in incident regular sinusoidal waves of small wave steepness, this will be sufficient from a hydrodynamical point of view. Further, if steady state conditions are assumed, i.e. there are no transient effects present due to initial conditions, the linear dynamic motions and loads are harmonically oscillating with the same frequency as the wave loads that excite the ship (the same frequency as the wave encounter frequency). This will allow for computations in the frequency domain.

The encounter frequency, ω , is given from the relation :

$$\omega = \omega_0 + \frac{\omega_0^2 U}{g} \cos\beta \quad (4.18)$$

where ω_0 is the wave frequency, U is the forward velocity of the vessel, β is the angle between the vessel and the wave propagation direction and g is the acceleration of gravity.

If the responses are assumed to be linear and harmonic, the linear coupled differential equation of motion for the six degrees of freedom can be written as:

$$\sum_{k=1}^6 [(M_{jk} + A_{jk})\ddot{\eta}_k + B_{jk}\dot{\eta}_k + C_{jk}\eta_k] = F_j e^{i\omega t}, \quad j = 1, \dots, 6 \quad (4.19)$$

where

- M_{jk} represents the elements of the generalized mass matrix
- A_{jk} represents the elements of the added mass matrix
- B_{jk} represents the elements of the linear damping matrix
- C_{jk} represents the elements of the of the stiffness matrix
- F_j represents the complex amplitudes of the wave exciting forces and moments, with the physical forces and moments given by the real part of $F_j e^{i\omega t}$. F_1, F_2, F_3, F_4, F_5 and F_6 refer to the amplitudes of the surge, sway and heave exciting forces and the amplitudes of the roll, pitch and yaw exciting moments, respectively.
- ω is the angular frequency of encounter
- η_k represents surge, sway, heave, roll, pitch and yaw motion amplitudes, respectively. The dots and double dots denotes time derivatives, and are velocity and acceleration terms, respectively.

The different contributions to the equations of motion are the *mass forces* due to the mass of the vessel, and follows directly from Newton's law. This can be expressed in terms of the motion of the ship, η_k , as

$$F_j = -M_{jk}\ddot{\eta}_k \quad (4.20)$$

where M_{jk} are the components of the generalized mass matrix for the ship.

The *steady-state added-mass and damping forces* are due to forced harmonic rigid body motions when there are no incident waves. The forced motion of the vessel generates outgoing waves and oscillating fluid pressures on the hull surface. By integration of these fluid pressure forces over the wetted body surface of the hull, the resulting forces and moments on the body are obtained. These forces and moments

are proportional to the body acceleration and velocity. The hydrodynamic added mass and damping loads due to the harmonic motion mode, η_k , can be written as

$$F_j = A_{jk}\ddot{\eta}_k - B_{jk}\dot{\eta}_k \quad (4.21)$$

where A_{jk} and B_{jk} are the added mass and damping coefficients, respectively.

The *restoring forces and moments*, which are body geometry and mass distribution dependent, can be written as

$$F_j = -C_{jk}\eta_k \quad (4.22)$$

where C_{jk} are the restoring coefficients.

Figure 4.5 depicts the concept of the added mass, damping, and restoring forces and moments.

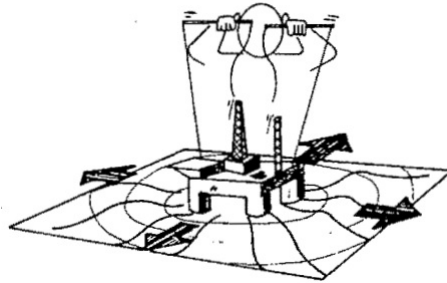


Figure 4.5: Added mass, damping and, restoring forces and moments [29]

The *linearized wave exciting forces and moments* are the loads on the body when the body is restrained from oscillating and there are incident waves present. These forces are divided into Froude-Kriloff and diffraction forces. The Froude-Kriloff force is the force excited on the vessel due to the undisturbed pressure field on the body, which again is induced by the unsteady pressure of the undisturbed waves. The diffraction force is the additional force because of the fact that the body changes this pressure field.

The motion transfer functions are then given by the amplitude η_a , and phase angle θ , and defined as

$$\eta_k(t) = \eta_{ka}\cos(\omega t + \theta_k), k = 1\dots6 \quad (4.23)$$

Figure 4.6 depicts the concept of the linearized wave excitation forces and moments.

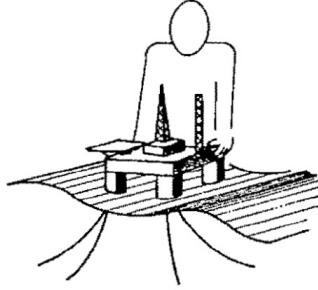


Figure 4.6: Excitation loads [29]

Viscous roll damping

When predicting the roll motions, viscous roll damping from the hull and bilge keels are included. The roll equation of motion is written as

$$\begin{aligned}
 & (M_{42} + A_{42})\ddot{\eta}_2 + B_{42}\dot{\eta}_2 + \\
 & (M_{44} + A_{44})\ddot{\eta}_4 + (B_{44}^P + B_{44}^{V_1})\dot{\eta}_4 + B_{44}^{V_2}|\dot{\eta}_4|\dot{\eta}_4 + C_{44}\eta_4 + \\
 & (M_{46} + A_{46})\ddot{\eta}_6 + B_{46}\dot{\eta}_6 = F_4,
 \end{aligned} \tag{4.24}$$

where the the potential, linear and quadratic viscous damping terms are denoted by the superscripts P, V_1 and V_2 , respectively.

The quadratic viscous damping term makes the equation non-linear and is solved by iteration. The viscous roll damping components taken into consideration by VeRes, are as follows:

- Frictional damping caused by skin friction stresses on the hull
- Eddy damping caused by pressure variation on the naked hull
- Bilge keel damping

For more details on the viscous damping it is referred to [28].

4.3.3 Vessel Model (VeSim)

Hydrodynamic properties of the vessel and the wave induced vessel responses, calculated by respectively HullVisc and VeRes, are pre-processors used to calculate the retardation functions. The retardation functions are calculated in the Vessel Model plug-in for VeSim and are used to solve the vessel's motions in 6 degrees of freedom. The Vessel Model plug-in consists of ship resistance, manoeuvring forces,

added mass, damping and restoring forces, and viscous roll damping. In addition to these pre-processors, input data is given to propulsive units and wind force. The following procedure of calculating the accelerations, velocities, motions, radiation forces and manoeuvring forces as part of the generation of the retardation functions, is a shortened and rendered edition of what presented in the VeSim documentation library [23].

Calculation of accelerations, velocities and motions

The 6 degrees of freedom motion responses can be obtained by assuming that the vessel is moving as a rigid body and neglecting hydroelastic effects. Given a body-fixed reference frame, the equations of motion in the time domain can be given as:

$$(m + A_\infty)\ddot{\eta} + C(\dot{\eta})\dot{\eta} + D_1\dot{\eta} + D_2f(\dot{\eta}) + K\eta + \int_0^t h((t - \tau)\dot{\eta}(\tau))d\tau = q(t, \eta, \dot{\eta}) \quad (4.25)$$

where

- η is the 6 degree of freedom motion vector (surge, sway, heave, roll, pitch and yaw),
- m is the body mass matrix,
- A_∞ is the added mass at infinite frequency,
- C is the coriolis matrix,
- D_1 is the linear damping matrix,
- D_2 is the quadratic damping matrix,
- f is the vector function,
- K is the restoring matrix,
- $h(\tau)$ is the retardation function, and
- q is the excitation forces

The excitation forces on the right hand side of equation (4.25) are be given by

$$q(t, \eta, \dot{\eta}) = q_{wind} + q_{wave}^{(1)} + q_{wave}^{(2)} + q_{prop} + q_{man} + q_{ext} \quad (4.26)$$

where

- q_{wind} is the wind drag force,
- $q_{wave}^{(1)}$ is the first order wave excitation force,
- $q_{wave}^{(2)}$ is the second order wave drift force,
- q_{prop} is the propulsion force,
- q_{man} is the manoeuvring forces, and
- q_{ext} is the remaining forces

To solve for the accelerations, velocities and motions in the time domain, Newton's second law has been applied;

$$M\ddot{\eta} = \sum F_i$$

where \mathbf{M} is the 6 x 6 inertia matrix, $\ddot{\eta}$ is the generalized acceleration vector and F_i is the linearly superimposed forces and moments vector.

By changing the notation, Newton's second law can be written as

$$M\dot{v} = \sum F_i$$

where v is the generalized velocity vector and the dot symbolizes the acceleration derivative.

$$\mathbf{v} = [u, v, w, p, q, r]^T$$

where the linear velocities in surge, sway and heave are given by $(u, v, w) = (\dot{\eta}_1, \dot{\eta}_2, \dot{\eta}_3)$ and the corresponding angular velocities in roll, pitch and yaw are given by $(p, q, r) = (\dot{\eta}_4, \dot{\eta}_5, \dot{\eta}_6)$.

By introducing the same notation for equation (4.25), it can be re-written as

$$(m + A_\infty)\dot{v} = q(t, \eta, v) - \int_0^t h(t - \tau)v(\tau)d\tau - K\eta - D_1v + D_2f(v) + K\eta - C(v)v, \quad (4.27)$$

with the sum of all the forces and moments being equal to

$$\sum F_i = q(t, \eta, v) - \int_0^t h(t - \tau)v(\tau)d\tau - K\eta - D_1v + D_2f(v) + K\eta - C(v)v. \quad (4.28)$$

The accelerations can then be solved by the sum of mass and added mass divided by the sum of forces

$$\dot{v} = (m + A_\infty)^{-1} \sum F_i. \quad (4.29)$$

To obtain the velocities, the accelerations are integrated using an ODE1 Euler method.

Radiation forces

Radiation forces are computed by applying a convolution integral technique on the retardation functions. A convolution integral is a mathematical operation applied on two functions and producing a third function. This third function is a modified version of the original functions, giving the area overlap between the two functions. Convolution has the similar principal as that of cross-correlation.

$$F = \int_0^t h(t - \tau)\dot{\eta}(\tau)d\tau \quad (4.30)$$

By transforming the frequency-dependent added mass and damping, the retardation function can be computed

$$h(\tau) = \frac{1}{2\pi} \int_{-\infty}^{+\infty} [c(\omega) + i\omega a(\omega)]e^{i\omega\tau} d\omega, \quad (4.31)$$

where

$$\begin{aligned} a(\omega) &= A(\omega) - A_\infty \\ c(\omega) &= C(\omega) - C_\infty \end{aligned}$$

and

- $A(\omega)$ is the frequency dependent added mass matrix
- $C(\omega)$ is the frequency dependent potential damping matrix
- C_∞ is the damping matrix at infinite frequency, and
- $C_\infty = 0$

If the assumption of $c(\omega) = c(-\omega)$, $a(\omega) = a(-\omega)$, and $h(\tau) = 0$ for $\tau > 0$ is used, the retardation function can be rewritten as

$$h(\tau) = \frac{2}{\pi} \int_0^{+\infty} c(\omega)\cos \omega\tau d\omega = -\frac{2}{\pi} \int_0^{+\infty} \omega a(\omega)\sin \omega\tau d\omega, \quad \text{for } \tau > 0 \quad (4.32)$$

Manoeuvring forces

When addressing manoeuvring problems, the damping terms in the horizontal motions (surge, sway, yaw) and how they are determined is very important. Friction and fluid viscosity are the main sources of damping. Friction and wave resistance are the main force contributors in the longitudinal (surge) direction. While cross flow separation will be the main force acting in the transverse (sway) direction. When addressing the vessel in its surrounding fluid, the relative velocity between the two can be expressed in terms of

$$u_D^{(i)} = u_w^{(i)}(\theta, x) + u_c^{(i)}(x) - u_v^{(i)}(x), \quad i = 1, 2 \quad (4.33)$$

where

- i $i=1$ for surge motion and $i=2$ for sway motion
- x is the longitudinal point of the vessel
- $u_w^{(i)}$ is the wave particle velocity at the centre of buoyancy (COB) and is assumed constant along the vessel
- $u_c^{(i)}$ is the current velocity
- $u_v^{(i)}$ is the vessel velocity

Longitudinal resistance in surge

The longitudinal polynomial resistance $F_D^{(1)}$ is generated from the resistance curve, which is provided from empirical methods of vessels in calm water.

$$F_D^{(1)} = R_0 + R_1 u_D^{(1)} + R_2 (u_D^{(1)})^2 + R_3 (u_D^{(1)})^3 + \dots \quad (4.34)$$

Cross flow drag forces in sway and yaw

Cross flow drag is a non-linear force, which is described as the drag force that occurs when a flow separates at the opposite side of a structure exposed to an inflowing fluid. The cross flow will generate drag forces in the opposite direction of the inflow direction and a lift force in the perpendicular direction. The cross flow drag force on a strip can be expressed as

$$f_D^{(2)}(\theta, x) = C_D(\theta, x) u_D^{(2)}(\theta, x) |u_D^{(2)}(\theta, x)| \quad (4.35)$$

where

C_D is the cross flow drag coefficient past an infinitely long cylinder. It is computed in terms of empirical formulas

When considering cross flow drag in sway and yaw motions, the longitudinal relative velocity components are assumed to have no effect on the transverse force.

The total cross flow drag in sway and yaw are obtained by integrating the cross flow drag force over the length of the vessel;

$$F_D^{(2)}(\theta) = \frac{1}{2}\rho \int_L c_D(\theta, x)D(x)u_D^{(2)}(\theta, x)|u_D^{(2)}(\theta, x)|dx, \quad (4.36)$$

$$F_D^{(6)}(\theta) = \frac{1}{2}\rho \int_L c_D(\theta, x)D(x)u_D^{(2)}(\theta, x)|u_D^{(2)}(\theta, x)|dx \quad (4.37)$$

where

$$C_D(\theta, x) = \frac{1}{2}\rho c_D(\theta, x)D(x) \quad (4.38)$$

and

- $i = 6$ is the superscript for yaw motion
- ρ is the density of water
- L is the length of the vessel
- $D(x)$ is the sectional draught in the longitudinal direction

Horizontal manoeuvring forces

The numerical manoeuvring model covers the three horizontal motions *surge*, *sway* and *yaw*. The motions are derived as follows [30]:

Surge:

$$\begin{aligned} (m - X_{\dot{u}})\dot{u} = & \\ (m + X_{vr})vr + (mx_g + X_{rr})r^2 + X_{res} + X_{vv}v^2 + & \\ X_{vvv}v^4 + X_{prp} + X_{rud} + X_{thr} + X_{wi} + X_{cu} + X_{wa} + X_{tug} & \end{aligned} \quad (4.39)$$

Sway:

$$\begin{aligned} (m - Y_{\dot{v}})\dot{v} + (mx_g - Y_{\dot{r}})\dot{r} = & \\ -mur + Y_vv + Y_{Uv}Uv + Y_r r + Y_{Ur}Ur - X_{\dot{u}}ur + Y_{cf} + Y_{prp} & \\ + Y_{rud} + Y_{thr} + Y_{wi} + Y_{cu} + Y_{wa} + Y_{tug} & \end{aligned} \quad (4.40)$$

Yaw:

$$\begin{aligned}
 (I_{zz} - N_{\dot{r}})\dot{r} + (mx_g - N_{\dot{v}})\dot{v} = & \\
 - mx_g u r + N_r r + N_{U_r} U r + N_v v + N_{U_v} U v + N_{cf} + N_{prp} + & \quad (4.41) \\
 N_{rud} + N_{thr} + N_{wi} + N_{cu} + N_{wa} + N_{tug} &
 \end{aligned}$$

where

I_{zz}	is the ship mass moment of inertia
m	is the ship mass
N_r	is the linear yaw damping coefficient
$N_{\dot{r}}$	is the added mass moment of inertia coefficient in yaw
N_{U_r}	is the Froude number dependent linear damping coefficient
N_{U_v}	is the Froude number dependent linear damping coefficient
N_v	is the linear yaw damping coefficient due to sway velocity
$N_{\dot{v}}$	is the linear yaw added mass coefficient due to sway acceleration
r	is the yaw velocity
\dot{r}	is the yaw acceleration
u	is the surge velocity
U	is the total ship Speed
\dot{u}	is the surge acceleration
v	is the sway velocity
\dot{v}	is the sway acceleration
x_g	is the distance of centre of gravity from midship
$X_{\dot{u}}$	is the added mass coefficient in surge
X_{res}	is the ship resistance
X_{rr}	is the longitudinal resistance due to yaw velocity
X_{vr}	is the longitudinal resistance due to combined sway and yaw velocity
X_{vv}	is the longitudinal resistance due to sway velocity
X_{vvvv}	is the longitudinal resistance due to sway velocity
Y_r	is the linear sway damping coefficient due to yaw velocity
$Y_{\dot{r}}$	is the linear sway added mass coefficient due to yaw acceleration
Y_{U_r}	is the Froude number dependent linear damping coefficient
Y_{U_v}	is the Froude number dependent linear damping coefficient
Y_v	is the linear sway damping coefficient
$Y_{\dot{v}}$	is the linear sway added mass coefficient

subscripts:

cf	non-linear damping according to cross-flow principle
prp	propeller contribution
rud	rudder contribution
thr	tunnel thruster contribution
wi	wind contribution
cu	current contribution
wa	wave drift contribution
tug	tug contribution

Propeller, rudder, thruster and wind forces

The input data giving the propeller characteristics is based on the work by J. Strøm-Tejsen and R.R. Porter [31]. They developed analytical expressions for the performance of an arbitrary CP propeller as a function of blade-area ratio, blade-pitch setting and any possible combination of propeller and shaft velocity. The Gutsche and Schroeder propeller series used in the experiment covers all of the geometrical and operational parameters except variation in number of propeller blades, which often is different for each ship. For detailed information about the analytical model, it is referred to the paper developed by Stroem-Tejsen and Porter.

The parameters included in the calculation of rudder forces are calculated and are as follows [3]:

- Free stream characteristics of rudders, which contributes to rudder lift and drag
- Effective aspect ratio as function of gap between top of rudder and hull surface, which changes with rudder angle
- Propeller race diameter and race velocity by means of momentum theory
- Flow velocity for the parts of rudder above, in and below propeller race
- Flow velocity over the complete rudder as a weighted average of these velocities

The tunnel thruster forces calculations are mainly based on the nominal propeller thrust [30]. The model can account for up to three tunnel thrusters, in both the aft and bow section. Effects of force increase or decrease taken into account are [30]

- pressure on the hull in the vicinity of thruster opening
- angle in the vertical and horizontal plane of the ship in the vicinity of the thruster
- tunnel length
- number of grids
- flow velocity and direction
- anti suction tunnels

For further information on the tunnel thruster model it is referred to [23] and [30].

The wind forces are calculated with wind force and moment coefficients and are proportional to the wind speed squared. All wind directions relative to the ship are taken into account with 10 deg intervals. The wind model supports both static and dynamic wind spectra [23] [30].

Chapter 5

Full-scale trials

Full-scale sea trials of MF Landegode were carried out in Beiarfjorden outside Bodø, Norway from Thursday 29th of August to Saturday 31st of August 2013. The sea trials were part of the MAROFF project for the promotion of innovation and environmental value creation in the maritime industries [32]. The main focus was the investigation of speed and manoeuvring performance, and obtaining well documented full-scale results of the manoeuvres.

By obtaining well documented full-scale trials, the results can be compared with results from manoeuvring simulations and model tests. Processing the full-scale results and making a comparison between the full-scale results and manoeuvring simulations are further treated.

During the three days in Bodø, different manoeuvre tests were carried out. The tests included

- Zig-zag tests
- Stopping tests
- Spiral tests
- Thruster turning tests with ahead, astern and zero speed
- Low speed manoeuvre tests
- Accelerating turn tests, and
- Turning circle tests followed by pull-out tests

The different manoeuvres investigated are the zig-zag manoeuvres, stopping tests, turning circle manoeuvres and low speed manoeuvres with main focus on thruster turning tests and accelerating turn tests.

In the following, a presentation of the instrumentation and data acquisition, an analysis of the manoeuvring trials and the results from the different manoeuvres will be addressed.

The data of the full-scale trials and Matlab scripts used to process the results along with plots from the trials are provided on an additional storage device.

5.1 Gauges and data acquisition

During the sea trials, MF Landegode was equipped with Kongsberg Seapath 330. This equipment was used to record the data during the sea trials.

5.2 Analysis of trials

The data obtained from the full-scale measurements are post-processed and tuned in Matlab to gather necessary and desirable information on the specific manoeuvres. This section will review the data, location, test conditions and influencing parameters during the full-scale trials. Finally, a review of the post-processed specific manoeuvres and the final results are presented.

Data sets

Data set 1: 29th of August 2013 from 12:22 to 15:15 GMT. The tests carried out this day were Test:1001-1016 containing thruster tests at zero speed and ahead speed, as well as three zig-zag tests (1014, 1015 and 1016), where test 1015 was a failed test.

Data set 2: 30th of August 2013 from 09:47 to 14:45 GMT. The tests carried out this day were Test:3001-3029 containing turning circle tests, spiral tests, zig-zag tests, thruster turning tests at zero speed and accelerating turn tests.

Data set 3: 31st of August 2013 from 09:47 to 14:00 GMT. The tests carried out this day were Test:5001-5021 containing acceleration tests, speed trials, stopping test and thruster turning tests with astern, zero and ahead speed.

Position

Seapath gives the position of MF Landegode in longitude and latitude, both in [m],[km] and [deg], where [m] is the parameter used. Both [m] and [deg] is given as geographic-coordinates. The heading is recorded in [deg]. A figure depicting the position of different manoeuvres is shown in Figure 5.1.






Figure 5.1: MF Landegode's position 30/08/2013. Mark A and B is the position of the port and starboard turning circle, respectively. Mark C and D is the position of the 20/20 and 10/10 zig-zag manoeuvre to port, respectively.

Test conditions

Table 5.1 lists the weather statistics for the three respective days of the sea trials. Non-specific weather observations, i.e. the cloud cover, temperature and wind direction, as well as speed are gathered from the meteorological institute of Norway [33]. The current velocity is calculated using the model described below and the wave height is gathered from the wave buoy used during the trials.

Table 5.1: Test conditions for the respective days

Date:	29/08/2013	30/08/2013	31/08/2013
Cloud cover:	Partly clouded	Clouded-partly clouded	Sunny-partly clouded
Temperature [$^{\circ}C$]:	11,20	11,95	17,22
Wind [m/s, direction]:	9,8 from west-southwest	2,6 from east-southeast	5,0 from east-southeast
	 [247, 5 $^{\circ}$]	 [112, 5 $^{\circ}$]	 [112, 5 $^{\circ}$]
Wave height, H_{m0} [m]:	0,32338	0,4351	0,24144
Current speed [m/s]	0,2521	0,0480	0,1027

To calculate the wind generated current velocity, the following procedure has been used [34].

Note! The calculations in the model is based upon [cm] and not [m].

$$\tau = \rho_{air} k_w W^2 \quad (5.1)$$

where

$$\begin{aligned} \tau &= \text{the wind stress exerted on the water surface by the wind,} \\ \rho_{air} &= \text{the density of air (0,001225[g/cm}^3\text{)]} \\ k_w &= \begin{cases} W < 100 \text{ cm/s} = 1.25/((W/100)^{0.2})0.001 \\ 100 \text{ cm/s} < W < 1500 \text{ cm/s} = ((W/100)^{0.5})(0.001/2) \\ W > 1500 \text{ cm/s} = 0.0026 \end{cases} \\ W &= \text{sustained wind speed in cm/s at 10 m elevation above the water surface} \end{aligned}$$

The model predicts wind generated currents in shallow waters. If the shallow water region is approximated to $10m < depth < 300m$, this model can be applied for the trial area depicted in Figure 5.1, which have depths of approximately 240-300m [35].

A relation between the wind shear stress acting on the water surface and the water shear stress acting on the sea bed can be expressed as follows

$$\tau_{bed} = k\tau_{surface} \quad (5.2)$$

where

$$\begin{aligned} \tau_{bed} &= \text{shear stress exerted on the seabed by the water flow near the seabed} \\ k &\approx 0.2, \text{ and} \\ \tau_{surface} &= \text{shear stress exerted on the water surface by the wind} \end{aligned}$$

If depth-averaged current velocity is assumed the velocity profile can be expressed as

$$v = 2.5u_* \ln\left(\frac{30z}{kD_{50}}\right) \quad (5.3)$$

where

- v = horizontal velocity as a function of the vertical coordinate positive in the direction of the wind shear stress
 u_* = $\sqrt{\frac{\tau_{bed}}{\rho_{water}}}$
 \ln = natural logarithm (log to the base e)
 z = the vertical coordinate with the origin at the seabed
 k = relative seabed roughness (relative to the sediment grain size, D_{50}), and
 D_{50} = median grain size

If equation (5.3) is integrated over the water depth, y_0 , the equation can be written

$$\begin{aligned}
 V &= 2.5u_* \ln\left(\frac{11y_0}{kD_{50}}\right) \\
 &= 2.5\sqrt{\frac{\tau_{bed}}{\rho_{water}}} \ln\left(\frac{11y_0}{kD_{50}}\right)
 \end{aligned}
 \tag{5.4}$$

where

- V = depth averaged velocity, and
 y_0 = water depth
 ρ_{water} = the density of water ($1,0[g/cm^3]$)

By substituting the expression for shear stress exerted on the sea bed in equation (5.2) into equation (5.4), the equation can be expressed as

$$V = 2.5\sqrt{\frac{0.2\tau_{surface}}{\rho_{water}}} \ln\left(\frac{11y_0}{kD_{50}}\right).
 \tag{5.5}$$

A median grain size is assumed to be $D_{50} \approx 1 \text{ mm}$ [36].

Error sources

As Table 5.1 suggest, the trial conditions were more or less stable. No extreme weather changes was experienced and the different manoeuvring tests had more or less the same point of reference in conjunction to the weather. The different results gathered from the same manoeuvre, e.g. a turning circle, proposes a valid basis for repeatability. There was knowledge of little current in the trial area, as the calculations suggests. The affect of present current is taken into account when analysing the turning circle manoeuvre. The effect was found be present, but of small significance. Other interfering sources may be

- The measuring gauge, e.g. the calibrations, frequency of data acquisition,
- The time of command given to execute ship manoeuvres,
- Play (offset) in the rudder or steering mechanism,
- Effective water velocity at the rudder,
- Effect of shallow waters,
- The effect of draft and trim conditions,
- Actual propeller and engine efficiency,
- Initial approach speed

5.3 Turning circle manoeuvre

Turning circles were performed on Friday the 30th of August. Both port and starboard turning circles were 360° circles with a 35° rudder angle. The trials were conducted with maximum continuous revolutions (MCR) at 85%.

5.3.1 Post-processing

The data recovered from the trial manoeuvre was post-processed in Matlab. The Matlab scripts are provided on an additional storage device. The parameters that have been evaluated are the north and east position [m], the vessel velocity [m/s] and the rudder angle [deg].

When evaluating the turning circle, the initial plot has been altered to give a more representable plot than originally. First, the approach trajectory was rotated so that the vessel's approach course was set along the x-axis. The rotation was performed utilizing a transformation matrix which rotates the trajectory by an angle θ , counter-clockwise about the origin, expressed as;

$$\begin{bmatrix} x' \\ y' \end{bmatrix} = \begin{bmatrix} \cos\theta & -\sin\theta \\ \sin\theta & \cos\theta \end{bmatrix} \begin{bmatrix} x \\ y \end{bmatrix}$$

where x and y are the original positions and x' and y' are the rotated coordinates. Figure 5.2 and 5.3 depicts the original and rotated trajectory for both the port and starboard turning circle.

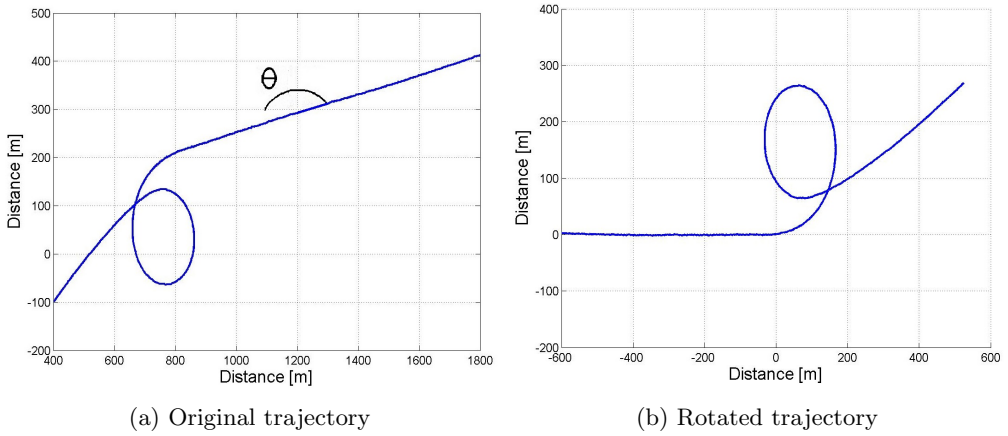


Figure 5.2: Port turning circle trajectory before and after rotation

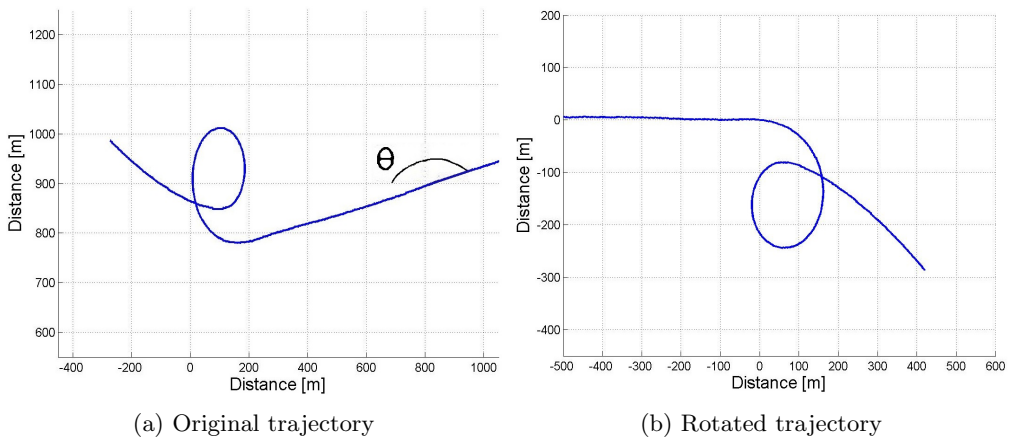


Figure 5.3: Starboard turning circle trajectory before and after rotation

Environmental conditions have an affect on the manoeuvrability and resistance of the vessel. It is therefore preferable for the vessel to conduct the full-scale trials in calm and stable weather conditions. The turning circle manoeuvres were carried out Friday 30th of August when the wind was at its lowest of the three days and the wave height was at its highest, at 0,4351m as listed in Table 5.1. To account for the effect of current, IMO's prediction guidance has provided an empirical model to correct for these influences [9]. Because the correction model demands a turning test of 720°, (which is not carried out for MF Landegode), some of the early steps in determining the current velocity has been disregarded. The current velocity was alternatively calculated, using equation (5.5).

The trajectory is corrected with the relation

$$\begin{aligned}\vec{x}'(t) &= \vec{x}(t) - \vec{v}_{cx}t \\ \vec{y}'(t) &= \vec{y}(t) - \vec{v}_{cy}t\end{aligned}\tag{5.6}$$

where $\vec{x}(t)$ and $\vec{y}(t)$ are measured x- and y-position vectors, $\vec{x}'(t)$ and $\vec{y}'(t)$ are the corrected position vectors, \vec{v}_{cx} and \vec{v}_{cy} are the current velocity in x and y direction, respectively, and t is the time in seconds. A corrected trajectory is shown in Figure 5.4. It should be mentioned that the correction of influencing current has been performed before turning the plot as illustrated in Figure 5.2 and 5.3. Hence, Figure 5.4 will present a misleading illustration of the current direction, given the direction of the wind, with regard to the corrected trajectory. Figure 5.4 is used to give a more visually representable plot. Figure 5.5 however, illustrates the initial corrected trajectory prior to the transformation.

Transfer and advance is measured at the point where the vessel has changed the heading by 90° , after the rudder execute. Tactical diameter is measured at a 180° change of heading. A plot of the turning circle with marked advance, tactical diameter and transfer is presented in Figure 5.4.

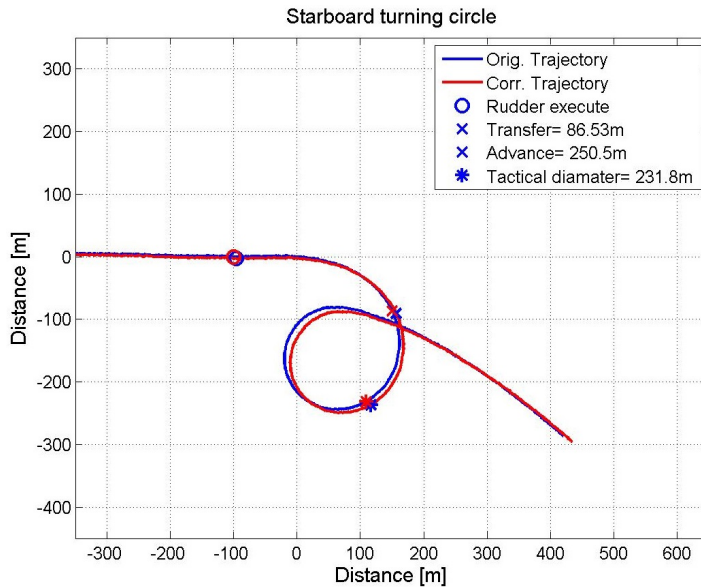


Figure 5.4: Starboard turning circle with original [blue] and corrected trajectory [red]

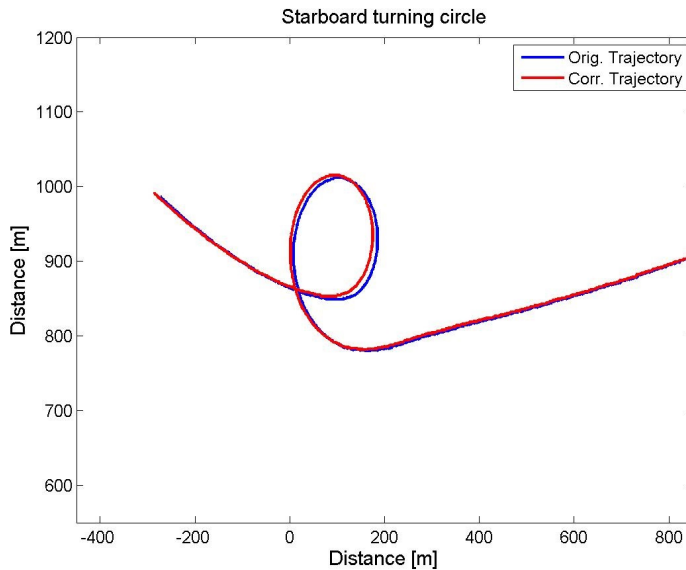


Figure 5.5: Starboard turning circle with corrected trajectory before rotation

5.3.2 Results

Both the port (run 3006) and the starboard (run 3005) turning circles have been processed, and the results are further presented. The manoeuvres should ideally be identical under similar conditions. As Table 5.2 and 5.3 presents, this is not the case. Both the tactical diameter and the advance is larger in the port manoeuvre. Different sources influencing the manoeuvre can be the reason for the deviation. The fact that the two tests were conducted in the same direction, given the effect of wind, current and waves, a boost and a braking force can occur for either of the trials. I.e. the port manoeuvre can experience a braking force in the diameter and the starboard manoeuvre can experience a boost effect, resulting in a smaller and bigger diameter, respectively. This can be observed from the corrected results of the two tests in Table 5.2 and 5.3, respectively. There is about 4% difference between the two trials which indicates that there is agreement between the two. But the fact that the port manoeuvre, turning into the wind, has a larger turning diameter than the starboard manoeuvre, turning with the wind, indicates that there is an influencing error source as the results are contradictory to what would appear to be the obvious outcome. To give a more qualified judgement of the precision-error of the full-scale trials, more turning circle manoeuvres should be conducted.

When the turning circle manoeuvre is performed, the propeller pitch and RPM are continuously changed to preserve and minimize engine strain throughout the manoeuvre.

Plots of the different turning circles are given in Appendix C.1.

Table 5.2: Full-scale port turning circle results

		Run 3006	Run 3006 corrected	IMO
Tactical diameter	[m]	254	251,8	450
Transfer	[m]	96,2	95,2	-
Advance	[m]	255,2	256,7	405
Rudder angle	[°]	34	34	-
Approach speed	[kn]	17,82	17,82	-
Final speed	[kn]	7,74	7,74	-

Table 5.3: Full-scale starboard turning circle results

		Run 3005	Run 3005 corrected	IMO
Tactical diameter	[m]	231,8	233,8	450
Transfer	[m]	86,5	87,5	-
Advance	[m]	250,5	252,0	405
Rudder angle	[°]	34	34	-
Approach speed	[kn]	17,7	17,7	-
Final speed	[kn]	6,5	6,5	-

5.4 Zig-zag manoeuvre

The zig-zag trials were performed on Thursday 29th of August and on Friday 30th of August. The tests performed on Thursday were test no. 1014 and 1015, a 10/10 and 20/20 test, respectively, and both to starboard. The 20/20 zig-zag manoeuvre became a 20/13 zig-zag manoeuvre due to wrong orders on the bridge. As one of the manoeuvres on Thursday was wrong and the fact that the tests were carried out on two different days, only the trials performed on Friday will be evaluated.

Run 3008 and 3009 gives the starboard zig-zag manoeuvre for the 10/10 and 20/20 test, respectively. Run 3007 and 3012 gives the port 10/10 and 20/20 zig-zag manoeuvre tests, respectively.

There has been no correction of influencing environmental conditions when evaluating the results of the zig-zag manoeuvres. The manoeuvre is too complicated to mathematically account for weather conditions and no straight forward correction method can be applied. For complicated manoeuvres such as the zig-zag manoeuvre, simulation techniques are used [10].

At the application of the counter rudder, the ship's continuous turn in the initial direction is measured as the overshoot angle. The first and second overshoot angle is measured as the maximum heading angle reached after the second and third rudder execute, respectively. The time from 1st and 2nd counter rudder to 1st and 2nd overshoot angle is measured correspondingly.

5.4.1 Results

Table 5.4: Full-scale zig-zag results

		Starboard		Port		IMO	
		10/10	20/20	10/10	20/20	10/10	20/20
Approach speed	[kn]	19,0	18,8	19,1	19,1	-	-
Time from 1st counter rudder to 1st overshoot angle	[s]	9,6	10,1	9,6	10,0	-	-
Time from 2nd counter rudder to 2nd overshoot angle	[s]	8,8	8,8	9,1	9,0	-	-
1st overshoot angle	[°]	7,5	15,1	7,2	14,4	10,0	25,0
2nd overshoot angle	[°]	5,9	8,4	8,2	10,1	25,0	-

From Table 5.4, showing the 10/10 and 20/20 zig-zag manoeuvre for both starboard and port, a compliance between the starboard and port tests can be observed. The largest deviation is in the 2nd overshoot angle, between the 10/10 starboard and port manoeuvre, where the difference is about 28%. A difference of about 17% can be observed in the 20/20 manoeuvre. The rest of the results has a difference of less than 5%. Given that the tests are carried out in different conditions, e.i. the conditions will not be of 100% similarity, the compliance between the tests are good. From the IMO criteria, it is clear that the vessel is well within the requirements.

Plots of the different zig-zag manoeuvres are presented in Appendix C.2.

5.5 Stopping test

The stopping test was performed on Saturday 31st of August. Run 5020 is the only stopping test performed, and it was not executed as specified in IMO MSC/Circ.1053 [9]. The IMO requirements states that the ship must be at full ahead speed when the full astern command is given. This can cause great strain on the engine and conducting several tests were hence avoided with this vessel. The vessel is therefore not travelling at full speed during the test. The measured approach speed

of the vessel was recorded as approximately 9,2 knots, whereas the top speed of the vessel is stated as approximately 22 knots, see Appendix A. This manoeuvre is therefore not evaluated as a standard IMO test and will not be compared with the associated requirements of the manoeuvre. When performing the manoeuvre, the speed of the vessel is reduced by reversing the pitch of the propeller instead of setting the machinery in reverse. This will, in addition to tuning the RPM of the engine and the thrust, reduce engine strain.

5.5.1 Results

Table 5.5: Full-scale stopping test results

		Run 5020
Track length	[m]	183,72
Ship length	[-]	2,0

From Table 5.5 the full-scale trial results are presented. Figure 5.6 depicts the trajectory of the vessel and Figure 5.7 depicts the speed and propeller pitch of the vessel as figure a) and b), respectively.

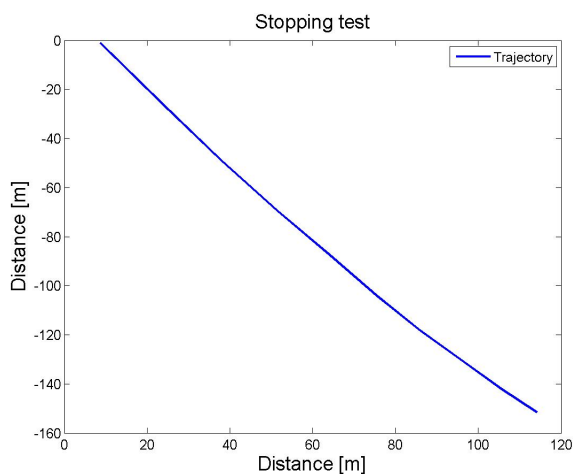


Figure 5.6: Full-scale stopping test trajectory

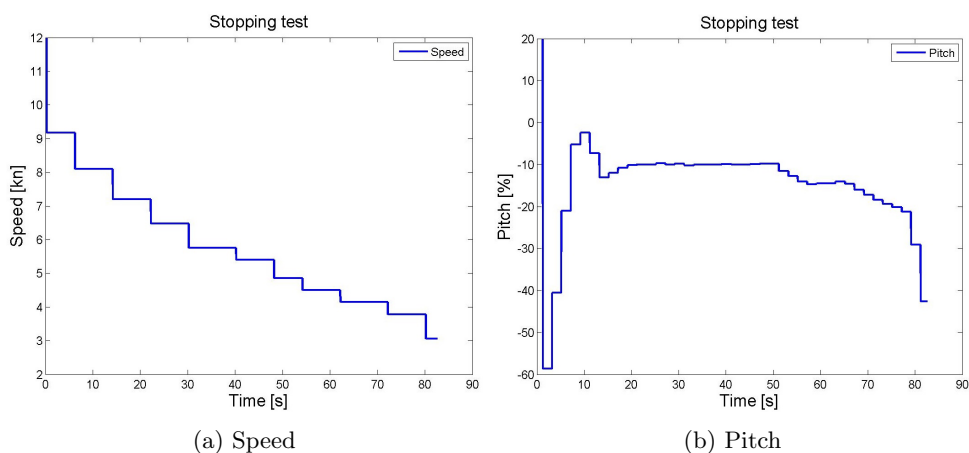


Figure 5.7: Full-scale stopping test speed and propeller pitch

5.6 Thruster turning manoeuvre

The thruster turning manoeuvres were performed on Thursday 29th, Friday 30th and Saturday 31st of August. All combinations of thruster 1, 2 and 3 have been performed at zero, forward and astern speed. Only the combination of all three thrusters at zero speed will be evaluated in this section, as this manoeuvre is most likely to be used in the quay area and is thus of highest interest.

Run 1005 was conducted with bow thrusters (numbered 1 and 2) set at 100% MCR towards starboard and the stern thruster (numbered 3) set at 100% MCR towards port.

The data to be recovered from the test are as described in Section 3.3.1.

5.6.1 Results

Figure 5.8 shows the result from the thruster turning test as heading versus time. The manoeuvre execute is given by the red circle and the different time values for heading reaches of 15, 30, 60, return to 60, return to 30 and return to 0 degrees are given by the red triangles. Table 5.6 lists the measured time and heading angle results depicted in Figure 5.8.

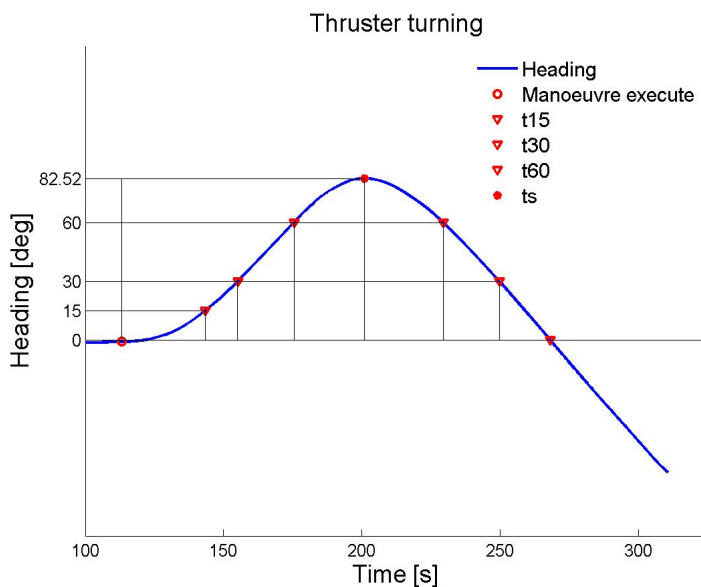


Figure 5.8: Vessel heading from the full-scale thruster turning manoeuvre

Table 5.6: Full-scale thruster turning results

		Run 1005
t_{15}	[s]	30.3
t_{30}	[s]	42
t_{60}	[s]	62.4
t_s	[s]	87.9
t_{60R}	[s]	116.4
t_{30R}	[s]	136.6
t_{0R}	[s]	154.9
Δt_s	[s]	25.5
ψ_s	[deg]	82.52
$\Delta\psi_s$	[deg]	22.52

5.7 Accelerating turn manoeuvre

Accelerating turn tests were performed on Friday 30th of August. Combinations in use of thrusters, engine power and rudder angle were conducted. The manoeuvre analysed, run 3020, was conducted with all three thrusters operating at 100% MCR, with thruster 1 and 2 (bow thrusters) set towards starboard, and thruster 3

(stern thruster) set towards port. The engine was set at 75% MCR and the rudder was set hard over at 65° , initiating a starboard turn. The propulsion plant settings at the start of the manoeuvre were not altered throughout the test.

The data to be recovered from the test are as described in Section 3.3.1.

5.7.1 Results

Figure 5.9 presents the trajectory and the heading reach as figure a) and b), respectively. In Figure a), showing the trajectory of the test, the manoeuvre execute is given by the red circle, while the red triangle and star gives the reach of 90° and 180° heading change, respectively. Table 5.7 presents the results of the manoeuvre.

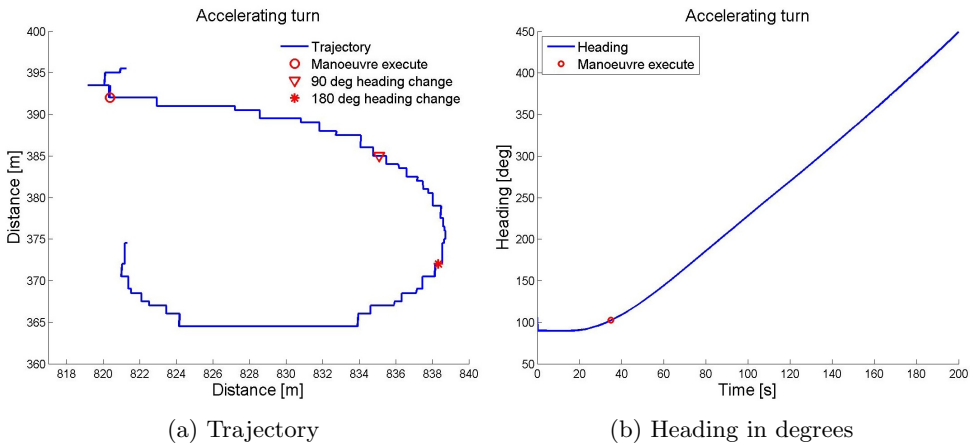


Figure 5.9: Full-scale accelerating turn trajectory and heading in degrees

Table 5.7: Full-scale accelerating turn results

		Run 3020
Advance	[m]	14.72
Transfer	[m]	7.0
Tactical diameter	[m]	20.0
Time to turn 90°	[s]	48.27
Time to turn 180°	[s]	91.23
Speed at 90° change of heading	[kn]	0.66
Speed at 180° change of heading	[kn]	0.63

Chapter 6

Simulations in VeSim

The simulation of the manoeuvres are conducted in VeSim. VeSim uses two different input plug-ins and requires additional information on propulsive units and environment. The plug-in tools are HullVisc and VeRes, which calculates the hydrodynamic properties, as well as the transfer functions for the vessel motions and loads in the frequency domain, respectively. For an overview of the structure of VeSim see Figure 4.2.

The hydrodynamic coefficients calculated by HullVisc can be of questionable validity. This is because of the method used by HullVisc for calculations is a regression analysis of benchmarking vessels. The benchmark vessels are of older design and not in the same category as MF Landegode.

The simulated manoeuvres should ideally have the same environmental conditions as the full-scale trials. As the simulated manoeuvres are carried out using the "Calm water manoeuvring" option of the Vessel Simulator, there will not be a 100% similarity between the simulated and the full-scale manoeuvres. This is because the wind, current and wave forces are excluded in this model. A certain grade of deviation is therefore to be expected.

The simulated manoeuvres are the *turning circle manoeuvre*, the *zig-zag manoeuvre*, an altered version of the *full astern stopping manoeuvre*, the *thruster turning manoeuvre (thruster twist manoeuvre)* and the *accelerating turn manoeuvre*. Figure 6.1 presents a list over the different calm water manoeuvres executable in VeSim.

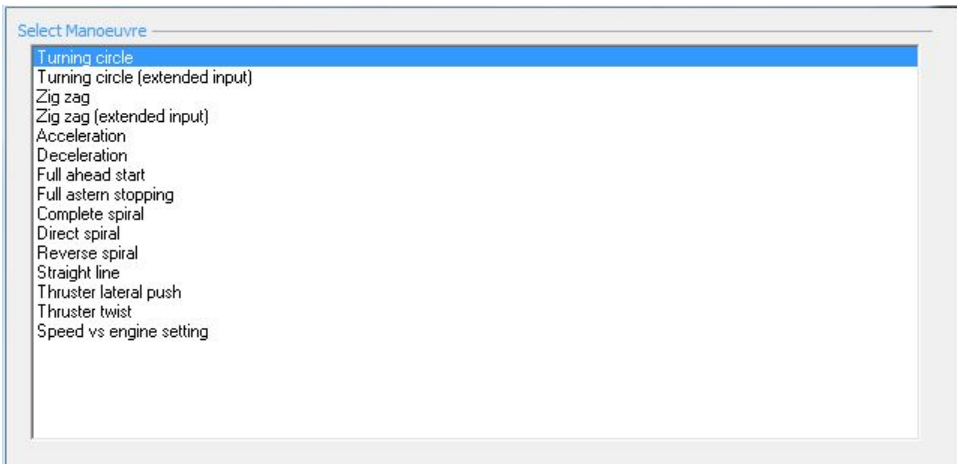


Figure 6.1: List of available manoeuvres in the calm water simulation model

The main parameters needed for the propulsion input are:

- Propeller x, y and z position
- Propeller diameter, pitch and blade area
- Rudder height, root chord and total area
- Wake fraction and thrust deduction
- Engine-propeller gear ratio and mechanical efficiency
- Engine MCR, RPM and moment of inertia

The vessel geometry used for the simulations is an adopted model developed by MARINTEK [37]. The vessel lines and principal characteristics are pre-defined in this geometry model. The loading condition for the designed waterline is set to $T = 4,20m$, where T is the vessel's draught. Additionally, the operational condition, with a midship draught of $T_m = 3,60m$ and a trim in the fore part of $+0.752m$ resulting in a fore part draught of $T_{FP} = 2,848m$ and an aft part draught of $T_{AP} = 4,352m$, is pre-defined. The bow thrusters and the aft thruster are only taken into account when the thruster turning (thruster twist) and the accelerating turn manoeuvre are simulated.

Every manoeuvre is simulated with the operational draught and trim described above.

6.1 Results from VeSim

The following sections present the results obtained from the simulations and present them in form of tables and a brief discussion. The tables will give a comparison of the simulated manoeuvres with the IMO requirements as in the full-scale trials. As the vessel geometry model is symmetric about the centreline, it was expected the results would be identical to port and starboard, this was however not the case. The different tables will list results of both starboard and port manoeuvres.

6.1.1 Turning circle manoeuvre

When simulating the turning circle, the user must set the desired initial vessel speed, maximum heading (i.e. the heading when the test is accomplished), the rudder angle to be used, if the manoeuvre is to starboard or port, and whether or not to include a pullout test and its duration.

When evaluating the results of the simulated turning circle manoeuvre, one should have in mind that the simulation is conducted without changing the pitch and RPM of the propeller, which was the case for the full-scale manoeuvre. Some differences between the full-scale and simulated manoeuvres are hence expected.

The results of the simulation is shown in the table below.

Table 6.1: Simulated turning circle results

	Port	Starboard	IMO
Tactical diameter [m]	246	251	450
Transfer [m]	126	128	-
Advance [m]	315	318	405
Rudder angle [°]	35	-35	-
Approach speed [kn]	17,6	17,6	-
Final speed [kn]	3,5	3,6	-

From Table 6.1 showing the the simulated turning circle manoeuvre, the results are well within the IMO requirements [9]. Regarding the simulated results, they appear to be of genuine validity with some discrepancy from the full-scale results in Table 5.2. But if the trajectory plot of the simulated manoeuvre is interpreted, one can clearly observe the inequality between the full-scale and simulated manoeuvre. This also confirms the inadequate quality of the coefficients calculated by HullVisc. The simulated trajectory plot is shown in Appendix D.1.

6.1.2 Zig-zag manoeuvre

The parameter input needed in the zig-zag manoeuvre are the initial vessel speed, the commanded rudder angle, the heading change achieved before rudder change and the number of overshoot angles to be calculated.

The result of the simulations are shown in the following Table 6.2.

Table 6.2: Simulated 10/10 and 20/20 zig-zag results

		Port		Starboard		IMO	
		10/10	20/20	10/10	20/20	10/10	20/20
Approach speed	[kn]	17,5	17,6	17,6	17,6	-	-
Time from 1st counter rudder to 1st overshoot angle	[s]	7,5	12,5	7,3	12,5	-	-
Time from 2nd counter rudder to 2nd overshoot angle	[s]	7,2	12,4	7,3	12,4	-	-
1st overshoot angle	[°]	3,6	11,1	3,5	10,8	10,0	25,0
2nd overshoot angle	[°]	3,6	11,2	3,8	11,5	25,0	-

Table 6.2 giving the result of the zig-zag manoeuvre indicates that the simulated manoeuvre is of desirable validity and well within the IMO requirements for both the 10/10 and the 20/20 manoeuvre. The main results and plots of the simulation is presented in Appendix D.2

6.1.3 Stopping test

When simulating the stopping manoeuvre, named "Full astern stopping" in VeSim, the user needs to determine the initial vessel speed and the commanded engine setting astern. The simulator does not give the user the possibility of altering the pitch of the propeller instead of reversing the engine. When evaluating this manoeuvre and comparing to the full-scale test, one need to bear in mind the different approach methods used for this manoeuvre, i.e. the use of reverse engine and propeller pitch. With this in mind, the results of the simulation are shown in the following Table 6.3.

Table 6.3: Simulated stopping test results

	VeSim simulation
Track length [m]	214
Ship length [-]	2,4

Table 6.3 lists the result of the simulated stopping manoeuvre. The results are not compared with the IMO requirements as the manoeuvre is not performed with a maximum approach speed as described in the IMO MSC/Circ.1053 , but with an approach speed of 9,2 knots, as in the full-scale manoeuvre [9]. The main results and plots of the simulation are presented in Appendix D.3

6.1.4 Thruster turning manoeuvre

The thruster turning manoeuvre, as described in the "International Standard ISO 13643-2", is not a standard manoeuvre in the list of executable manoeuvres in VeSim. However, a similar manoeuvre called "Thruster twist" is available, but this manoeuvre will only rotate the vessel about its own axis in a continuously directional motion by use of thrusters, until the end of the time sequence is reached.

To simulate the thruster turning manoeuvre, the manoeuvre must be manually commanded in the time domain simulator. By doing so, the thrusters are commanded to 100% by the command "Tunnel_Thruster1_Actuator cmd_revs 100.0" in the scenario manager tab, as illustrated in Figure 6.2. The time of the thruster executions are found by evaluating the yaw angle [deg] from the thruster twist manoeuvre. The time needed to reach a 60° heading change is logged from the thruster twist and used in the time domain simulation to give the command to reverse the thrusters. By plotting the yaw angle versus time, the time needed for reaching a heading of 15, 30, 60, maximum, return to 60, return to 30 and return to 0 degrees can be obtained, including the overshoot angle and time.

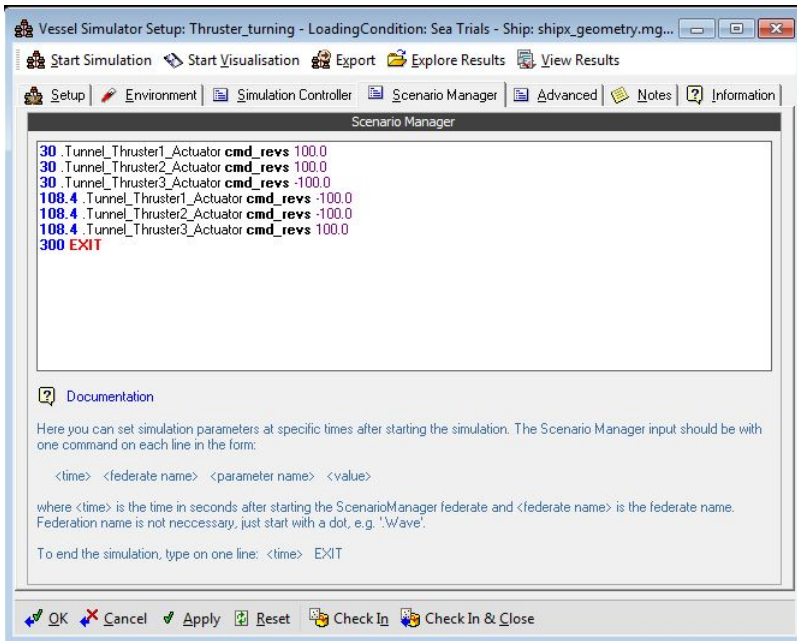


Figure 6.2: Scenario manager in the time domain simulator

Table 6.4 lists the results obtained from the manual time domain simulation. Figure 6.3 depicts the heading of the vessel and the time steps corresponding to Table 6.4. The time of manoeuvre execute in Figure 6.3 is at $t=30$ sec.

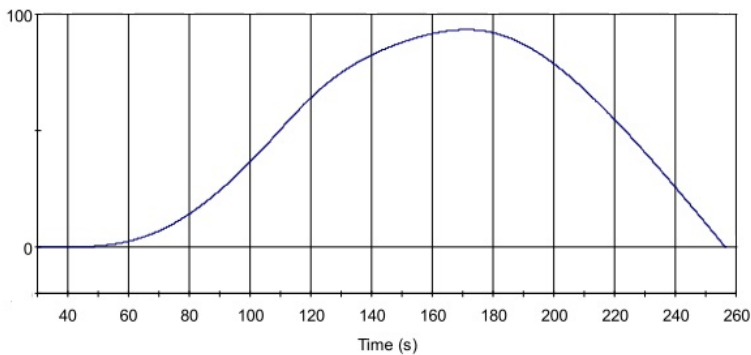


Figure 6.3: Vessel heading (yaw-angle) from the simulated thruster turning manoeuvre

Table 6.4: Simulated thruster turning results

	VeSim simulation
t_{15} [s]	50.8
t_{30} [s]	64.7
t_{60} [s]	86.8
t_s [s]	141.2
t_{60R} [s]	186.0
t_{30R} [s]	207.2
t_{0R} [s]	226.5
Δt_s [s]	54.4
ψ_s [deg]	93.2
$\Delta\psi_s$ [deg]	33.2

The main results and plots of the simulated manoeuvre is presented in Appendix D.4.

6.1.5 Accelerating turn manoeuvre

The accelerating turn manoeuvre is also not a basic manoeuvre from the selected list of executable manoeuvres. But the "Turning circle (extended input)" manoeuvre allows the user to provide input for multiple parameters that is not included in the basic turning circle manoeuvre input. E.i. the use of thruster power. The advance, transfer and tactical diameter are given by the standard output in the ShipX plot, but the speed at-, and the time to turn 90° and 180° are found by manually plotting the yaw angle [deg] and speed [m/s] versus time, and further extracting the corresponding values.

The results of the accelerating turn manoeuvre is listed in Table 6.5 below.

Table 6.5: Simulated accelerating turn results

	VeSim simulation
Advance [m]	23
Transfer [m]	7.0
Tactical diameter [m]	28
Time to turn 90° [s]	65.9
Time to turn 180° [s]	110.7
Speed at 90° change of heading [kn]	1.07
Speed at 180° change of heading [kn]	2.74

The main results and plots of the simulated manoeuvre is presented in Appendix D.5.

6.2 Comparison of simulated and full-scale results

Here, a comparison of the simulated and full-scale manoeuvring trials will be presented as a set of different graphs, most with a best fit trend line. Different combinations of colour and markers are used to indicate the different characteristic measurements of the manoeuvre currently analysed. These marker and colour combinations are listed in the corresponding table for each manoeuvre. The different graphs are a graphical presentation of the full-scale and simulated results.

From the different graphs a clear observation can be made on whether the simulations are over- or underestimated. As the graphs indicate, most of the simulated results are overestimated. This can be a result of the underestimated hydrodynamic coefficients calculated by HullVisc. Other error sources in predicting the manoeuvres may be from the mathematical model used in VeSim and VeRes, as viscous effect, cross flow drag, propeller, rudder and thruster forces.

6.2.1 Turning circle manoeuvre

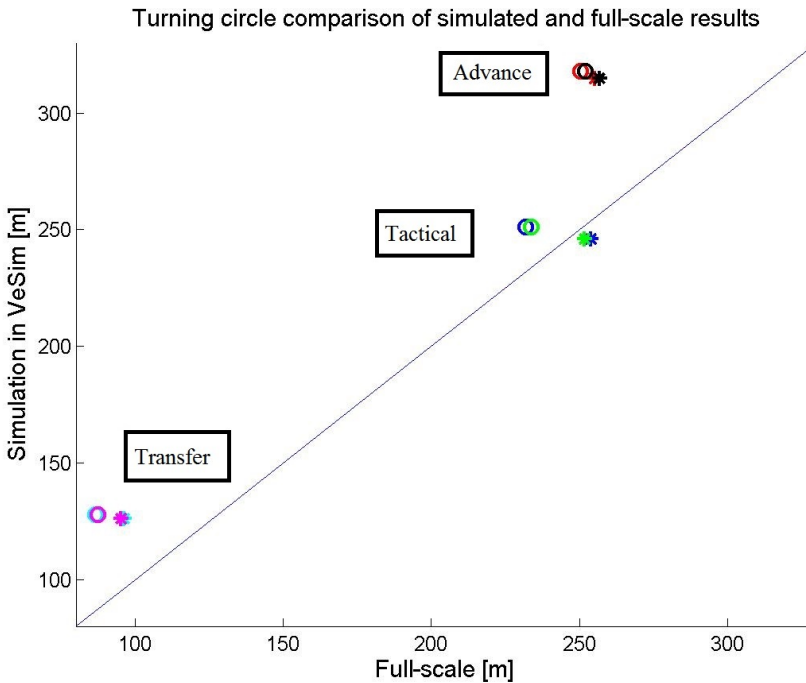


Figure 6.4: Comparison of full-scale and simulated turning circle results

Table 6.6: Markers for comparison of simulated and full-scale turning circle results

	Original			Corrected		
	Advance	Transfer	Tactical	Advance	Transfer	Tactical
Port	Red *	Cyan *	Blue *	Black *	Magenta *	Green *
Starboard	Red o	Cyan o	Blue o	Black o	Magenta o	Green o

Figure 6.4 depicts the simulated and full-scale turning circle manoeuvre. Both the original full-scale results and the current corrected results are plotted in the figure. The linear blue line indicates the best fit trend line where the results from simulations and full-scale would be similar. Table 6.6 explains the different marker and colour combinations used in Figure 6.4, where "original" and "corrected" refers to the current correction.

From Figure 6.4 it can be observed a clear tendency of overestimation of the simulated manoeuvres. Only the port tactical diameter is underestimated, but however fairly close to the full-scale trial result. As is the starboard tactical diameter, both presented as listed in Table 6.6. The Advance and transfer is overestimated in a large extent as they are not very close to the best fit line. The fact that the different calculations have a different percentage of error margin may indicate an unstable simulation of the manoeuvre. This is mainly concerning the calculation of advance, since this parameter is the one farthest away from what was the desired outcome.

6.2.2 Zig-zag manoeuvre

In Figure 6.5 the different overshoot angles are plotted for each rudder angle in both the port (positive values) and starboard (negative values) direction. The circle markers indicate simulated manoeuvres, the x markers indicate full-scale manoeuvres, whereas the red and blue colour represent the first and second overshoot angle, respectively. The results are as listed in Table 5.4 and 6.2 for the full-scale and simulated manoeuvres, respectively.

Figure 6.5 give an impression of the similarity between the 10/10 and 20/20 manoeuvre, and the 1st and 2nd overshoot angle to both starboard and port. As the figure illustrates, there is a high rate of compliance between the simulated starboard and port manoeuvre, for both the 10/10 and the 20/20 rudder angle. The full-scale measurements show a fair rate of compliance, but with a segregate in the 10/10 port 2nd overshoot angle, as it is larger than the 1st overshoot angle which contradicts the tendency of the other full-scale results. This may be an error in the specific run and should be evaluated with care. The figure also illustrates the similarity between the 1st and 2nd overshoot angle in the simulated manoeuvre, as they are almost identical, unlike the full-scale results.

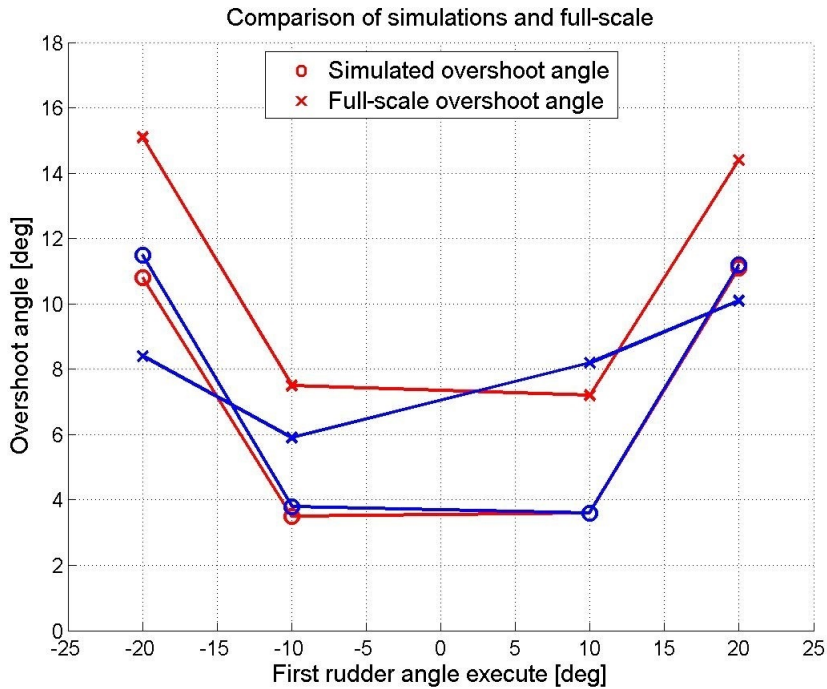


Figure 6.5: Comparison of full-scale and simulated zig-zag overshoot angles

In Figure 6.6 the same results are plotted, but as a best fit trend line between the simulation and full-scale measurements. The corresponding colour and marker combinations are listed in Table 6.7. As the figure illustrates, the 2nd overshoot in the 20/20 starboard and port manoeuvre is the only overestimated calculation in VeSim, whereas the other calculations are underestimated. It can also be observed that there is a tendency of underestimating the calculations with the same magnitude, as the markers are about the same proportion of magnitude below the best fit line. This indicates that there is a certain stability in the simulations, albeit they are, for the most part, underestimated.

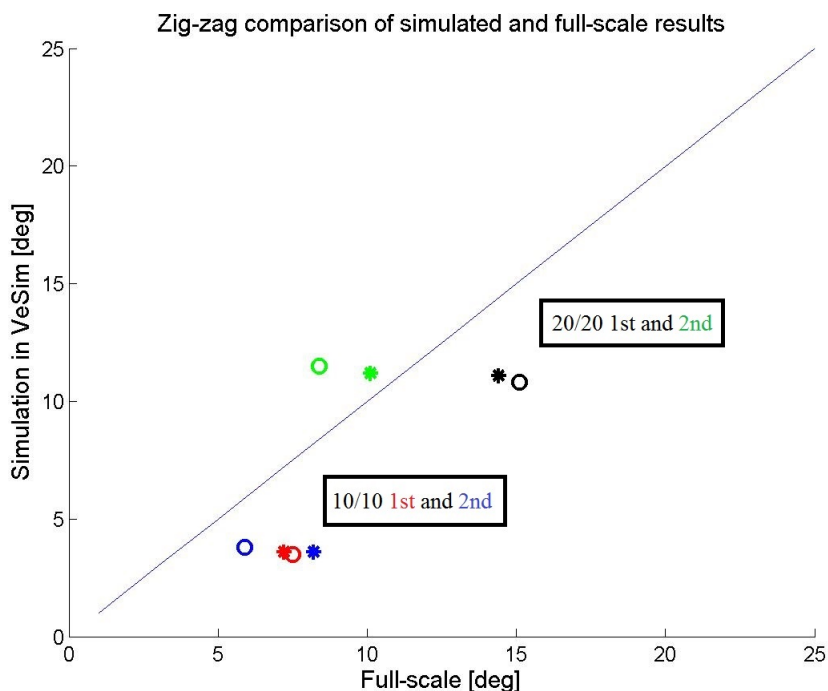


Figure 6.6: Comparison of full-scale and simulated zig-zag results

Table 6.7: Markers for comparison of simulated and full-scale zig-zag results

	10/10		20/20	
	1st overshoot	2nd overshoot	1st overshoot	2nd overshoot
Port	Red *	Blue *	Black *	Green *
Starboard	Red o	Blue o	Black o	Green o

6.2.3 Thruster turning manoeuvre

Figure 6.7 depicts the different time calculations of the thruster turning manoeuvre. The full-scale and simulated results listed in Table 5.6 and 6.4, respectively, are plotted with marker and colour combinations as listed in Table 6.8. Figure 6.8 is a dummy figure, intended for illustrating the use of the different colour combinations presented in Table 6.8. As Figure 6.7 illustrates, the time simulated results are overestimated for all heading reaches. A tendency of increasing the margin of error can be observed as the different simulated heading angles are reached after increasing time steps. The simulation model is stable considering not having calculations that disperse from the trend in a large extent, but increases the time needed to obtain the desired heading reach with a constant degree of error.

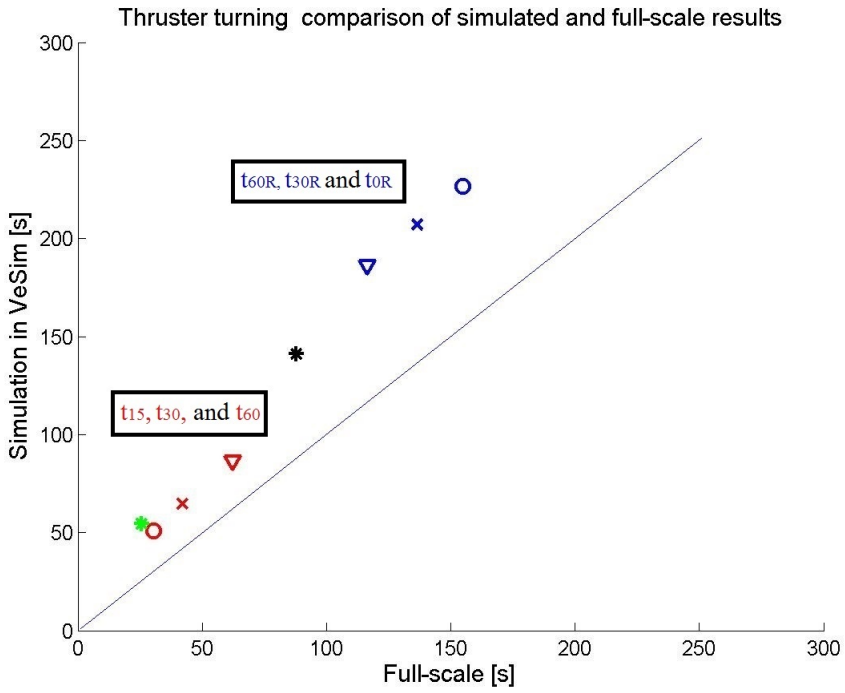


Figure 6.7: Comparison of full-scale and simulated thruster turning results

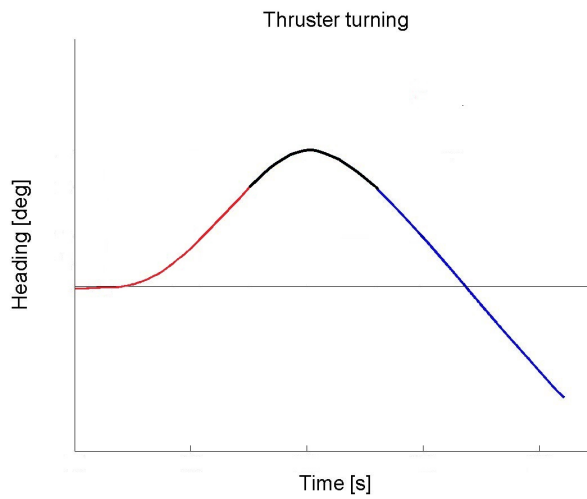


Figure 6.8: Heading with colour equivalent to time parameters

Table 6.8: Markers for comparison of simulated and full-scale thruster turning results

		Marker
t_{15}	[s]	Red o
t_{30}	[s]	Red x
t_{60}	[s]	Red ∇
t_s	[s]	Black *
t_{60R}	[s]	Blue ∇
t_{30R}	[s]	Blue x
t_{0R}	[s]	Blue o
Δt_s	[s]	Green *

6.2.4 Accelerating turn manoeuvre

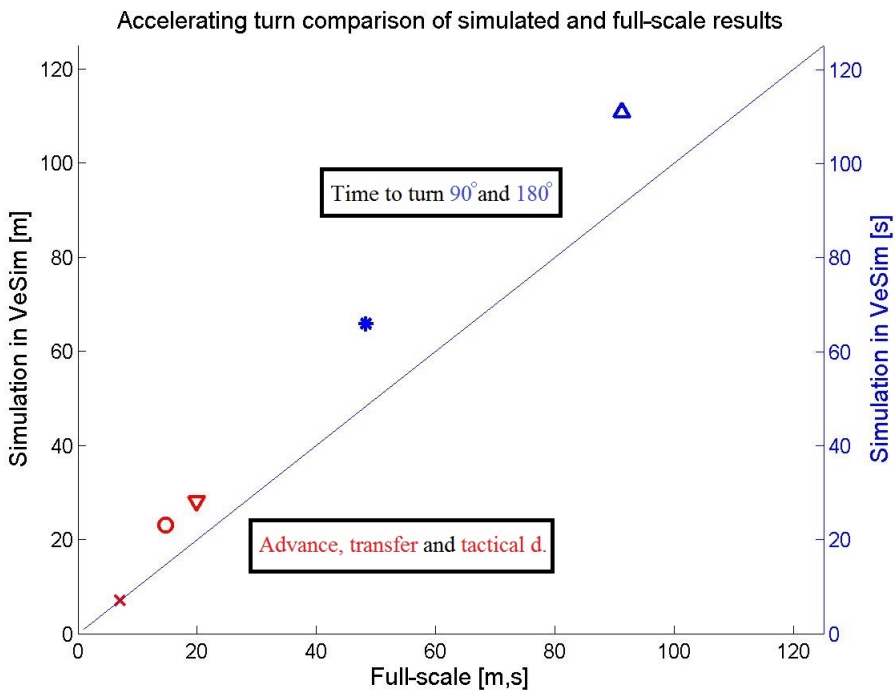


Figure 6.9: Comparison of full-scale and simulated accelerating turn results

Table 6.9: Markers for comparison of simulated and full-scale accelerating turn results

		Marker
Advance	[m]	Red o
Transfer	[m]	Red x
Tactical diameter	[m]	Red ∇
Time to turn 90°	[s]	Blue *
Time to turn 180°	[s]	Blue Δ

In Figure 6.9, the results of the full-scale and simulated accelerating turn manoeuvre, listed in Table 5.7 and 6.5, respectively, are plotted in combinations of marker and colour. The different combinations are listed in Table 6.9. The left y-axis in Figure 6.9 refers to the simulations in metres and the right y-axis refers to the time in seconds. As the figure illustrates, the simulated transfer calculation is 100% identical to the full-scale measurement, as it appears exactly on the best fit trend line. The advance and tactical diameter are however overestimated, but in the same magnitude of error, indicating a stable simulation model. This is also the case for the time to turn 90 and 180 degrees, indicated in Figure 6.9 as described in Table 6.9.

Chapter 7

Summary and Conclusion

7.1 Discussion

7.1.1 Manoeuvring results compared with IMO MSC Res. 137(76)

The different manoeuvres described as the standards, e.g. the turning circle, zig-zag and stopping test manoeuvre, will be evaluated according to the IMO requirements described in Section 3.2.

Full-scale sea trials

The full-scale sea trial results are listed in Table 5.2 and 5.3 for the port and starboard turning circle, respectively, and in Table 5.4 and 5.5 for the zig-zag and stopping test manoeuvre, respectively.

Table 5.2 and 5.3 shows that all the manoeuvre parameters are well within the requirements. As briefly discussed in Section 5.3.2, the port manoeuvre, turning into the wind has larger turning circle parameters than the starboard manoeuvre, turning with the wind. In one way this is counter-intuitive, as one would expect that turning with the wind should give the vessel a boost, especially regarding the transfer and tactical diameter parameter when looking at Figure 5.5. But this is obviously not the case, as the two tables emphasizes. When correcting for current forces, the starboard parameters increase and the port parameters decrease, as was expected. In the case of this vessel, only these two turning tests were conducted. To check whether this was an occasional incident or in fact the turning abilities of the vessel are this different from starboard to port, more turning circle tests should be conducted. The repeatability of the tests would have to be addressed, e.g. if the identical tests conducted render similar results, i.e. if two turning circles to port render similar results.

For the zig-zag manoeuvres, given by Table 5.4, the results are well within the required abilities. Results show that there is a fairly good compliance between the port and starboard tests, with a difference of about 28% in the 2nd overshoot angle of the 10/10 manoeuvre as the largest. The difference between the other parameters are less than 5% between the starboard and port manoeuvre. But as a study of repeatability, more identical tests should be conducted. Neither the turning circle manoeuvre nor the zig-zag manoeuvre were subjects of several identical tests.

The results of the only stopping test performed is listed in Table 5.5. The test is not performed in the specified manner as described in the IMO regulations [9]. This is because the specified manoeuvre can cause great engine strain and is of this reason avoided as much as possible. An alternative manoeuvre, utilizing the propeller pitch and RPM instead of reversing the engine to 100% MCR, was performed. The results listed in Table 5.5 cannot be compared with the requirements set by the IMO.

Simulated manoeuvres

The simulated IMO standard manoeuvres are listed in Table 6.1, 6.2 and 6.3 for the turning circle, zig-zag and stopping test manoeuvre, respectively.

The results of the turning circle manoeuvre listed in Table 6.1 indicates that all the parameters of the manoeuvre are well within the requirements. The port and starboard manoeuvre varies in little degree, which can indicate that there is a minor error in the center line symmetry of the physical ShipX model or that the calculation method varies from port to starboard, albeit the manoeuvre should, in theory, be identical to both port and starboard. Although the initial results of the turning circle looks to be of satisfying validity, regarding the IMO requirements, there is a reason for concern regarding the simulation model when looking at the track plot of the manoeuvre. The track plot can be seen in Appendix D.1. This illustrates that there is an overestimation of the turning ability of the vessel after obtaining a 180° change of heading. Instead of completing a full circle, the vessel seems to drift with a large yaw motion. This indicates that there is a miscalculation in the hydrodynamic coefficients affecting the straight line stability of the ship. As discussed in Section 4.3.1, this may occur because of the fact that HullVisc uses a semi-empirical model to calculate the coefficients where the benchmark vessels are of older design and mostly based on offshore vessels. The turning circle parameters are within the IMO requirements, but because of the most likely incorrect calculation of hydrodynamic coefficients, the results should be evaluated with care.

The simulated zig-zag manoeuvre, presented in Table 6.2 are within the required abilities. From the results, it can be observed that the simulation model predicts almost identical overshoot angles for both the 1st and 2nd overshoot angle. The full-scale trials of the zig-zag manoeuvre have a tendency of smaller 2nd overshoot angles compared to the 1st, and this is not the case in the simulated manoeuvre. But, regarding the IMO requirements, the model predictions are of satisfactory

result.

The stopping test simulation results are presented in Table 6.3. As the results of the full-scale test, the simulated manoeuvre is also not conducted as defined in the IMO regulations, and cannot be compared with its requirements.

7.1.2 Simulation results compared with full-scale results

The following figures depict the percentage deviation of the simulated manoeuvres compared with the full-scale trials. The scale varies from 0 – 100% where less than 100% is underestimation and more than 100% is overestimation, and consequently 200% is equivalent to two times the value of the full-scale result.

Figure 7.1 depicts the percentage of how much the simulated turning circle manoeuvre differs from the full-scale sea trials, for both the original results and the results of correcting for the current forces as Figure a) and b), respectively. From the figures, the only parameter that is almost identical is the port tactical diameter, as it is fairly near 100%. From the other parameters, it is clear that VeSim overestimates the results as discussed in Section 6.2.1. The parameter that deviates the most from the full-scale trials is the transfer, which is about 50% larger than the full-scale measurement. Correcting for current forces does not affect the results in a decisive manner as can be observed from the two figures. It can also be observed that the full-scale starboard manoeuvre has a tendency of having smaller values than to port, giving less overestimation of the simulation, as the simulated manoeuvres are more or less identical, as seen in Table 6.1.

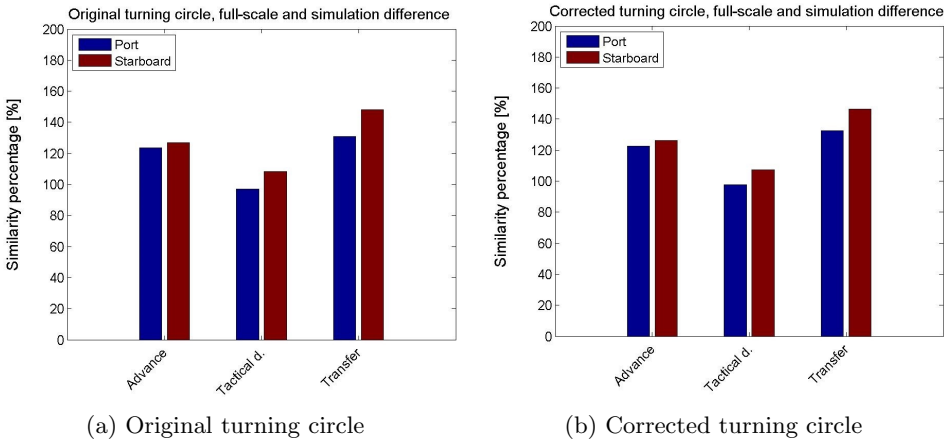


Figure 7.1: Full-scale turning circle and simulation in percentage difference

In Figure 7.2 the simulated stopping test is compared with the full-scale test. As the figure illustrates, the simulations are overestimated with approximately 20%

in both track length and ship length. This manoeuvre is quite different between the full-scale procedure and simulation procedure. This result must therefore be interpreted with care.

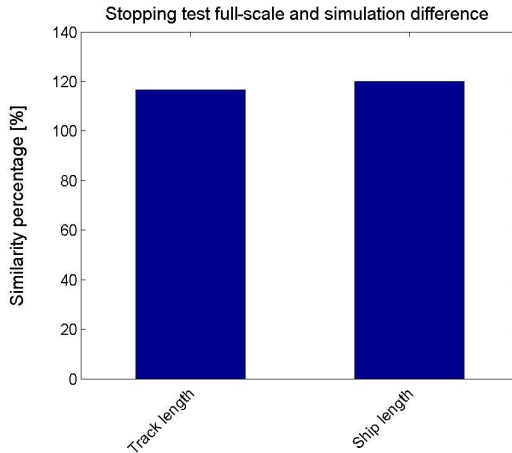


Figure 7.2: Full-scale stopping test and simulation in percentage difference

Figure 7.3 shows the comparison of the simulated and full-scale zig-zag manoeuvre, as how much the simulation differs from the full-scale trials. In this case, the simulation model underestimates the different overshoot angles, except for the 20/20 2nd overshoot angle, which is exceeded in the amount of almost 40% to the starboard side and only 10% to the port side. The clear difference between starboard and port can also be seen in the 10/10 manoeuvre for the 2nd overshoot, where the starboard overshoot angle is quite smaller than what measured to port, hence the larger difference to starboard, albeit the simulation is underestimated in this particular manoeuvre. The reason for the larger difference to starboard than to port has its origin in the full-scale trials as seen in Table 5.4. Here, the 1st overshoot angle to starboard and port differs with almost 40% and the 2nd overshoot angle to starboard and port differs with approximately 20%. The simulated zig-zag manoeuvres are however, quite stable regarding the similarity of the starboard and port manoeuvres. Although, there are almost no difference in the 10/10 and 20/20 overshoot angles, which may seem to be incorrect according to the full-scale test results.

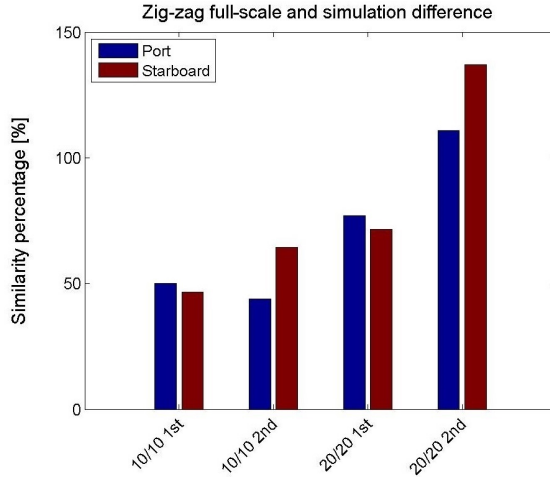


Figure 7.3: Full-scale zig-zag and simulation in percentage difference

The thruster turning differences in simulation and full-scale are illustrated in Figure 7.4. As the previous illustrations, this too differs in the sense of over- or underestimation of simulated results. It can be observed that the simulation model is overestimating the parameters in a fairly equivalent amount. The simulation results are about 50% larger than that of the full-scale results, except for the overshoot time (Δt_s) and the overshoot angle (ψ_s) which are significantly higher and lower than 50%, respectively. The equivalent overestimations may indicate that the model is stable, but calculates incorrect horizontal stability, with the calculated HullVisc coefficients in mind.

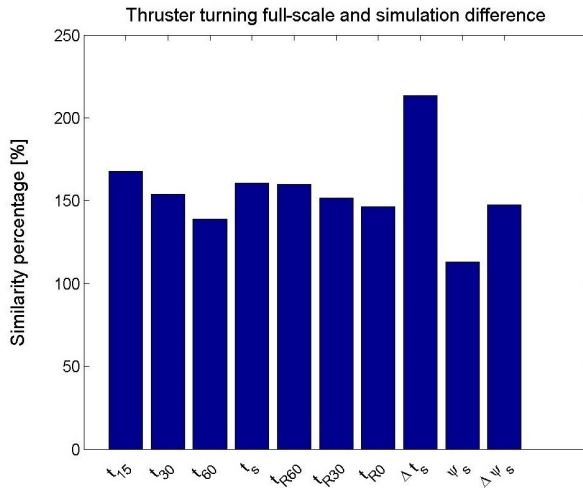


Figure 7.4: Full-scale thruster turning and simulation in percentage difference

The illustration of the accelerating turn simulation and full-scale difference is given in Figure 7.5. An equivalent magnitude of overestimation can also be seen in this manoeuvre. The parameters are all in the amount of about 50% larger than the full-scale results, except for the speed at 180° heading change and transfer, which are overestimated in an extreme magnitude and 100% identical to the full-scale results, respectively. The simulation model seems to be stable, neglecting the possible error source of hydrodynamic performance.

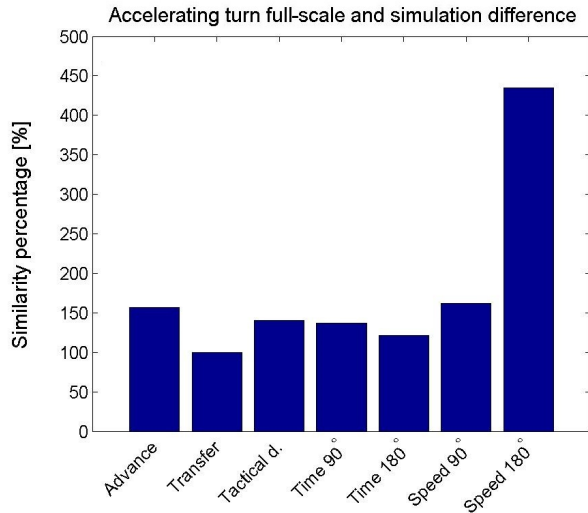


Figure 7.5: Full-scale accelerating turn and simulation in percentage difference

7.1.3 Influencing parameters in VeSim and error sources

The simulated manoeuvres are as described and illustrated, deviating in a varying extent from the full-scale trial measurements. The magnitude of the deviation differs for each manoeuvre, where the zig-zag manoeuvre parameters are fairly underestimated, and in the other manoeuvres as turning circle, thruster turning and accelerating turn, are overestimated. The main reason for this is believed to originate from the invalid calculation of the hydrodynamic coefficients by HullVisc, as it is based upon regression analysis and semi-empirical calculations.

Other influencing parameters that may lead to incorrect simulations may be the disparities that occur between port and starboard manoeuvres in the full-scale trials. This of course, does not affect the simulation model, but may lead to misjudgement of the model when comparing simulated and full-scale results. Albeit, this is not the case for the simulations performed, as they are quite off, regardless of the disparity of the full-scale measurements.

The calculation of propeller and rudder forces in the simulation model may influence the result. The propeller and rudder arrangement for MF Landegode can be

viewed in Appendix A. This arrangement is one of Rolls-Royce's integrated propeller and rudder systems that may offer effects that may not be covered by the mathematical model used for the calculation of propeller and rudder forces listed in Section 4.3.3.

Regarding the low speed manoeuvres, e.i. the thruster turn and accelerating turn manoeuvre, wind is an important parameter [38]. The simulations are carried out with no wind, but this is not possible for the full-scale trials. Although the wind speed was low at the day of the full-scale low speed manoeuvres, see Table 5.1, the vessel was in fact affected by it, resulting in simulation results that differ from the full-scale results. This effect has however been assumed to be of little importance as this is not the main source of prediction error.

Another source of miscalculation of the manoeuvre may lie within the mathematical model being unable to capture effects of ship behaviour and environments encountered in manoeuvring.

7.1.4 Verification and validation of the model

The difference between the full-scale and simulated manoeuvres give a clear indication of the simulations being overestimated in most cases. The simulation model present stable results, which indicate that the model is of desired validity. The error however, may be in the estimation of the hydrodynamic coefficients. PMM tests with a scaled model of Landegode has been conducted at MARINTEK. The results of these tests were not ready when the thesis was written. Using the calculated hydrodynamic coefficients from the PMM tests should give a more detailed indication of the validity of the coefficients calculated by HullVisc, and whether or not VeSim is a suitable simulation model for MF Landegode. In addition to using PMM coefficients, the simulations could be performed in a time domain simulation giving the user the opportunity to change the pitch and RPM throughout the manoeuvre, as in the full-scale trials. This may also improve the result of the simulation model. VeSim is, according to the results, a valid simulation tool in some degree, keeping in mind the possibility of future correction of the hydrodynamic coefficients. By studying the affect of the coefficients, more satisfying results would hopefully be obtained and a more tangible decision on the validity of the model could be made.

7.2 Summary and conclusion

Developing regulations for improving safety at sea has been a concern since international trading became a reality. The International Maritime Organization (IMO) has become the international adopted treaty which regulates the manoeuvring performance of ships to maintain the safety, security and preventing marine pollution at sea. The IMO has established three standard manoeuvring tests for vessels with lengths larger than $L \geq 100m$ to evaluate the performance of the vessel. This is the turning circle, zig-zag and stopping test manoeuvre. Requirements are provided for each individual manoeuvre to be fulfilled. In addition to the IMO performance

tests, additional manoeuvres to be evaluated has been listed from different organizations.

When designing a ship, early estimations of the manoeuvring performance is an essential part, and simulation models are therefore a critical tool. With a simulation model that can predict these characteristics based upon the main dimensions of the vessel, alterations and modifications can be made in an early design stage, and mission-related requirements can be tweaked for better performance. It is therefore important to have a validated simulation model predicting trustworthy calculations and performance characteristics.

A computer model of the case vessel, MF Landegode, has been provided by MARINTEK and adopted into the simulation model. The simulation model developed by MARINTEK, Vessel Simulator (VeSim), is a time domain simulation tool. The simulation model consists of two main pre-processors called HullVisc and VeRes, calculating the hydrodynamic coefficients, and forces and motions in the frequency domain, respectively. A flowchart of the structure of VeSim is illustrated in Figure 4.2, followed by a more detailed description of the different pre-processors and the mathematical models that have been used.

A set of full-scale trial data has been provided and processed for comparison with the simulated manoeuvres. The sea trials were conducted on the 29th, 30th and 31st of August 2013. The standard IMO performance tests and additional low speed manoeuvres were conducted and measured with equipment fitted to the vessel during the manoeuvres. The analysis of the trials, test conditions and the different manoeuvres analysed have been presented. Tables and figures illustrate the manoeuvres and the results obtained from each test. The results show that the IMO standard manoeuvres are within the required abilities set for each specific manoeuvre. The stopping test is, however not conducted as specified in the IMO regulations, but altered to save the engine from too much strain. The altered test cannot, from this reason, be compared with the IMO regulations.

The calm water simulations were carried out using the simulation model which has been described. The standard IMO manoeuvres were carried out using the simulation plug-in for calm water, which enables the user to choose from different pre-determined tests as Figure 6.1 illustrates. The low speed manoeuvres were carried out by using the described manual time domain simulation model and illustrated by Figure 6.2. All the IMO standard manoeuvres were well within the requirements. Even though the turning circle manoeuvre was within the requirements, the ship's track plot given in Appendix D.1 clearly illustrates that the prediction is flawed and that there is an aberration in the straight line stability of the vessel. This give rise to the most conceivable cause of error, that the hydrodynamic coefficients are spurious due to the fact that they are based upon a semi-empirical calculation with benchmark vessels of older design. The comparison between the full-scale trials and simulated manoeuvres give a clear indication of over- and underestimation of the

simulated manoeuvres in the range of 20 – 50% as an average value. This is also the case for the low speed manoeuvres.

The simulation model used is believed to be of satisfying validity, emphasizing the aberration in the HullVisc calculations and that this should be studied in detail before making a firm conclusion on whether or not to use VeSim as a validated simulation model. I.e. further investigation related to the hydrodynamic coefficients, especially with regard to PMM tests, should be conducted and implemented in the validation of this simulation model.

7.3 Recommendations for further work

For a more complete and reliable validated model, further work and study is necessary, especially regarding the validity of the hydrodynamic coefficients and the affect of these. There are conducted PMM tests with a scaled model of MF Landegode at MARINTEK. These were not analysed during the time of preparation for this thesis, but should be available during the autumn of 2014. The coefficients from the PMM tests should give a better indication on the validity of the HullVisc coefficients. A more detailed study of other means of calculating the hydrodynamic coefficients could be conducted to address this issue more thoroughly, and to have a more tangible perspective of the affect of the hydrodynamic coefficients.

In addition, more full-scale tests could be conducted to address the issue of repeating the manoeuvres and obtaining matching or similar results for each test to both starboard and port.

To address the low speed manoeuvres more accurately, an individual study of these manoeuvres and obtaining a more applicable simulation model with regard to wind forces, change of propeller pitch and RPM throughout the manoeuvre should be conducted. A study of the affect of changing the propeller pitch and RPM should in addition to low speed manoeuvres be performed on the IMO standard manoeuvres as well.

Much more work can be done regarding the validation of the simulation model, with the above mentioned studies being a good place to start.

References

- [1] Andreas R. Moss, "Simulation Model for MF Landegode." Project thesis, December 2013.
- [2] *Validation of Manoeuvring Simulation Models*, ITTC - Recommended Procedures and Guidelines, 2011.
- [3] Tor Einar Berg*, Edvard Ringen, "Validation of shiphandling simulation models," in *International Conference on Ocean, Offshore and Arctic Engineering (OMAE)*, ASME, 2011. *Corresponding author.
- [4] *"Esso Osaka Specialist Committee - Final Report and Recommendations to the 23rd ITTC"*, ITTC, 2002. Venice, Italy.
- [5] SIMMAN Workshop 2008. URL:<http://www.simman2008.dk/>, 2008. "[Accessed 14/11/2013]".
- [6] Ferry Revolution. URL: <http://ferryrevolution.jimdo.com/newbuilding-archive/2013/thorghatten-nord/>, 2013. "[Accessed 14/11/2013]".
- [7] International Maritime Organization, "Brief history of IMO." URL: <http://www.imo.org/About/Pages/Default.aspx>, 2013. [Accessed 06/10/2013].
- [8] International Maritime Organization, "IMO MSC/Res.137(76)," tech. rep., IMO, 2002. Standards for For Ship Manoeuvrability.
- [9] International Maritime Organization, "IMO MSC/Circ.1053," tech. rep., IMO, 2002. Explanatory Notes to the Standards for Ship Manoeuvrability.
- [10] International Towing Tank Conference, "Full scale measurements, manoeuvrability full scale, manoeuvring trials procedure," tech. rep., ITTC, 2002.
- [11] F.H.H.A. Quadvlieg, P. van Coevorden, "Manoeuvring criteria: More than IMO A751 requirments alone," tech. rep., MARIN, The Netherlands, 2003.
- [12] International Standard ISO 13643-2, "Ships and marine technology - manoeuvring of ships," tech. rep., International Standard ISO, 2013.

- [13] Yasuo Yoshimura, Yumiko Masumoto, “Hydrodynamic database and manoeuvring prediction method with high speed merchant ships and fishing vessels,” *Society of Naval Architects and Marine Engineers*, vol. 14, 2011.
- [14] “A new multi-purpose carriage in the MARINTEK towing tank.” ”[Accessed 12/12/2013]”.
- [15] Tor Einar Berg, *Lecture notes in TMR 4220, Naval Hydrodynamics, Ship Manoeuvring*. Dept. Marine Technology, NTNU, 2009.
- [16] Margaret Rouse, “Definition supercomputer.” URL: <http://whatis.techtarget.com/definition/supercomputer>, 2008. [Accessed 11/10/2013].
- [17] URL: <http://www.sintef.no/home/MARINTEK-old/Software-developed-at-MARINTEK/VERES/>. ”[Accessed 12/12/2013]”.
- [18] URL: <http://www.wamit.com/>. ”[Accessed 12/12/2013]”.
- [19] Odd Magne Faltinsen, *Hydrodynamics of high speed marine vehicles*. Cambridge University Press, 2005.
- [20] Thor Inge Fossen, *Handbook of Marine Craft Hydrodynamics and Motion Control*. A John Wiley and Sons Ltd, 2011.
- [21] Andrew Ross, *Nonlinear Manoeuvring Models for Ships*. PhD thesis, Norwegian Univeristy of Science and Technology (NTNU), 2008.
- [22] URL: <http://www.sintef.no/home/MARINTEK-old/MARINTEK-Publications/MARINTEK-Review/MARINTEK-Review-2—2009/Vessel-simulator-VeSim-combining-manoevring-and-seakeeping/>. ”[Accessed: 06.04.2014]”.
- [23] Dariusz Fathi, *MARINTEK Vessel Simulator (VeSim)*, 4.1.x ed.
- [24] URL: http://en.wikipedia.org/wiki/File:ECEF_ENU_Longitude_Latitude_relationships.svg. ”[Accessed 05/04/2014]”.
- [25] Dariusz Fathi, *SHIPX Workbench, Getting Started*. MARINTEK, URL:<http://www.ivt.ntnu.no/imt/software/shipx>. ”[Accessed 19/10/2013]”.
- [26] John Nicholas Newman, *Marine Hydrodynamics*. Massachusetts Institute of Technology, 1977.
- [27] ITTC, *ITTC Symbols and Terminology List*, Septmeber 2011.
- [28] Dariusz Fathi, *SHIPX Vessel Responses (VERES) Ship Motions and Global Loads Users’ Manual*. MARINTEK, NTNU, June 2012.
- [29] Odd Magne Faltinsen, *Sea Loads on Ships and Offshore Structures*. Cambridge, 1990.

-
- [30] Kjell Martinussen, Edvard Ringen, “Manoeuvring prediction during design stage,” tech. rep., MARINTEK AS, October 2000. International Workshop on Ship Manoeuvrability, HSVA, Hamburg, Germany.
- [31] J. Strøm-Tejsen and R.R. Porter, “Prediction of Controllable-Pitch Propeller Performance in Off-Design Conditions,” in *Third Ship Control Systems Symposium*, Paper VII B-1, Bath, 1972.
- [32] URL: <http://www.sintef.no/home/MARINTEK/News/MARINTEK-responsible-for-three-new-MAROFF-projects/>. ”[Accessed 28/05/2014]”.
- [33] URL: <http://www.yr.no>. ”[Accessed: 07/04/2014]”.
- [34] “Wind generated currents in shallow water.” URL: <http://www.dot.state.fl.us/rddesign/Drainage-/Research/CE/Wind-Generated-Currents.pdf>. ”[Accessed 19/03/2014]”.
- [35] URL: <http://cdip.ucsd.edu/?nav=documents&sub=faq&xitem=forecast>. ”[Accessed: 07/04/2014]”.
- [36] “Wentworth grain size chart.” URL: <http://upload.wikimedia.org/wikipedia/commons/e/e2/Wentworth-Grain-Size-Chart.pdf>. ”[Accessed 07/04/2014]”.
- [37] Ørjan Selvik, “E-mail correspondance,” October 14th 2013.
- [38] URL:<http://thenauticalsite.com/NauticalNotes/Manoeuv/MyMan-Lesson02-SHandling.htm>. ”[Accessed: 07/04/2014]”.
- [39] URL: <http://www.rolls-royce.com/marine/products/propulsors/promas/>. ”[Accessed 22/11/2013]”.

Appendix

Appendix A

Ship specifications: MF Landegode

MF Landegode

Car Ferry between Bodø and Moskenes

Name	MF Landegode
Owner	Torghatten Nord AS
Designed by	LMG Marine, Norway
Built by	Remontowa Shipyards in Gdańsk
Delivery year	2012
Port of Registry	Tromsø, Norway

Main dimensions

Draught	T	=3,6	m
Length	L _{pp}	=90	m
Breadth	B	=16,81	m
Displacement	∇	=2494,634	m ³
Block coefficient	C _B	=0,396	[-]
Weight	Δ	=2557	tons
Speed	V	=19	knots

Capacity

Passengers	390
Cars	120 PCU (Personal Car Unit)

Machinery

Main electric propulsion	Rolls Royce Bergen, B35:40V12PG with 5250 kW/750 rpm
Speed at 100% MCR	22 knots
Cruise speed	15-17 knots
Main Steering gear and propulsion	Rolls Royce Integrated propeller and rudder system "Promas"

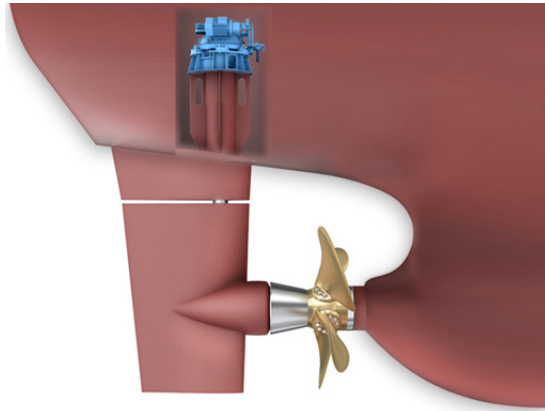


Figure A.1: Rolls Royce Integrated propeller and rudder system "PROMAS" [39]

Appendix B

Non-dimensional coefficients

The hydrodynamic coefficients calculated in HullVisc is described and made non-dimensional as follows:

Y_v : Linear sway damping due to sway velocity.

$$Y'_v = \frac{Y_v}{\frac{1}{2}\rho L_{pp}^2 U}$$

Y_r : Linear sway damping due to yaw velocity.

$$Y'_r = \frac{Y_r}{\frac{1}{2}\rho L_{pp}^3 U}$$

N_v : Linear yaw damping due to sway velocity.

$$N'_v = \frac{N_v}{\frac{1}{2}\rho L_{pp}^3 U}$$

N_r : Linear yaw damping due to yaw velocity.

$$N'_r = \frac{N_r}{\frac{1}{2}\rho L_{pp}^4 U}$$

$Y_{\dot{v}}$: Linear hydrodynamic mass in sway due to sway acceleration.

$$Y'_{\dot{v}} = \frac{Y_{\dot{v}}}{\frac{1}{2}\rho L_{pp}^3}$$

$Y_{\dot{r}}$: Linear hydrodynamic mass in sway due to yaw acceleration.

$$Y'_{\dot{r}} = \frac{Y_{\dot{r}}}{\frac{1}{2}\rho L_{pp}^4}$$

$N_{\dot{v}}$: Linear hydrodynamic mass moment of inertia in yaw due to sway acceleration.

$$N'_\dot{\delta} = \frac{N_{\dot{\delta}}}{\frac{1}{2}\rho L_{pp}^4}$$

$N_{\dot{r}}$: Linear hydrodynamic mass moment of inertia in yaw due to yaw acceleration.

$$N'_{\dot{r}} = \frac{N_{\dot{r}}}{\frac{1}{2}\rho L_{pp}^5}$$

X_{rr} : Longitudinal resistance due to yaw velocity.

$$X'_{rr} = \frac{X_{rr}}{\frac{1}{2}\rho L_{pp}^4}$$

$X_{\dot{u}}$: Hydrodynamic mass in surge due to surge acceleration.

$$X'_{\dot{u}} = \frac{X_{\dot{u}}}{\frac{1}{2}\rho L_{pp}^3}$$

X_{vr} : Longitudinal resistance due to combined sway and yaw velocity.

$$X'_{vr} = \frac{X_{vr}}{\frac{1}{2}\rho L_{pp}^3}$$

X_{vv} : Longitudinal resistance due to sway velocity.

X_{vvvv} : Longitudinal resistance due to sway velocity.

Where

- L_{pp} is ship length between perpendiculars
- ρ is water density
- U is total ship velocity

M' : Non-dimensional Mass.

$$M' = \frac{M}{\frac{1}{2}\rho L_{pp}^3}$$

X'_G : Non-dimensional Center of Gravity.

$$X'_G = \frac{X_G}{L_{pp}}$$

Y'_δ : Non-dimensional Rudder Force.

$$Y'_\delta = \frac{Y_\delta}{\frac{1}{2}\rho L_{pp}^2 U^2}$$

N'_δ : Non-dimensional Rudder Moment.

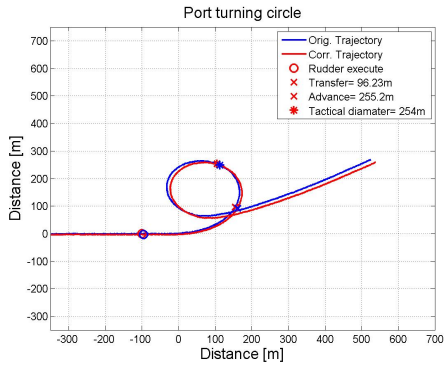
$$N'_\delta = \frac{N_\delta}{\frac{1}{2}\rho L_{pp}^3 U^2}$$

Appendix C

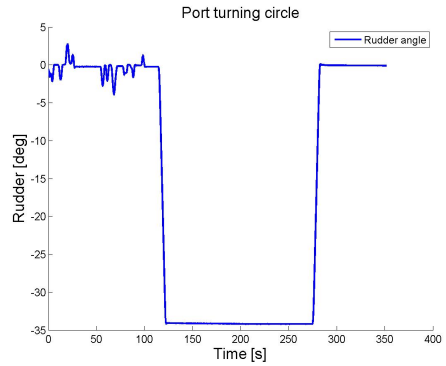
Full-scale manoeuvres

C.1 Turning circle manoeuvre

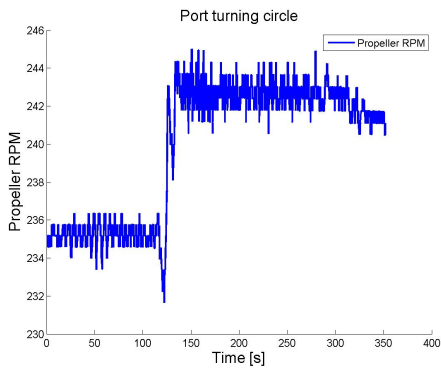
C.1.1 Port turning circle



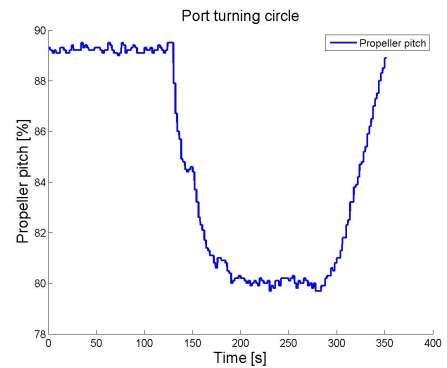
(a) Original and corrected trajectory



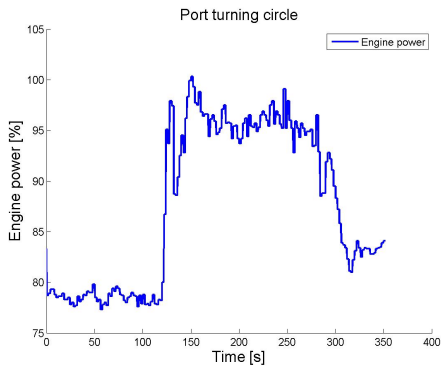
(b) Rudder angle



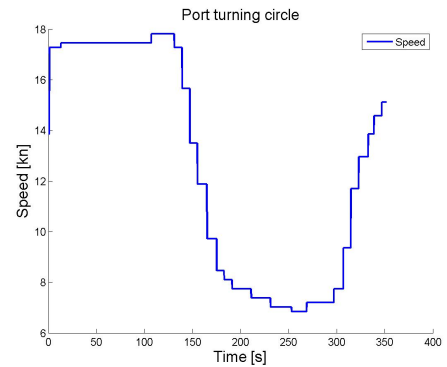
(c) Propeller RPM



(d) Propeller pitch



(e) Engine power



(f) Ship speed

Figure C.1: Full-scale port turning circle

C.1.2 Starboard turning circle

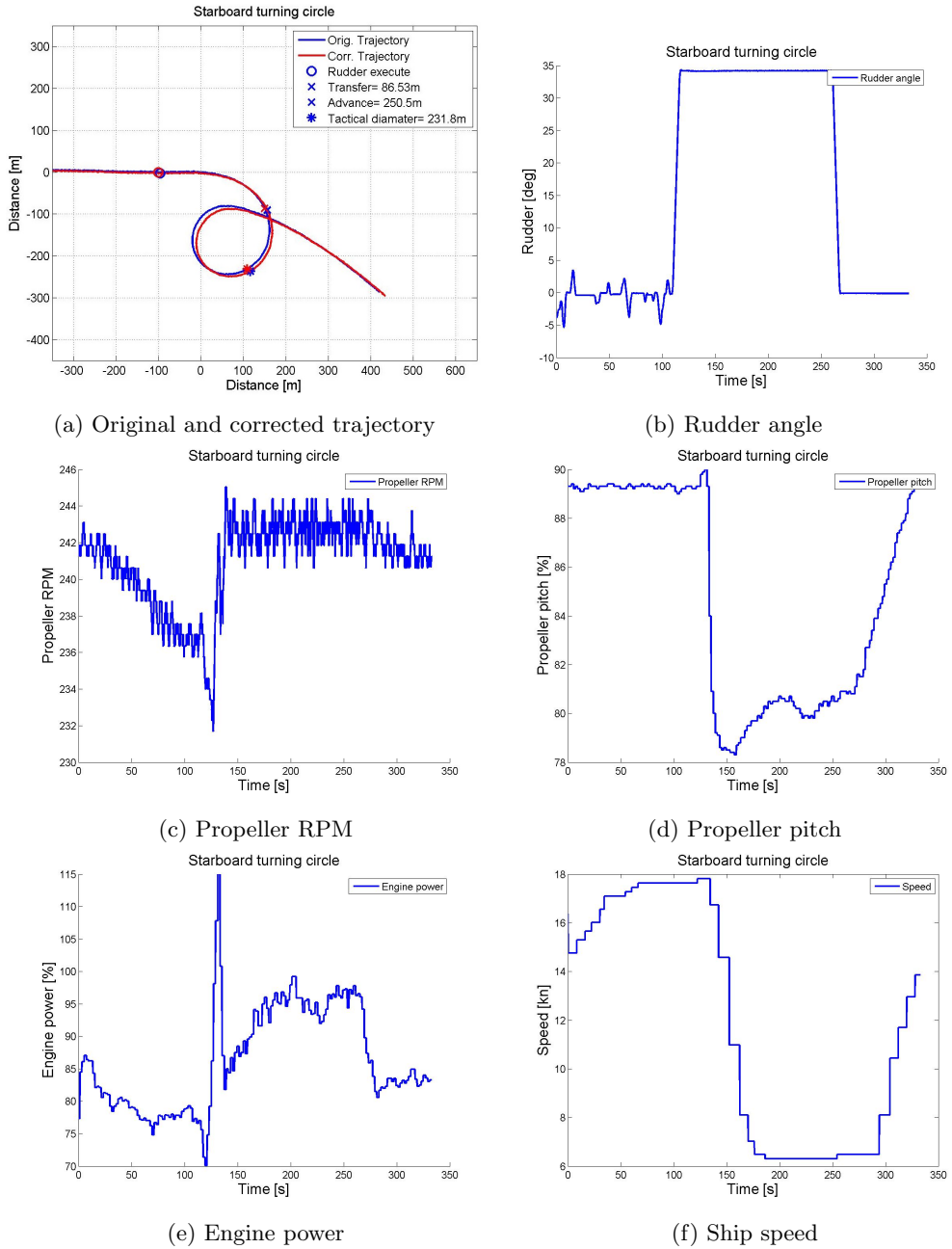
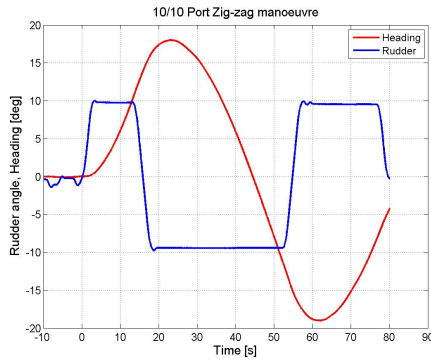


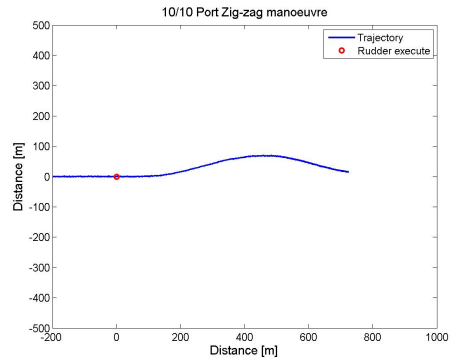
Figure C.2: Full-scale starboard turning circle

C.2 Zig-zag manoeuvre

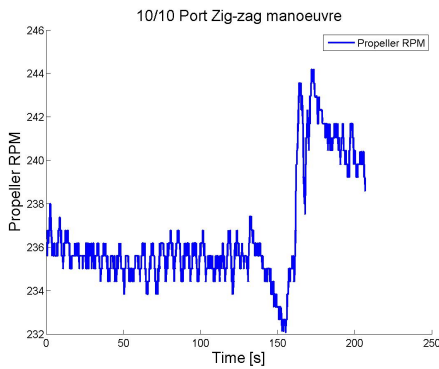
C.2.1 Port 10/10 zig-zag manoeuvre



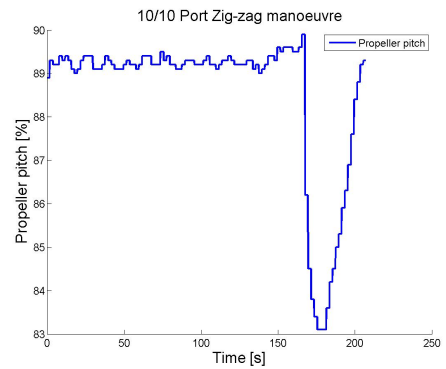
(a) Heading and rudder angle



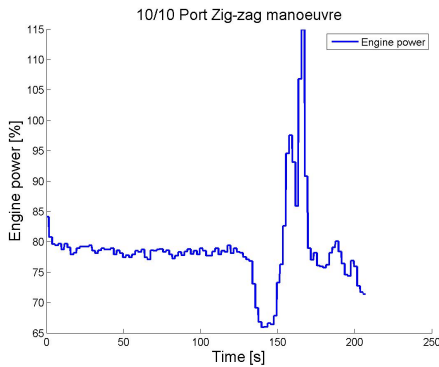
(b) Trajectory



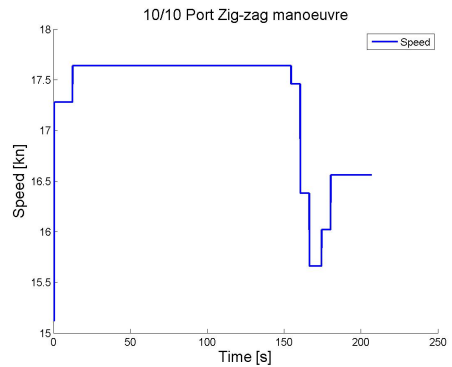
(c) Propeller RPM



(d) Propeller pitch



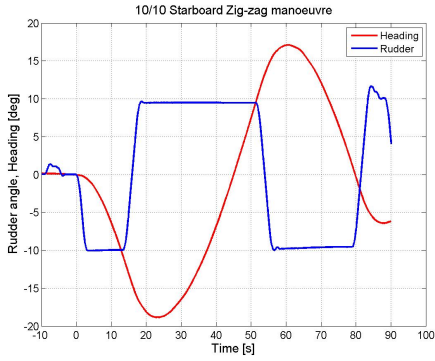
(e) Engine power



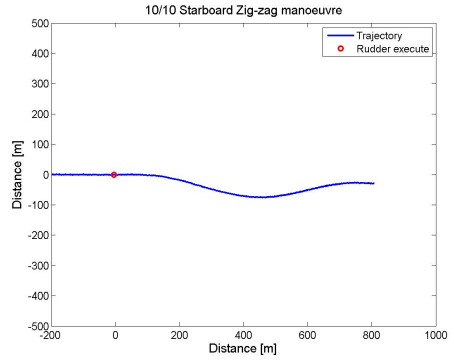
(f) Ship speed

Figure C.3: Full-scale port 10/10 zig-zag manoeuvre

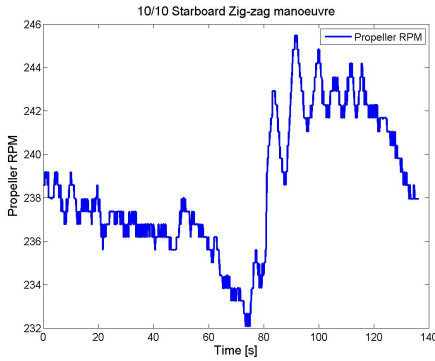
C.2.2 Starboard 10/10 zig-zag manoeuvre



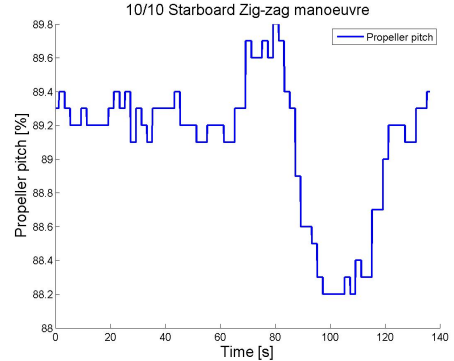
(a) Heading and rudder angle



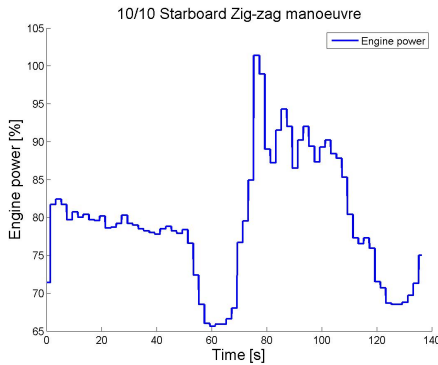
(b) Trajectory



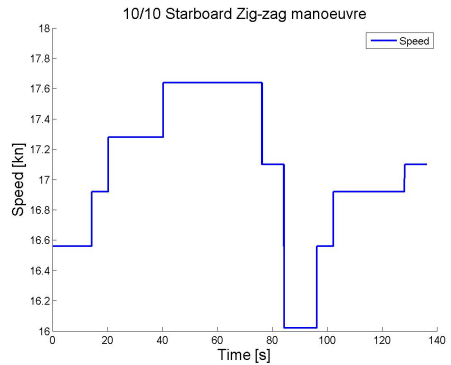
(c) Propeller RPM



(d) Propeller pitch



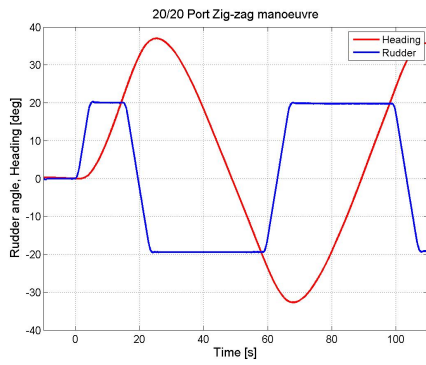
(e) Engine power



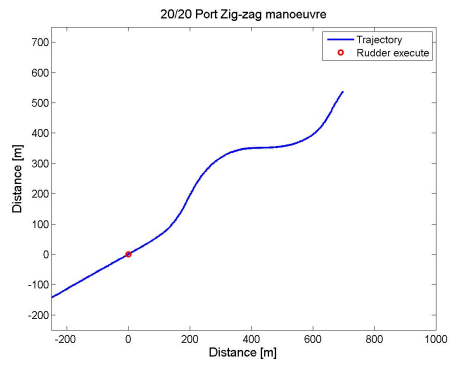
(f) Ship speed

Figure C.4: Full-scale starboard 10/10 zig-zag manoeuvre

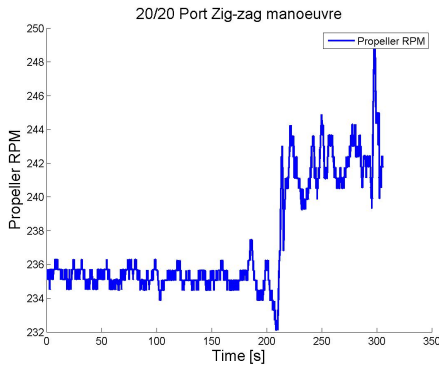
C.2.3 Port 20/20 zig-zag manoeuvre



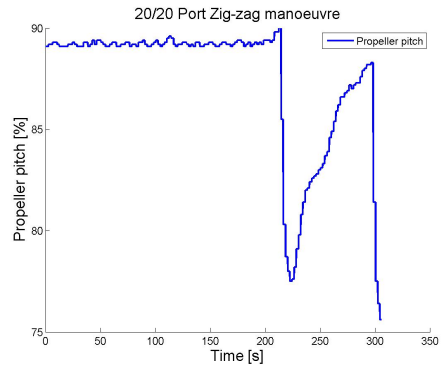
(a) Heading and rudder angle



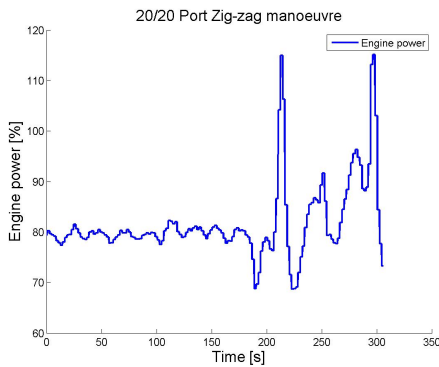
(b) Trajectory



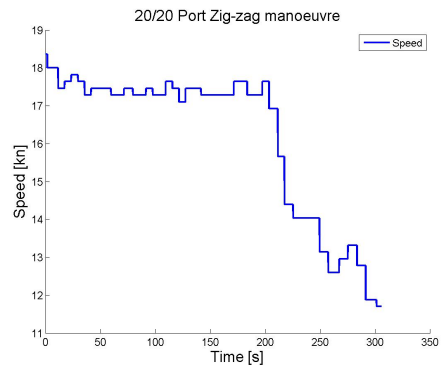
(c) Propeller RPM



(d) Propeller pitch



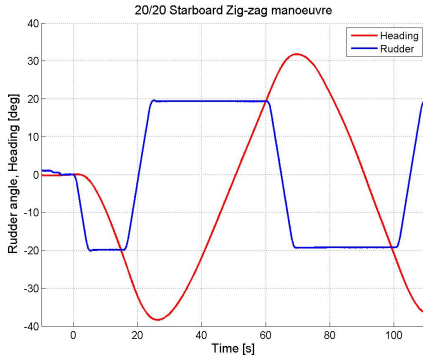
(e) Engine power



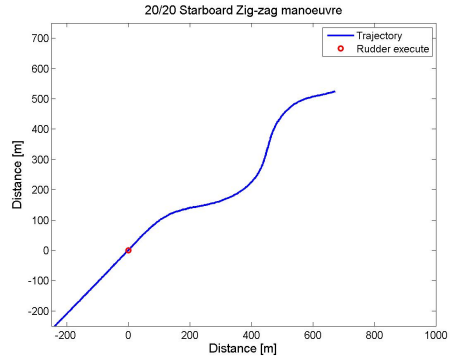
(f) Ship speed

Figure C.5: Full-scale port 20/20 zig-zag manoeuvre

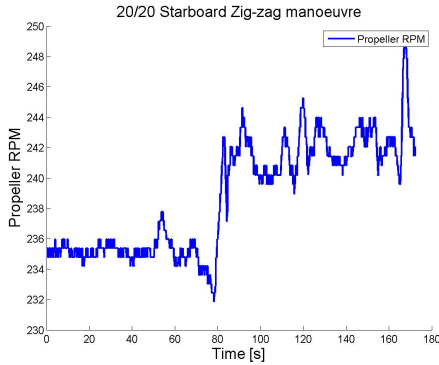
C.2.4 Starboard 20/20 zig-zag manoeuvre



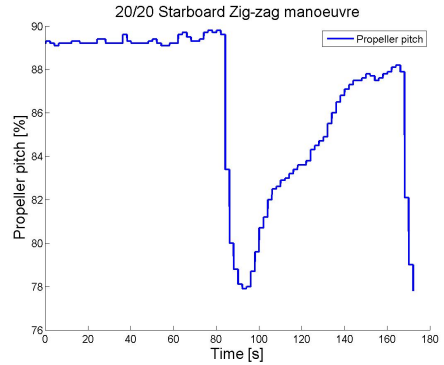
(a) Heading and rudder angle



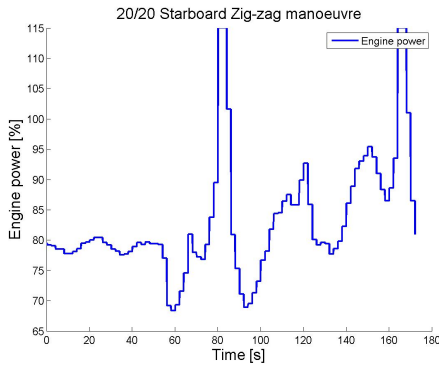
(b) Trajectory



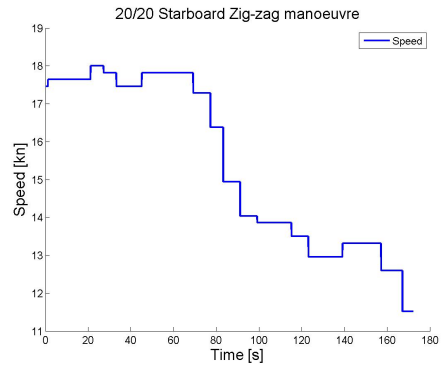
(c) Propeller RPM



(d) Propeller pitch



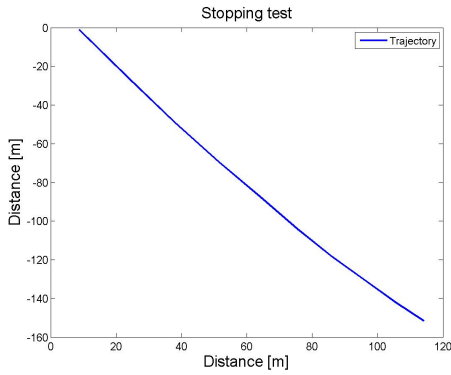
(e) Engine power



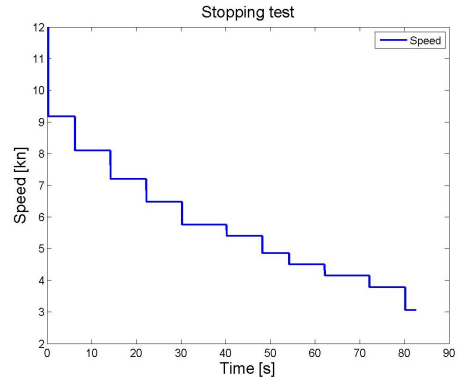
(f) Ship speed

Figure C.6: Full-scale starboard 20/20 zig-zag manoeuvre

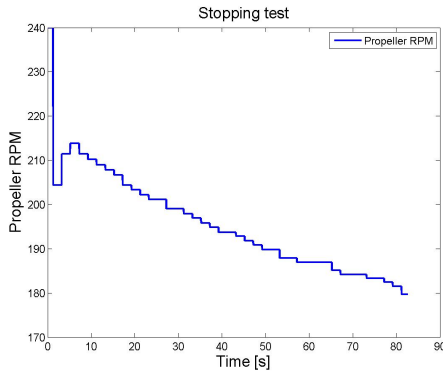
C.3 Stopping test manoeuvre



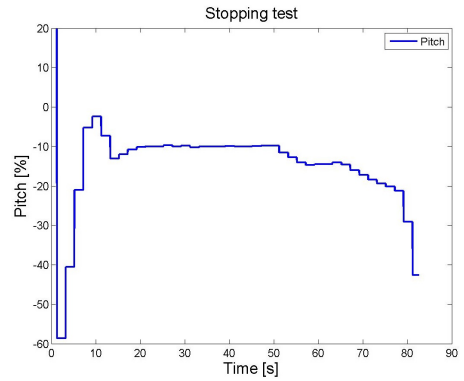
(a) Trajectory



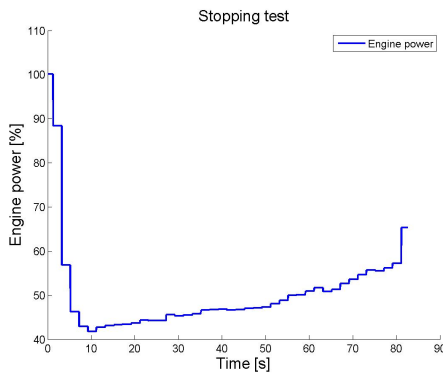
(b) Ship speed



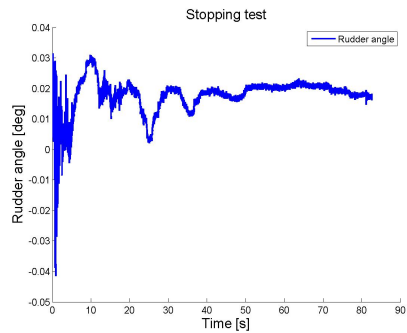
(c) Propeller RPM



(d) Propeller pitch



(e) Engine power



(f) Rudder angle

Figure C.7: Full-scale stopping test manoeuvre

C.4 Thruster turning manoeuvre

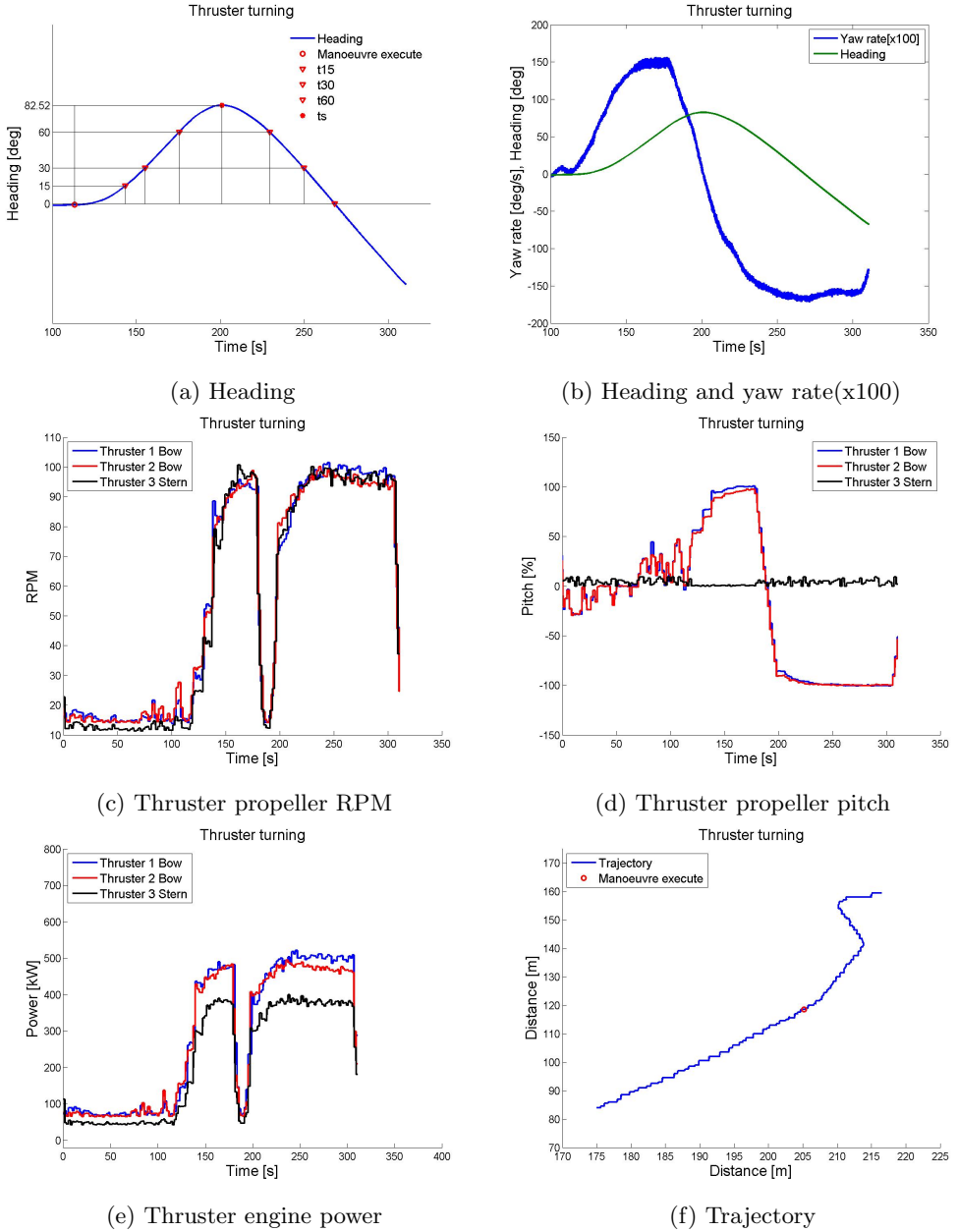
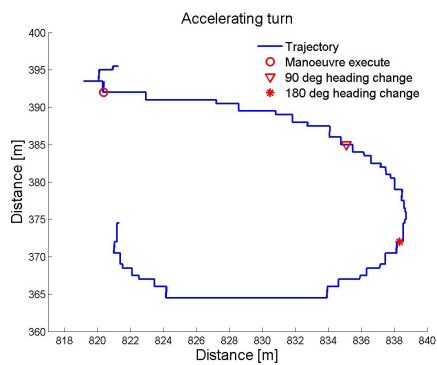
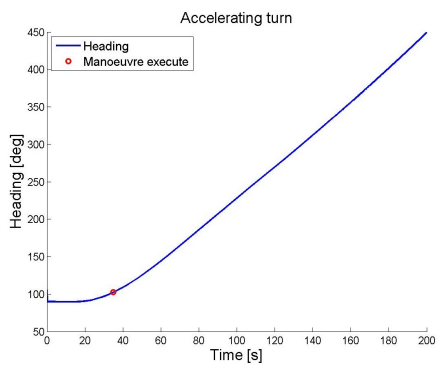


Figure C.8: Full-scale thruster turning manoeuvre

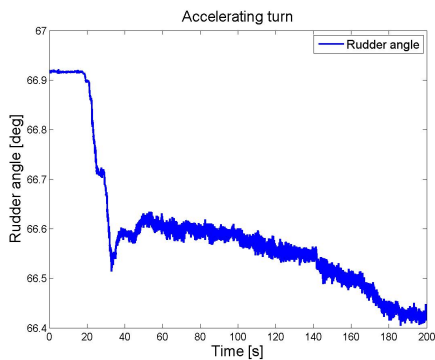
C.5 Accelerating turn manoeuvre



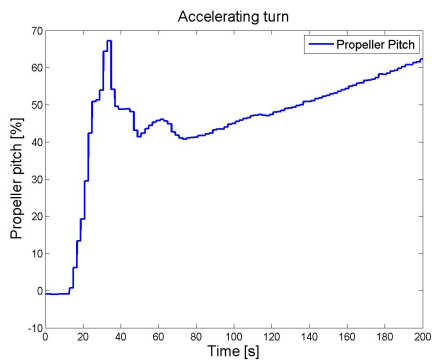
(a) Trajectory



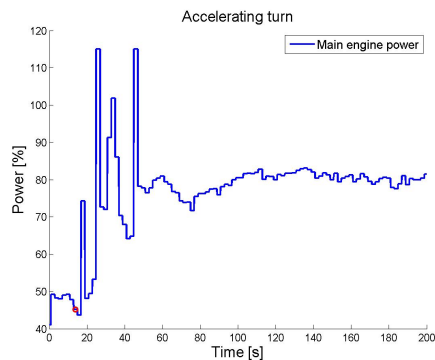
(b) Heading



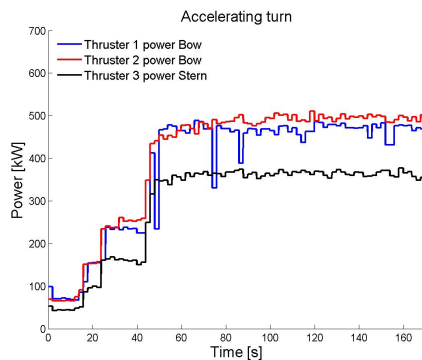
(c) Rudder angle



(d) Main propeller pitch



(e) Main engine power



(f) Thruster engine power

Figure C.9: Full-scale accelerating turn manoeuvre

Appendix D

VeSim simulated manoeuvres

D.1 Turning circle manoeuvre

D.1.1 Port turning circle

TURNING CIRCLE MANOEUVRE	ENCL.	1)
	REPORT	
	DATE	2014-05-21
	REF	

Turning circle

Turning Circle Manoeuvre Summary

Turning Circle 35 deg to port

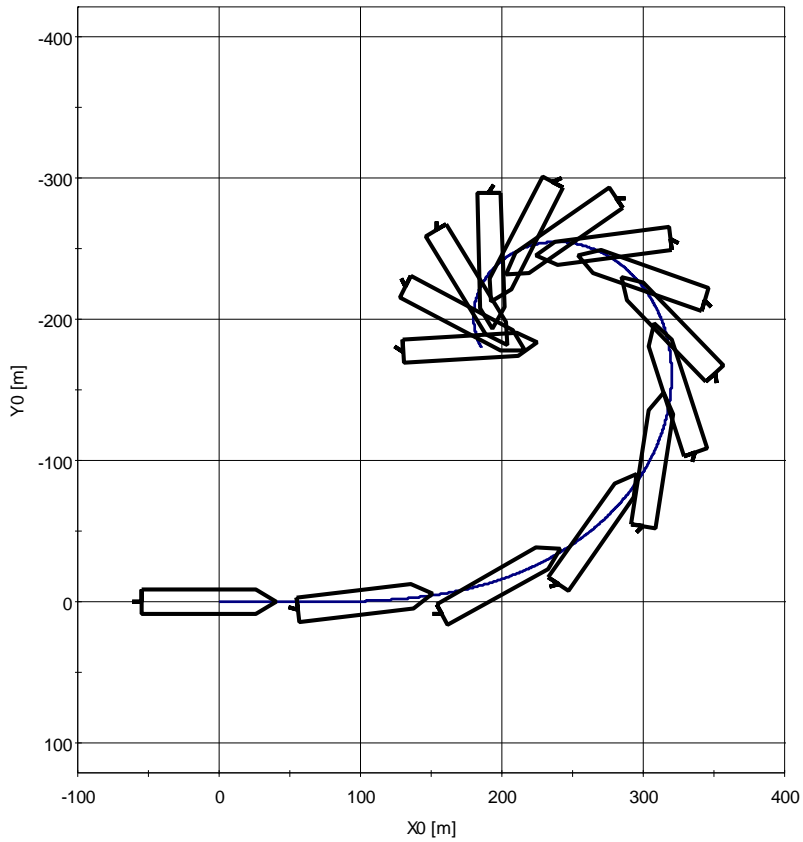
Rudder angle (to port)	35 deg
Heading change	-360 deg
Approach speed	17.6 knots
Speed at 90 deg / Approach speed	0.47 -
Speed at 180 deg / Approach speed	0.28 -
Speed at 270 deg / Approach speed	0.20 -
Final speed	3.5 knots
Final speed / Approach speed	0.20 -
Advance	315 m
Advance / Lpp	3.30 -
Transfer	126 m
Transfer / Lpp	1.32 -
Tactical diameter	246 m
Tactical diameter / Lpp	2.58 -
Final turning radius	43 m
Final turning radius / Lpp	0.45 -
Final rate of turn (to port)	2.37 deg/s
Final rate of turn (to port) * Lpp / U	2.20 -
Pivot point position	29 m
Pivot point position / Lpp	0.30 -
Drift angle at 270 deg	-41.8 deg

MARINTEK Vessel Simulator (VeSim) - Version 4.1.697 - 02-May-2014 11:48:27 - Licensed to: AM (NTNU)

Figure D.1: Port turning circle summary report

TURNING CIRCLE MANOEUVRE	ENCL	1)
	REPORT	
	DATE	2014-05-21
	REF	

TURNING CIRCLE MANOEUVRE



Turning circle

MARINTEK Vessel Simulator (VeSim) - Version 4.1.697 - 02-May-2014 11:48:27 - Licensed to: AM (NTNU)

Figure D.2: Port turning circle trajectory

D.1.2 Starboard turning circle

TURNING CIRCLE MANOEUVRE	ENCL	1)
	REPORT	
	DATE	2014-05-21
	REF	

Turning circle

Turning Circle Manoeuvre Summary

Turning Circle 35 deg to starboard

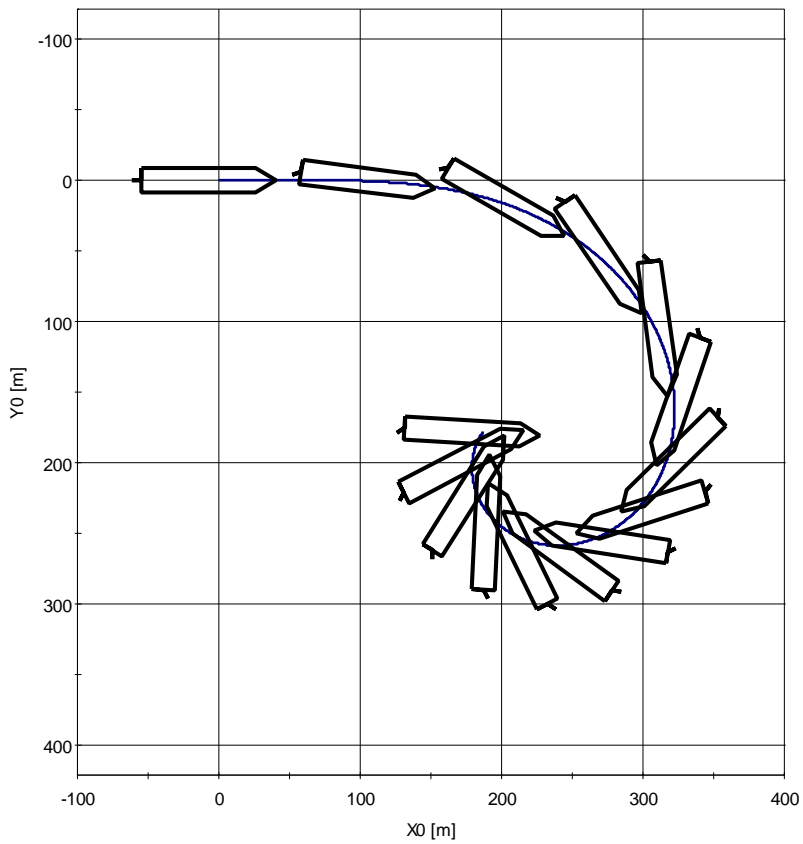
Rudder angle (to starboard)	35 deg
Heading change	360 deg
Approach speed	17.6 knots
Speed at 90 deg / Approach speed	0.47 -
Speed at 180 deg / Approach speed	0.29 -
Speed at 270 deg / Approach speed	0.20 -
Final speed	3.6 knots
Final speed / Approach speed	0.20 -
Advance	318 m
Advance / Lpp	3.32 -
Transfer	128 m
Transfer / Lpp	1.34 -
Tactical diameter	251 m
Tactical diameter / Lpp	2.62 -
Final turning radius	46 m
Final turning radius / Lpp	0.48 -
Final rate of turn (to starboard)	2.29 deg/s
Final rate of turn (to starboard) * Lpp / U	2.09 -
Pivot point position	29 m
Pivot point position / Lpp	0.30 -
Drift angle at 270 deg	39.5 deg

MARINTEK Vessel Simulator (VeSim) - Version 4.1.697 - 02-May-2014 11:54:13 - Licensed to: AM (NTNU)

Figure D.3: Starboard turning circle summary report

TURNING CIRCLE MANOEUVRE	ENCL.	1)
	REPORT	
	DATE	2014-05-21
	REF	

TURNING CIRCLE MANOEUVRE



Turning circle

MARINTEK Vessel Simulator (VeSim) - Version 4.1.697 - 02-May-2014 11:54:13 - Licensed to: AM (NTNU)

Figure D.4: Starboard turning circle Trajectory

D.2 Zig-zag manoeuvre

D.2.1 Port 10/10 zig-zag manoeuvre

ZIG-ZAG MANOEUVRE	ENCL.	1)
	REPORT	
	DATE	2014-05-21
	REF	

Zig zag

Zig-Zag Manoeuvre Summary

Zig-zag 10/10 to port

10 deg rudder angle, 10 deg heading, first turn to port

Approach speed	17.5 knots
Initial turning time	19.4 s / 1.83 -
Half period	46.4 s / 4.37 -
Time from 1st counter rudder to 1st overshoot angle	7.5 s / 0.71 -
Time from 2nd counter rudder to 2nd overshoot angle	7.2 s / 0.68 -
Time from 3rd counter rudder to 3rd overshoot angle	0.0 s / 0.00 -
1st overshoot angle	3.6 deg
2nd overshoot angle	3.6 deg
3rd overshoot angle	0.0 deg

Zig-Zag Manoeuvre IMO Summary

Zig-zag 10/10 to port

10 deg rudder angle, 10 deg heading, first turn to port

Approach speed 17.5 knots

Travel at 10 deg heading change

Calculated	174 m	(1.8)
IMO	239 m	(2.5)

First overshoot angle

Calculated	3.6 deg
IMO	10.3 deg

Second overshoot angle

Calculated	3.6 deg
IMO	25.5 deg

The IMO regulations are complied with in this manoeuvre.

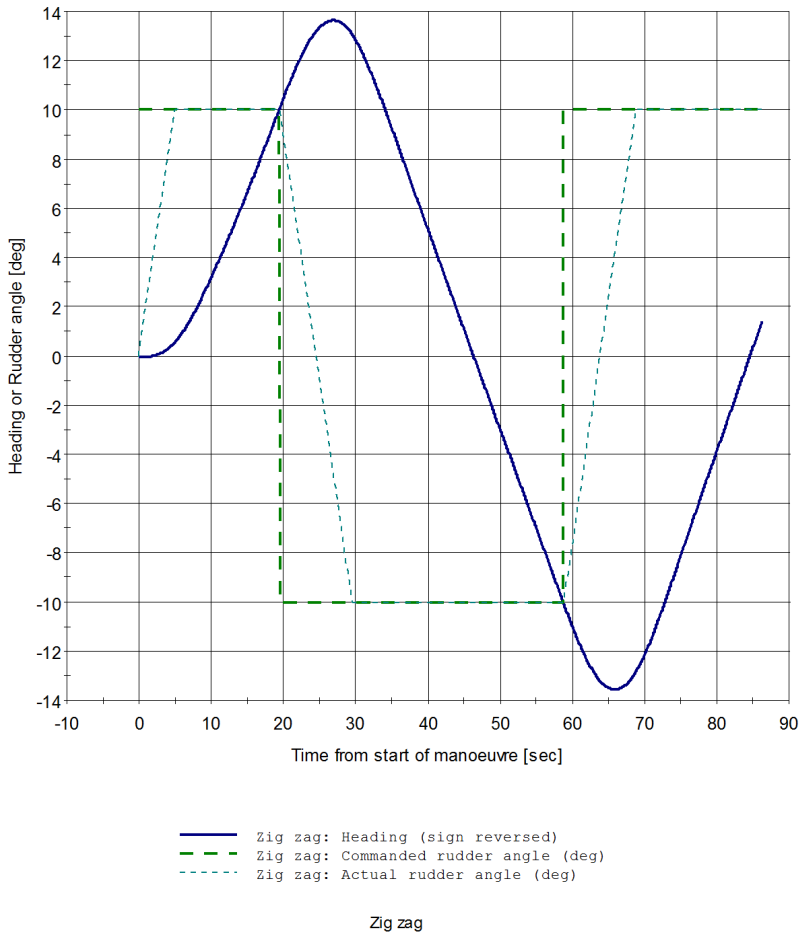
Warning

- IMO regulations does not apply to ships with Lpp less than 100 m, unless it is a chemical tanker or a gas carrier constructed on or after 1 July 1994.

Figure D.5: Port 10/10 zig-zag summary report

ZIG-ZAG MANOEUVRE	ENCL.	1)
	REPORT	
	DATE	2014-05-21
	REF	

Heading and Rudder Angle



MARINTEK Vessel Simulator (VeSim) - Version 4.1.697 - 02-May-2014 11:57:53 - Licensed to: AM (NTNU)

Figure D.6: Port 10/10 zig-zag heading and yaw angle

D.2.2 Starboard 10/10 zig-zag manoeuvre

ZIG-ZAG MANOEUVRE	ENCL	1)
	REPORT	
	DATE	2014-05-21
	REF	

Zig zag

Zig-Zag Manoeuvre Summary

Zig-zag 10/10 to starboard

10 deg rudder angle, 10 deg heading, first turn to starboard

Approach speed	17.6 knots
Initial turning time	19.5 s / 1.84 -
Half period	45.5 s / 4.30 -
Time from 1st counter rudder to 1st overshoot angle	7.3 s / 0.69 -
Time from 2nd counter rudder to 2nd overshoot angle	7.3 s / 0.69 -
1st overshoot angle	3.5 deg
2nd overshoot angle	3.8 deg

Zig-Zag Manoeuvre IMO Summary

Zig-zag 10/10 to starboard

10 deg rudder angle, 10 deg heading, first turn to starboard

Approach speed 17.6 knots

Travel at 10 deg heading change

Calculated	175 m	(1.8)
IMO	239 m	(2.5)

First overshoot angle

Calculated	3.5 deg
IMO	10.3 deg

Second overshoot angle

Calculated	3.8 deg
IMO	25.4 deg

The IMO regulations are complied with in this manoeuvre.

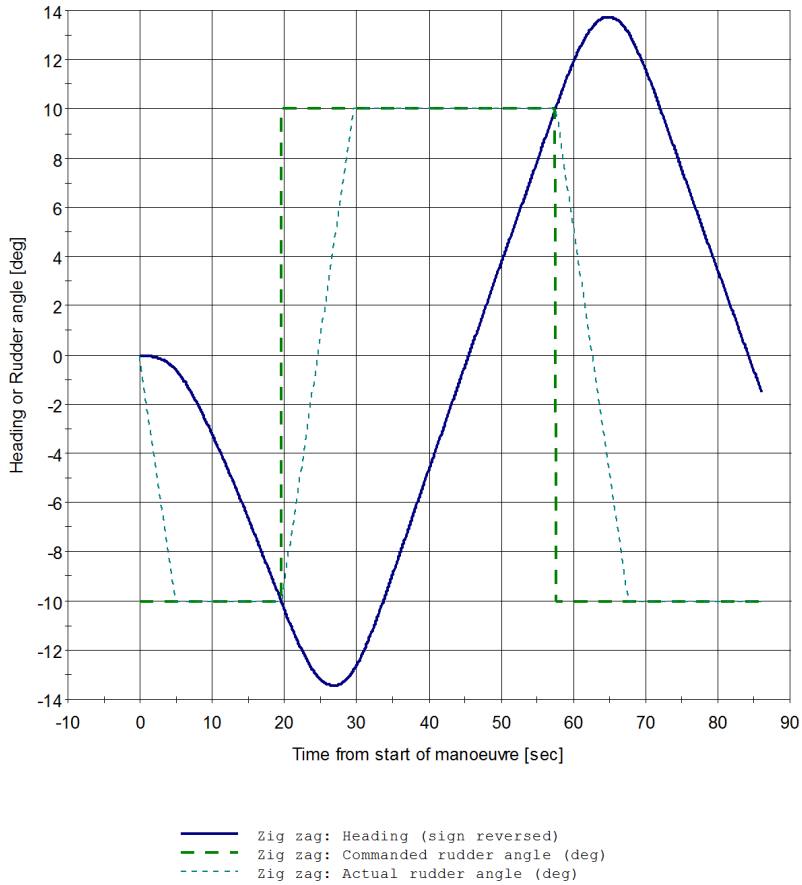
Warning

- IMO regulations does not apply to ships with Lpp less than 100 m, unless it is a chemical tanker or a gas carrier constructed on or after 1 July 1994.

Figure D.7: Starboard 10/10 zig-zag summary report

ZIG-ZAG MANOEUVRE	ENCL	1)
	REPORT	
	DATE	2014-05-21
	REF	

Heading and Rudder Angle



MARINTEK Vessel Simulator (VeSim) - Version 4.1.697 - 02-May-2014 12:04:42 - Licensed to: AM (NTNU)

Figure D.8: Starboard 10/10 zig-zag heading and yaw angle

D.2.3 Port 20/20 zig-zag manoeuvre

ZIG-ZAG MANOEUVRE	ENCL.	1)
	REPORT	
	DATE	2014-05-21
	REF	

Zig zag

Zig-Zag Manoeuvre Summary

Zig-zag 20/20 to port

20 deg rudder angle, 20 deg heading, first turn to port

Approach speed	17.6 knots
Initial turning time	22.0 s / 2.08 -
Half period	59.7 s / 5.64 -
Time from 1st counter rudder to 1st overshoot angle	12.5 s / 1.18 -
Time from 2nd counter rudder to 2nd overshoot angle	12.4 s / 1.17 -
Time from 3rd counter rudder to 3rd overshoot angle	0.0 s / 0.00 -
1st overshoot angle	11.1 deg
2nd overshoot angle	11.2 deg
3rd overshoot angle	0.0 deg

Zig-Zag Manoeuvre IMO Summary

Zig-zag 20/20 to port

20 deg rudder angle, 20 deg heading, first turn to port

Approach speed 17.6 knots

First overshoot angle

Calculated	11.1 deg
IMO	25.0 deg

The IMO regulations are complied with in this manoeuvre.

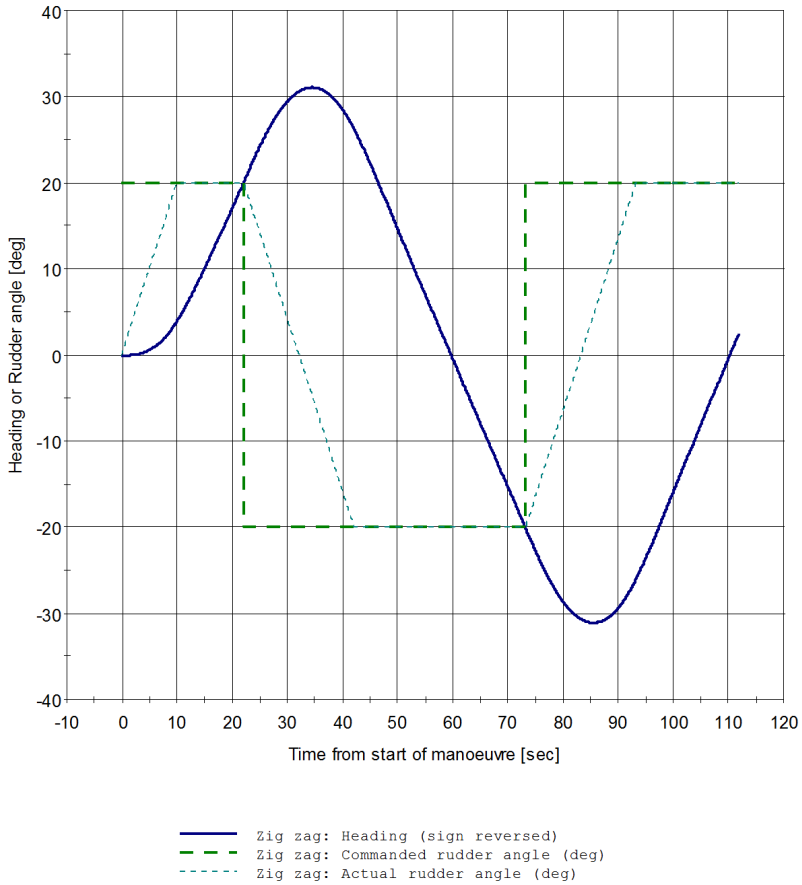
Warning

- IMO regulations does not apply to ships with Lpp less than 100 m, unless it is a chemical tanker or a gas carrier constructed on or after 1 July 1994.

Figure D.9: Port 20/20 zig-zag summary report

ZIG-ZAG MANOEUVRE	ENCL.	1)
	REPORT	
	DATE	2014-05-21
	REF	

Heading and Rudder Angle



Zig zag

MARINTEK Vessel Simulator (VeSim) - Version 4.1.697 - 02-May-2014 12:12:53 - Licensed to: AM (NTNU)

Figure D.10: Port 20/20 zig-zag heading and yaw angle

D.2.4 Starboard 20/20 zig-zag manoeuvre

ZIG-ZAG MANOEUVRE	ENCL.	1)
	REPORT	
	DATE	2014-05-21
	REF	

Zig zag

Zig-Zag Manoeuvre Summary

Zig-zag 20/20 to starboard

20 deg rudder angle, 20 deg heading, first turn to starboard

Approach speed	17.5 knots
Initial turning time	22.3 s / 2.10 -
Half period	59.3 s / 5.59 -
Time from 1st counter rudder to 1st overshoot angle	12.3 s / 1.16 -
Time from 2nd counter rudder to 2nd overshoot angle	12.6 s / 1.19 -
Time from 3rd counter rudder to 3rd overshoot angle	0.0 s / 0.00 -
1st overshoot angle	10.8 deg
2nd overshoot angle	11.5 deg
3rd overshoot angle	0.0 deg

Zig-Zag Manoeuvre IMO Summary

Zig-zag 20/20 to starboard

20 deg rudder angle, 20 deg heading, first turn to starboard

Approach speed 17.5 knots

First overshoot angle

Calculated	10.8 deg
IMO	25.0 deg

The IMO regulations are complied with in this manoeuvre.

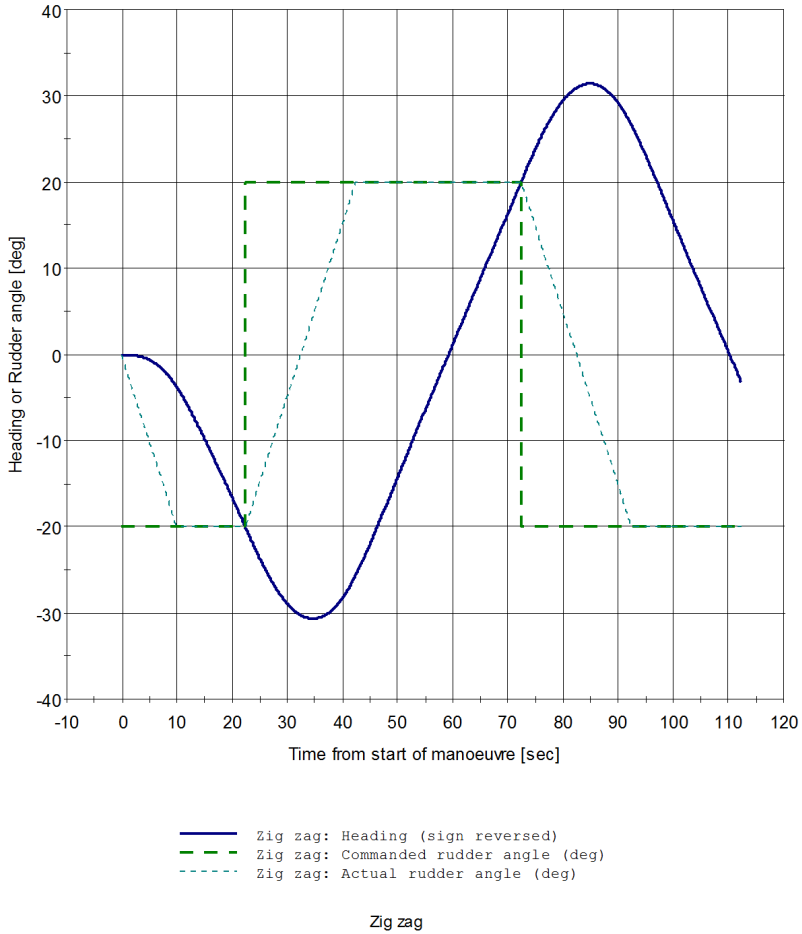
Warning

- IMO regulations does not apply to ships with Lpp less than 100 m, unless it is a chemical tanker or a gas carrier constructed on or after 1 July 1994.

Figure D.11: Starboard 20/20 zig-zag summary report

ZIG-ZAG MANOEUVRE	ENCL.	1)
	REPORT	
	DATE	2014-05-21
	REF	

Heading and Rudder Angle



MARINTEK Vessel Simulator (VeSim) - Version 4.1.697 - 02-May-2014 12:10:30 - Licensed to: AM (NTNU)

Figure D.12: Starboard 20/20 zig-zag heading and yaw angle

D.3 Full astern stopping manoeuvre

FULL ASTERN STOPPING MANOEUVRE	ENCL.	1)
	REPORT	
	DATE	2014-05-21
	REF	

Full astern stopping

Full Astern Stopping Manoeuvre Summary

Approach speed	9.2 knots
Track length	214 m
Track length / Lpp	2.2 -
Head reach	214 m
Head reach / Lpp	2.2 -
Lateral deviation	0 m
Lateral deviation / Lpp	0.00 -

Full Astern Stopping Manoeuvre IMO Summary

Approach speed 9.2 knots

Track length

Calculated	214 m	(2.2)
IMO	1434 m	(15.0)

The IMO regulations are complied with in this manoeuvre.

Warning

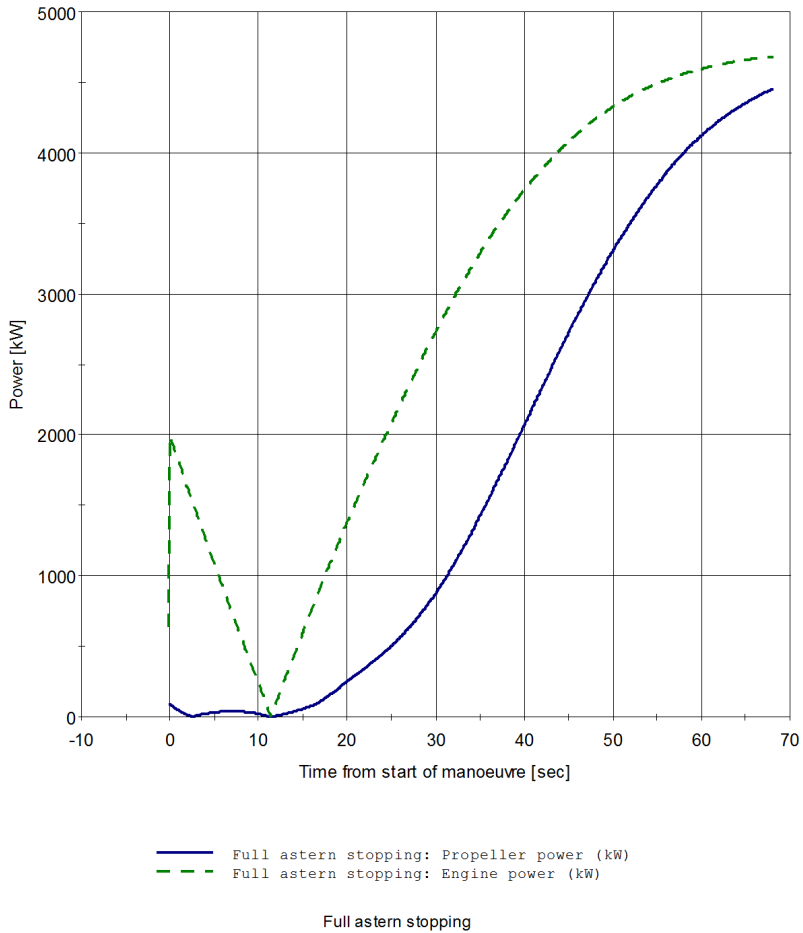
- IMO regulations does not apply to ships with Lpp less than 100 m, unless it is a chemical tanker or a gas carrier constructed on or after 1 July 1994.

MARINTEK Vessel Simulator (VeSim) - Version 4.1.697 - 02-May-2014 12:18:03 - Licensed to: AM (NTNU)

Figure D.13: Stopping test summary report

FULL ASTERN STOPPING MANOEUVRE	ENCL.	1)
	REPORT	
	DATE	2014-05-21
	REF	

Power

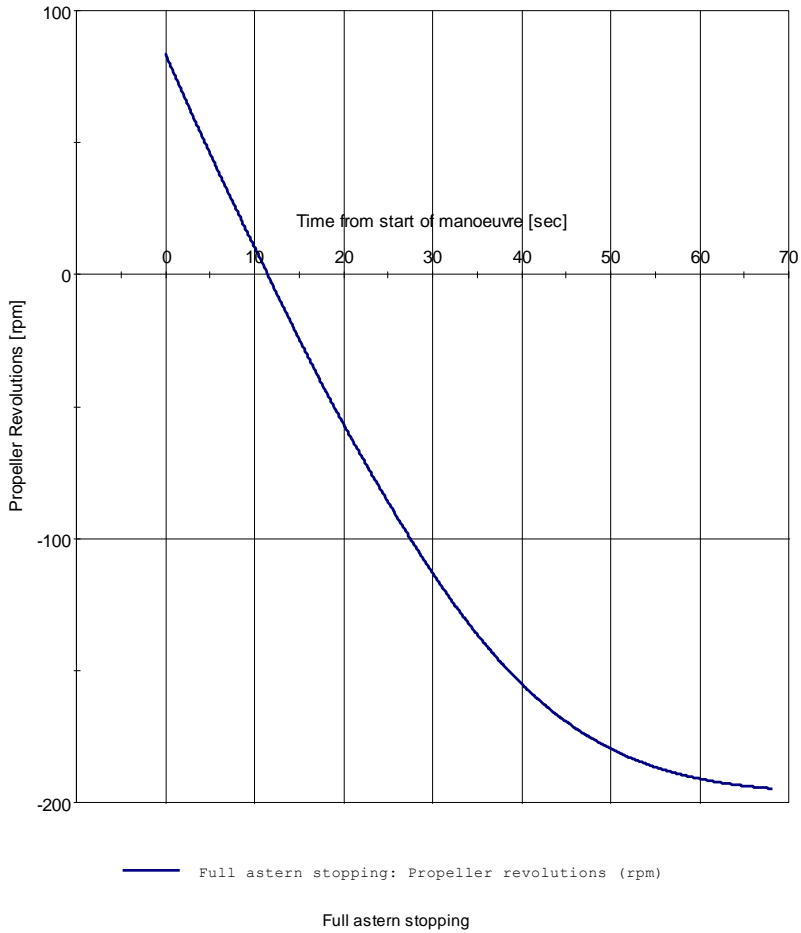


MARINTEK Vessel Simulator (VeSim) - Version 4.1.697 - 02-May-2014 12:18:03 - Licensed to: AM (NTNU)

Figure D.14: Stopping test engine power

FULL ASTERN STOPPING MANOEUVRE	ENCL.	1)
	REPORT	
	DATE	2014-05-21
	REF	

Propeller Revolutions

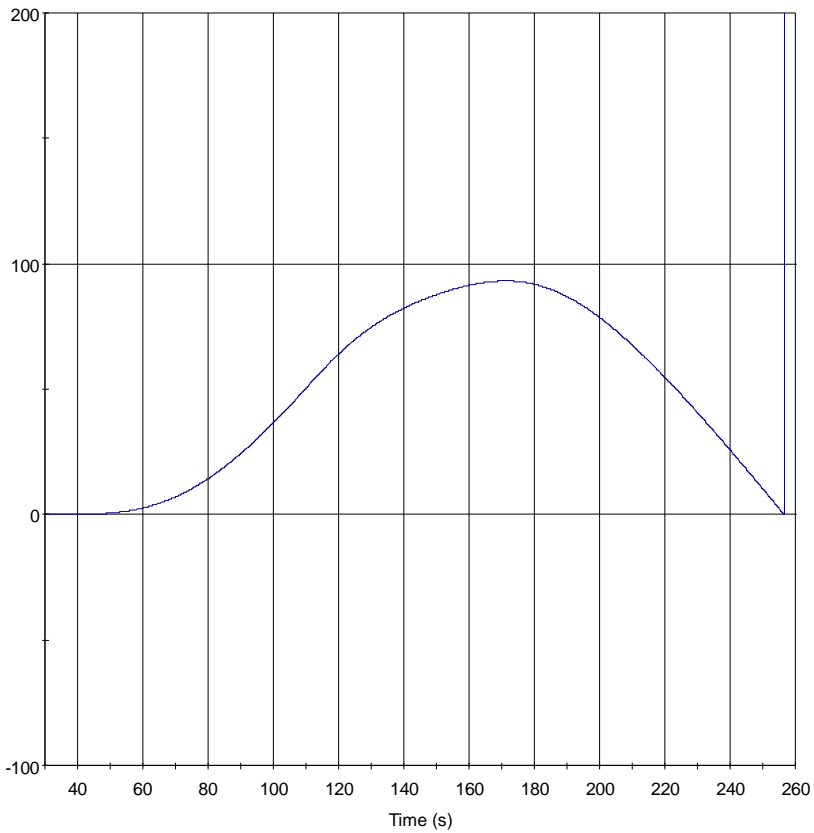


MARINTEK Vessel Simulator (VeSim) - Version 4.1.697 - 02-May-2014 12:18:03 - Licensed to: AM (NTNU)

Figure D.15: Stopping test propeller rpm

D.4 Thruster turning manoeuvre

Thruster Turning	ENCL.	1)
	REPORT	
	DATE	2014-05-21
	REF	



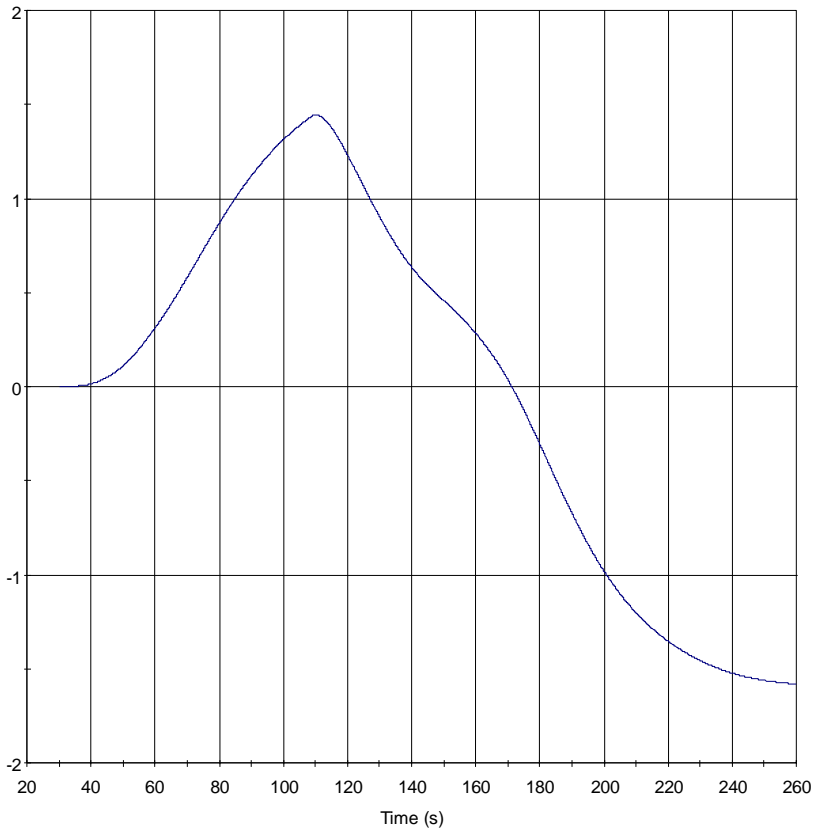
— Yaw angle of vessel (deg)

Selected time interval: 30.00 - 260.00 s
No filter applied.

ShipX (Time-Series Analysis) 09-May-2014 10:58:55 - Licensed to: AM (NTNU)

Figure D.16: Thruster turning heading

Thruster Turning	ENCL.	1)
	REPORT	
	DATE	2014-05-21
	REF	



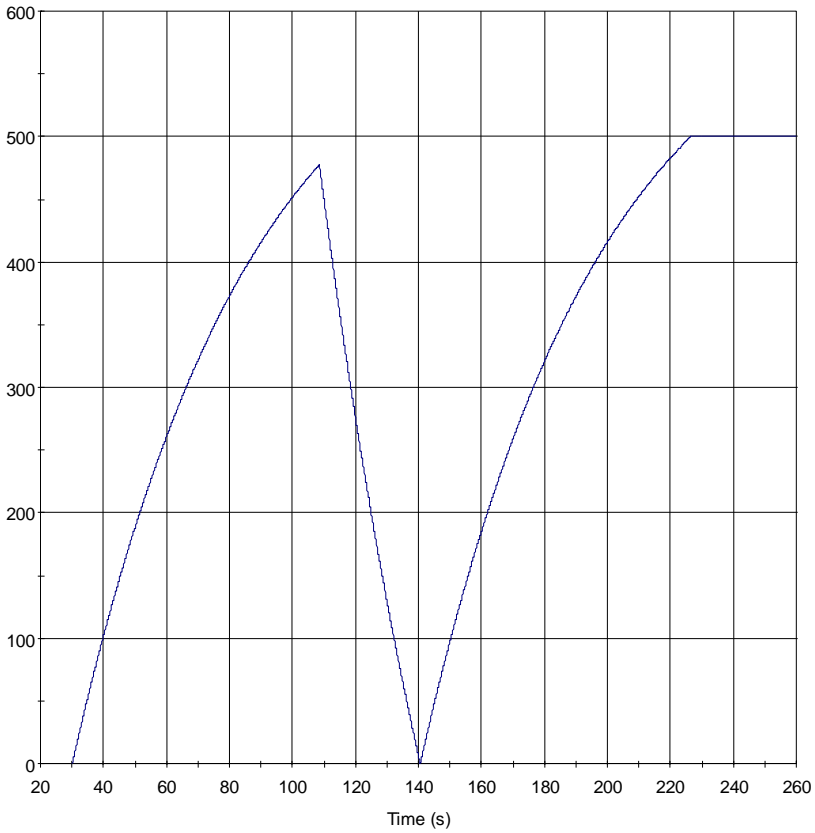
— Yaw velocity of vessel (deg/s)

Selected time interval: 30.00 - 260.00 s
No filter applied.

ShipX (Time-Series Analysis) 09-May-2014 11:02:51 - Licensed to: AM (NTNU)

Figure D.17: Thruster turning heading yaw rate

Thruster Turning Bow Thruster 1	ENCL.	1)
	REPORT	
	DATE	2014-05-21
	REF	



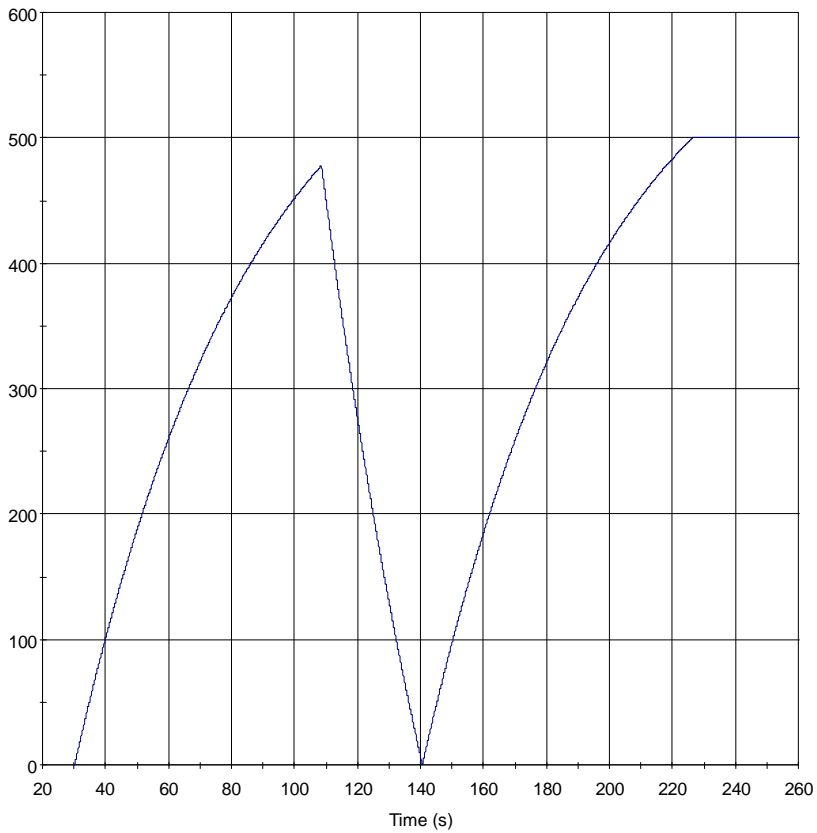
— Engine power (kW)

Selected time interval: 30.00 - 260.00 s
No filter applied.

ShipX (Time-Series Analysis) 09-May-2014 11:05:30 - Licensed to: AM (NTNU)

Figure D.18: Thruster turning thruster 1 power

Thruster Turning Bow Thruster 2	ENCL.	1)
	REPORT	
	DATE	2014-05-21
	REF	



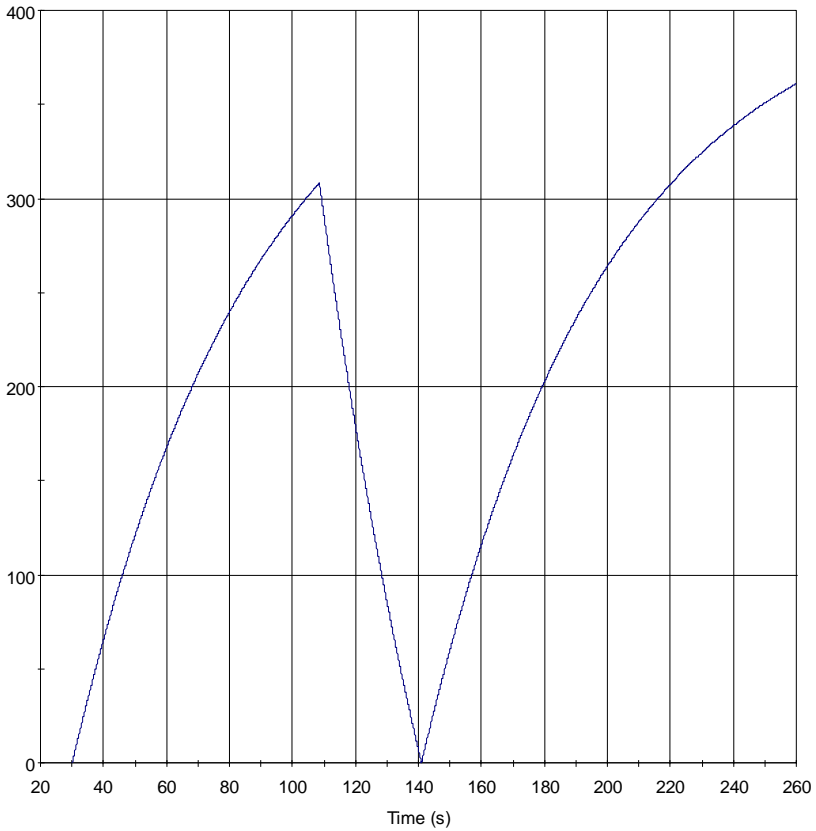
— Engine power (kW)

Selected time interval: 30.00 - 260.00 s
No filter applied.

ShipX (Time-Series Analysis) 09-May-2014 11:06:18 - Licensed to: AM (NTNU)

Figure D.19: Thruster turning thruster 2 power

Thruster Turning Stern Thruster 3	ENCL.	1)
	REPORT	
	DATE	2014-05-21
	REF	



— Engine power (kW)

Selected time interval: 30.00 - 260.00 s
No filter applied.

ShipX (Time-Series Analysis) 09-May-2014 11:07:04 - Licensed to: AM (NTNU)

Figure D.20: Thruster turning thruster 3 power

D.5 Accelerating turn manoeuvre

ACCELERATING TURN	ENCL.	1)
	REPORT	
	DATE	2014-05-21
	REF	

Turning circle (extended input)

Turning Circle Manoeuvre Summary

Turning Circle 65 deg to starboard

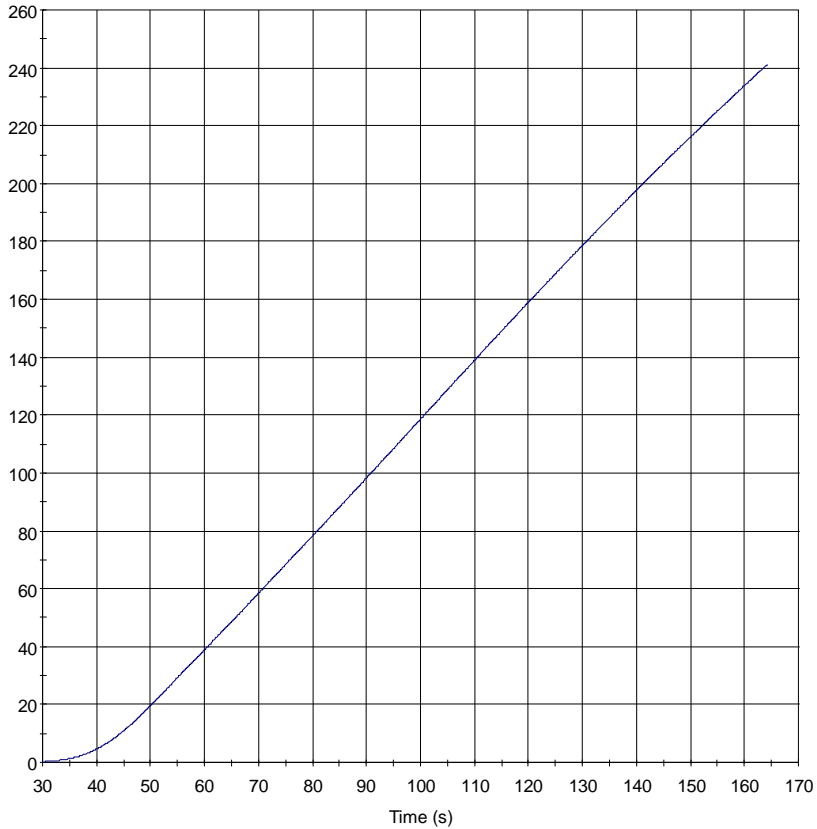
Rudder angle (to starboard)	65 deg
Heading change	240 deg
Approach speed	0.0 knots
Speed at 90 deg	1.3 knots
Speed at 180 deg	2.8 knots
Final speed	2.8 knots
Advance	23 m
Advance / Lpp	0.24 -
Transfer	7 m
Transfer / Lpp	0.07 -
Tactical diameter	28 m
Tactical diameter / Lpp	0.29 -
Final turning radius	43 m
Final turning radius / Lpp	0.45 -
Final rate of turn (to starboard)	1.93 deg/s
Final rate of turn (to starboard) * Lpp / U	2.22 -
Pivot point position	10 m
Pivot point position / Lpp	0.10 -
Drift angle at 180 deg	12.8 deg

MARINTEK Vessel Simulator (VeSim) - Version 4.1.697 - 09-May-2014 13:39:15 - Licensed to: AM (NTNU)

Figure D.21: Accelerating turn summary report

ACCELERATING TURN	ENCL. 1)
	REPORT
	DATE 2014-05-21
	REF

Heading



— Yaw angle of vessel (deg)

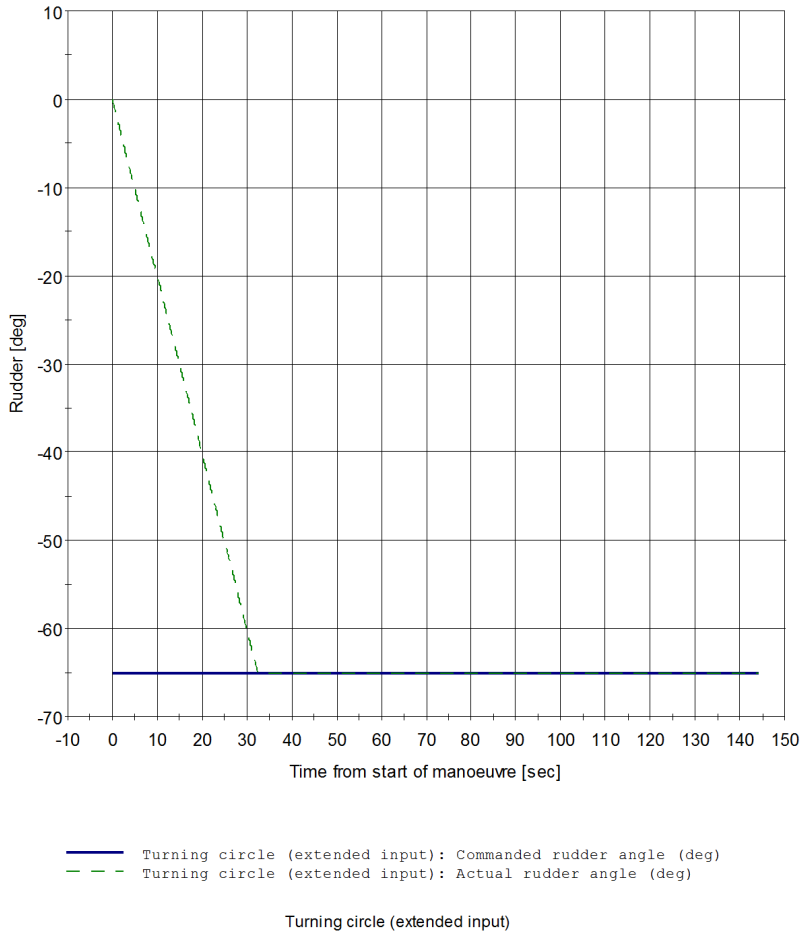
Selected time interval: 30.00 - 164.30 s
No filter applied.

ShipX (Time-Series Analysis) 09-May-2014 13:45:35 - Licensed to: AM (NTNU)

Figure D.22: Accelerating turn heading

ACCELERATING TURN	ENCL.	1)
	REPORT	
	DATE	2014-05-21
	REF	

Rudder

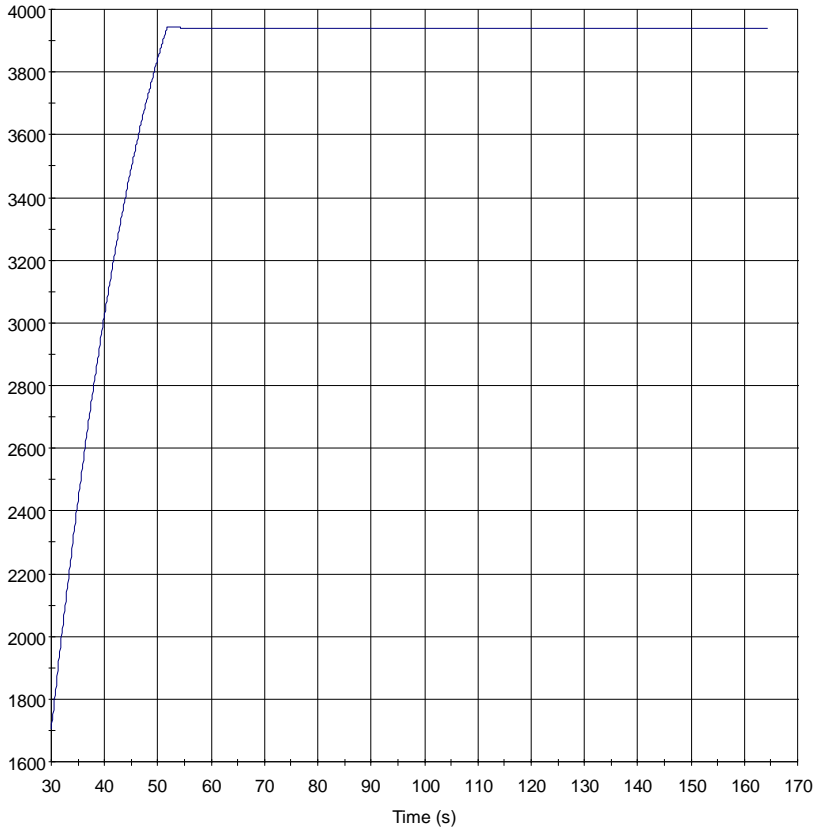


MARINTEK Vessel Simulator (VeSim) - Version 4.1.697 - 09-May-2014 13:39:15 - Licensed to: AM (NTNU)

Figure D.23: Accelerating turn rudder angle

ACCELERATING TURN	ENCL	1)
	REPORT	
	DATE	2014-05-21
	REF	

Engine power



— Engine power (kW)

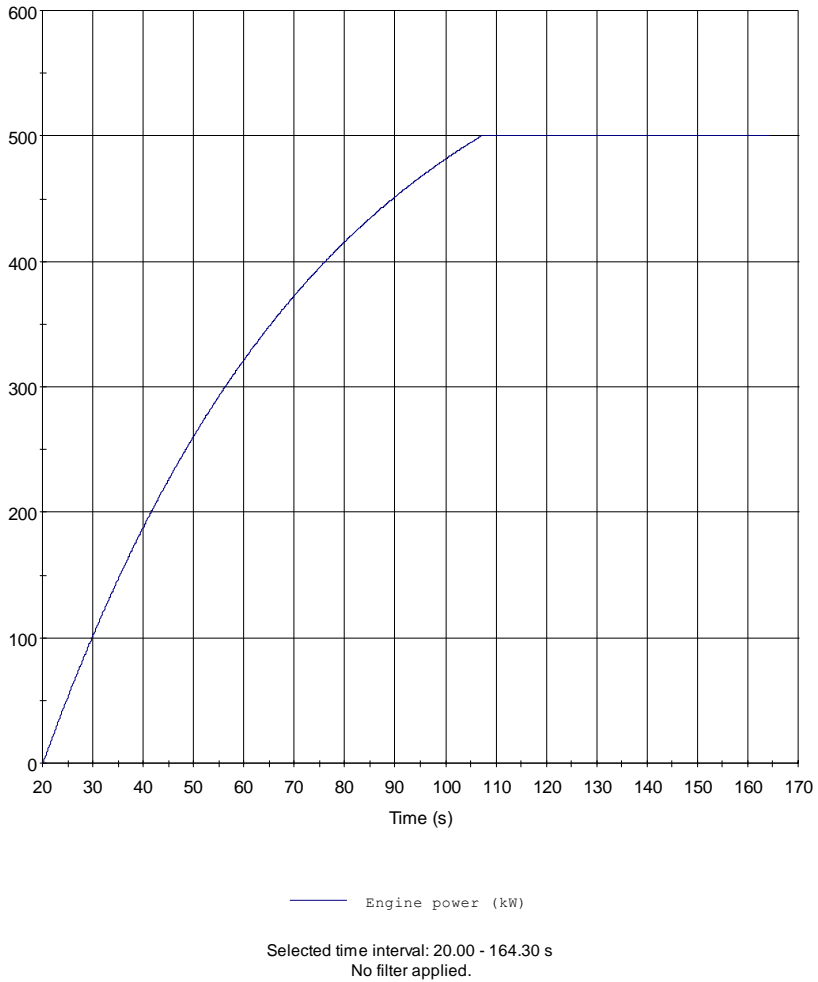
Selected time interval: 30.00 - 164.30 s
No filter applied.

ShipX (Time-Series Analysis) 09-May-2014 13:58:44 - Licensed to: AM (NTNU)

Figure D.24: Accelerating turn main engine power

ACCELERATING TURN	ENCL.	1)
	REPORT	
	DATE	2014-05-21
	REF	

Thruster Power Bow 1

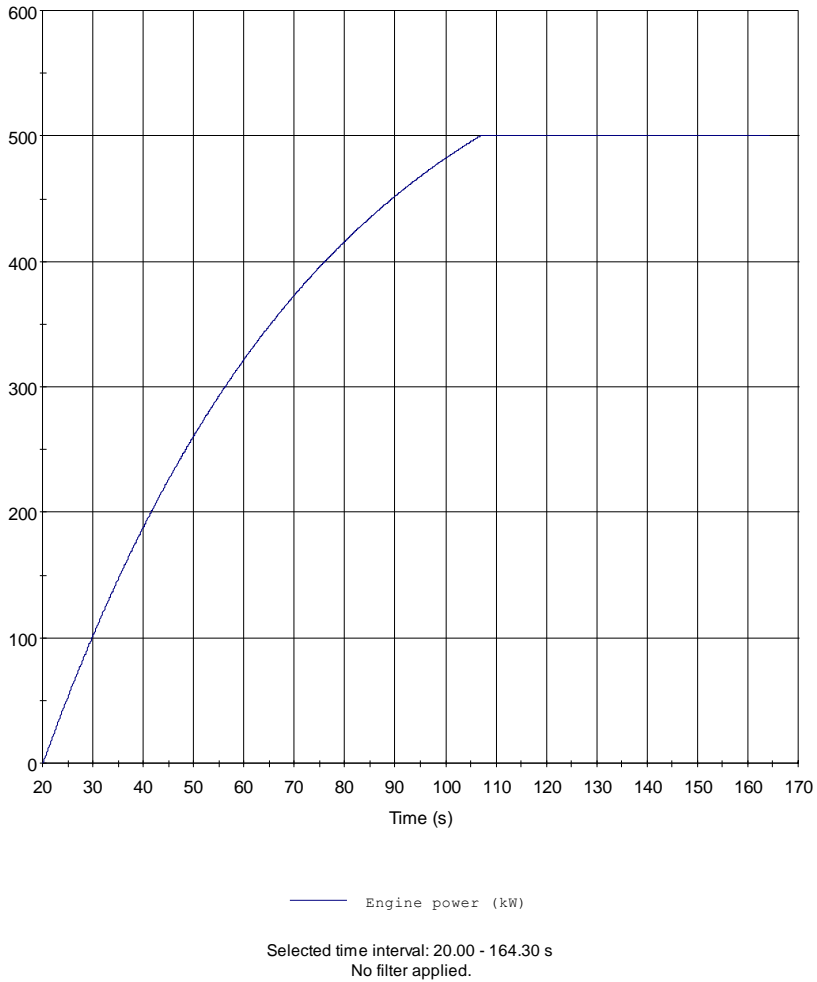


ShipX (Time-Series Analysis) 09-May-2014 14:07:55 - Licensed to: AM (NTNU)

Figure D.25: Accelerating turn thruster 1 power

ACCELERATING TURN	ENCL.	1)
	REPORT	
	DATE	2014-05-21
	REF	

Thruster Power Bow 2

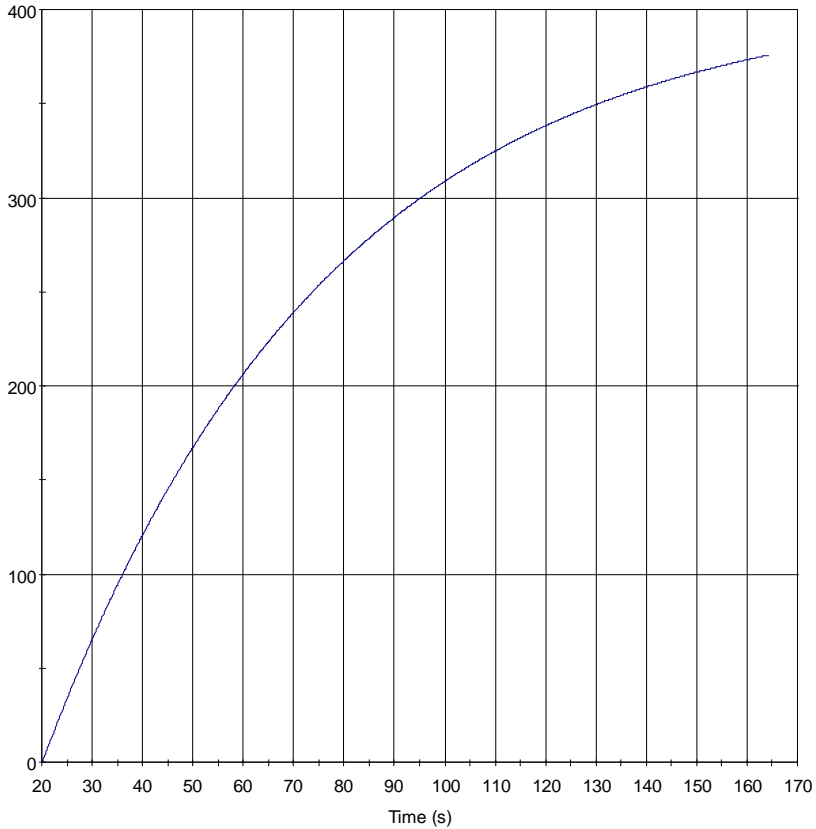


ShipX (Time-Series Analysis) 09-May-2014 14:08:35 - Licensed to: AM (NTNU)

Figure D.26: Accelerating turn thruster 2 power

ACCELERATING TURN	ENCL.	1)
	REPORT	
	DATE	2014-05-21
	REF	

Thruster Power Stern 3



— Engine power (kW)

Selected time interval: 20.00 - 164.30 s
No filter applied.

ShipX (Time-Series Analysis) 09-May-2014 14:09:26 - Licensed to: AM (NTNU)

Figure D.27: Accelerating turn thruster 3 power